EVALUATING MUTANT P53 GAIN-OF-FUNCTION PHENOTYPES AND MECHANISMS IN CANCER

By

Lindsay Nicole Redman Rivera

Dissertation

Submitted to the Faculty of the

Graduate School of Vanderbilt University

in partial fulfillment of the requirements

for the degree of

DOCTOR OF PHILOSOPHY

in

Biochemistry

December 18, 2021

Nashville, Tennessee

Approved

Jennifer A. Pietenpol, Ph.D.

David Cortez, Ph.D.

Scott Hiebert, Ph.D.

Carlos Lopez, Ph.D.

Jeffrey Rathmell, Ph.D.

To Eloisa

ACKNOWLEDGEMENTS

I am humbled by the fact that I am the first woman in my family to have pursued a doctoral degree. While I could write a novel thanking everyone who helped me get to this point in my life, I will attempt to use this section to acknowledge as many people as I can, especially the strong women who came before me.

First and foremost, I would like to thank my mentor Dr. Jennifer A. Pietenpol. Quite frankly, one reason I joined Jennifer's lab is because my mother told me to. After seeing Jennifer speak at the parents visitation time during my first year of graduate school, my mother knew that having a powerful role model like her would be invaluable for my career. I saw this too, which is why I rotated in Jennifer's lab, even though I had already convinced myself that I wanted to do chemical and not biological research. Jennifer's dedication to mentorship, her passion, and energy have unquestionably contributed to my success in graduate school. I constantly try to emulate her leadership skills, but not her sleep habits. While I am still not entirely convinced that she is human – maybe alien or robot – because of her uncanny ability to be a "GSD" and get stuff done, her humanity is evident through her passion and desire to help others and positively contribute to society. In all seriousness, I am truly grateful to have been trained by such an accomplished scientist, passionate leader, and strong woman.

Prior to graduate school, I have had several mentors who contributed significantly to my career trajectory. Dr. Shelley Lusetti from New Mexico State University allowed me to do research in her lab, and ultimately convinced me that I should apply to graduate school. She saw my potential and for that, I am grateful. Dr. Eva Birnbaum from the Los Alamos National Laboratories took a chance by allowing an administrative student just

out of high school to start working in a laboratory that handled high levels of radioactivity. She trusted me to not contaminate myself and taught me that a critical aspect of leadership is “putting out fires”. I am grateful to have been mentored by these two strong women. Other mentors who have contributed to my success and need to be acknowledged include Dr. Lee Uranga, Dr. Stosh Kozimor, Dr. Kevin John, Dr. Stuart Schreiber and Dr. Anneke Kramm. I am forever grateful for their contribution to my scientific training.

I want to thank the members of my thesis committee: Dr. David Cortez, Dr. Scott Hiebert, Dr. Carlos Lopez and Dr. Jeffrey Rathmell. Their feedback and attention have contributed to the quality of my thesis project and graduate experience. I am thankful for those who contributed to this work, including Dr. Quanhu (Tiger) Sheng, Dr. Katy Beckermann, Rachel Hongo, Dr. Ferrin Wheeler, and Dr. Paula Gonzalez Ericsson.

Members of the Pietenpol lab have made a seminal contribution to my thesis work and graduate school experience. Without Hailing Jin, this project would not have been possible. I cannot thank her enough for her technical assistance and for making me carefully understand and justify every experiment. Her aid undoubtedly contributed to the efficiency of my work. Kimberly Newsom is a critical member of the Pietenpol lab and was always willing and ready to help. She supported my work through her administrative and technical experience, and most importantly she supported me emotionally when I needed it the most. Every graduate student needs a Kim. Dr. Brian Lehmann supported my research by answering every question, big or small, and always gave me a reason to laugh when I needed it. Lynnette Stanton-Williams is a calming presence, a joy to talk to, and extremely helpful in navigating Jennifer’s hectic schedule. I am appreciative for other

former trainees in the lab; Dr. Johanna Schafer, Dr. Clayton Marshall, Dr. Scott Beeler, Dr. Tim Shaver and Dr. Gabriela Santos, as they provided support and assistance with my research, as well as helping me navigate other aspects of graduate school.

I am grateful for the opportunity to have conducted my graduate training at Vanderbilt, including the extra programs I have taken part in. Special thanks goes to individuals in the BRET office, especially Dr. Beth Bowman (I can't thank Beth enough) and Carolyn Berry; the Quantitative and Chemical Biology program and Dr. Hassane Mchaourab; Patty Mueller, Jen Smith and Dr. John York of the Biochemistry Department; Dr. Christina Keeton, Dr. Linda Sealy and Dr. Roger Chalkley and the Initiative for Maximizing Student Diversity (IMSD) program (2R25GM062459), as well as my IMSD peers; Dr. Scott Hiebert and the training grant (2T32CA009582); Faith Bishop, Dr. Vandana Abramson, Dr. Mark de Caestecker and Dr. James Luther with the Vanderbilt Program in Molecular Medicine; the team in the ASPIRE program; and the NCI for a Ruth L. Kirchstein National Research Service Award (1F31CA247356).

Last but not least, my graduate school experience would not have been possible without the support of family and friends. Thank you to my parents for providing me with the means and instilling in me the willpower and perseverance necessary to pursue my education. Thank you to my grandparents for always reminding me to have faith. Thank you to my cousins and siblings for supporting me in often the smallest but most meaningful ways. Thank you to my friends both old and new, who I leaned on heavily during difficult times. Thank you to the dogs of course, for their un-endless love and company. And thank you to Emilio, my perpetual lab partner, for way too many things to name.

TABLE OF CONTENTS

LIST OF TABLES

LIST OF FIGURES

LIST OF ABBREVIATIONS

A	Adenine
ANOVA	Analysis of variance
ARF	Alternate reading frame (aliases: p14, p19; gene: *CDKN2A*)
ARF-BP1	ARF-Binding Protein 1 (gene: *HUWE1*)
AS	Aneuploidy Score
ATM	Ataxia telangiectasia mutated protein
ATR	Ataxia telangiectasia and Rad3-related protein
BAX	BCL2 associated X protein
BBC3	BCL2 binding component 3
BCL2	B-cell lymphoma 2
bp	Base pair(s)
BRCA	Breast invasive carcinoma
BRCA2	Breast cancer gene 2
C	Cytosine
CBP	CREB-binding protein
CCLE	Cancer cell line encyclopedia
CDK	Cyclin-dependent kinase
CDKN1A	Cyclin-dependent kinase inhibitor 1A (protein: p21)
cDNA	Complementary DNA
CHIP	Carboxy-terminus of Hsc70 interacting protein (gene: *STUB1*)
CHK1	Checkpoint-kinase 1
CHX	Cycloheximide
CMA	Cytogenomic microarray analysis
COP1	Constitutive photomorphogenesis protein 1
CpG	Cytosine and guanine joined by a phosphodiester bond
CY3	Cyanine 3
DCDFDA	Dichlorofluorescin diacetate

DEG(s)	Differentially expressed gene(s)
DMEM	Dulbecco's modified Eagle's medium
DNA	Deoxyribonucleic acid
Dox	Doxorubicin
E3	Ubiquitin ligase
E6-AP	E6-associated protein
ECL	Enhanced chemiluminescence
EGFR	Epidermal growth factor receptor
ELISA	Enzyme-linked immunoassay
ER	Estrogen receptor
FBS	Fetal bovine serum
FDR	False discovery rate
FFPE	Formalin-fixed and paraffin embedded
FGA	Fraction of the genome altered
FITC	Fluorescein isothiocyanate
G	Guanine
GAPDH	Glyceraldehyde 3-phosphate dehydrogenase
GOF	Gain-of-function
gRNA	Guide RNA
GSEA	Gene set enrichment analysis
h	Hour(s)
HA-Ub	HA-tagged ubiquitin
HAUSP	Herpes virus-associated ubiquitin specific protease (alias: USP7)
HDAC	Histone deacetylase
HDAC1	Histone deacetylase 1
HDR	Homology-directed repair
HER2	Human epidermal growth factor receptor 2
HLA	Human leukocyte antigen
HRP	Horseradish peroxidase

HSP70	Heat shock 70 kDa protein
HSP90	Heat shock 90 kDa protein
IC_{50}	Half-maximal inhibitory concentration
IgG	Immunoglobulin G
IB	Immunoblotting
IF	Immunofluorescence
IHC	Immunohistochemistry
IP	Immunoprecipitation
kDa	Kilodalton
KPC	*Kras*$^{G12D/+}$;*Trp53*$^{R172H/+}$;*Pdx1-Cre* mice
LFS	Li-Fraumeni syndrome
LOF	Loss-of-function
LogR	Log_2 ratio
LOH	Loss of heterozygosity
LUSC	Lung squamous cell carcinoma
MDM2	Mouse double minute 2 homolog
min	Minute(s)
MitoSOX	Mitochondrial superoxides
MKRN1	Makorin ring finger protein 1
MRE11	Meiotic recombination 11
mRNA	Messenger RNA
MTG	Mitotracker green
Myc	V-Myc avian myelocytomatosis viral oncogene homolog
NBF	Neutral buffered formalin
NCI	National Cancer Institute
NES	Normalized enrichment score
NIH	National Institutes of Health
NSDHL	NAD(P) dependent steroid dehydrogenase-like
nt	Nucleotide

OV	Ovarian serous cystadenocarcinoma
p21	Cyclin-dependent kinase inhibitor 1 (gene: *CDKN1A*)
p53	Tumor protein p53 (gene: *TP53*)
p63	Tumor protein p63 (gene: *TP63*)
p73	Tumor protein p73 (gene: *TP73*)
PAM	Protospacer adjacent motif
PARP	Poly (ADP-ribose) polymerase
PBS	Phosphate buffered saline
PCA	Principal component analysis
PCR	Polymerase chain reaction
PI	Propidium iodide
Pirh2	P53-induced RING-H2 protein (gene: *RCHY1*)
PPMID	Protein phosphatase, Mg2+/Mn2+ dependent 1D
PTEN	Phosphatase and tensin homolog
PTM	Post-translational modification
Ras	Rat sarcoma virus oncogene
RB	Retinoblastoma
RIPA	Radioimmunoprecipitation assay buffer
RNA	Ribonucleic acid
RNA-seq	RNA sequencing
ROS	Reactive oxygen species
RPPA	Reverse phase protein array
s.d.	Standard deviation
s.e.m.	Standard error of the mean
SDS-PAGE	Sodium dodecyl sulfate polyacrylamide gel electrophoresis
Ser15	Serine 15
shRNA	Short hairpin RNA
SNP	Single nucleotide polymorphism
SV40	Simian virus 40

T	Thymine
TCGA	The Cancer Genome Atlas
TMA	Tissue microarray
TMRE	Tetramethylrhodamine, ethyl ester
TOPORS	Top1 binding arginine/serine rich protein
TRIM24	Tripartite motif containing 24
TSA-IF	Tyramide signal-amplified immunofluorescence
UCEC	Uterine corpus endometrial carcinoma
UCS	Uterine carcinosarcoma
UV	Ultraviolet
WES	Whole exome sequencing
WGD	Whole-genome doubling
WT	Wild-type

CHAPTER I

INTRODUCTION

Genomic alterations required for cellular transformation and carcinogenesis can range from small genetic events like single nucleotide mutations to extensive alterations such as duplication of the entire set of human chromosomes. Chromosomal alterations were once proposed to be the root cause of cancer (Boveri, 2008; Hansemann, 1890), and it is now understood that mutations in specific genes ultimately lead to tumorigenesis.

The most frequently mutated gene across human cancers, *TP53*, which encodes the protein p53 (Kandoth et al., 2013), is also the most well studied. Called “the guardian of the genome” (Lane, 1992), p53 functions as a transcription factor and tumor suppressor by regulating gene expression programs that control the cell cycle, are involved in genome maintenance, and induce apoptosis of damaged cells. Mutation in p53 leads to a loss of DNA binding, thus its tumor-suppressive function (Cho et al., 1994; Kern et al., 1992), and allows for the accumulation of genomic alterations that lead to the development of cancer.

In addition, mutated versions of p53 have also been reported to acquire a diverse set of novel oncogenic activities that lead to the emergence of various tumor-promoting phenotypes in cells. The existence of this neomorphic “gain-of-function” (GOF) activity is hotly debated within the p53 field. There is no agreement for the exact mechanisms by which mutant p53 can promote diverse and often context-specific oncogenic

phenotypes; although, proposed mechanisms attribute altered transcriptional activities and protein-protein interactions to the mutant protein. As mutant p53 frequently accumulates to high levels in transformed cells, this feature has also been proposed to underlie mutant p53 GOF by enhancing oncogenic protein activities and interactions.

The study of mutant p53 GOF is challenging because of the experimental limitations of the models used and the heterogeneous cellular features that occur after the loss of p53 function. Therefore, this dissertation aimed to evaluate mutant p53 GOF phenotypes and mechanisms using genetically engineered and controlled epithelial isogenic cell line models. This chapter will review the study and function of both wild-type and mutant p53 proteins, emphasizing reported mutant p53 GOF activities and associated phenotypes such as accumulation of the mutant protein.

Tumor Protein p53

Discovery and History

In the 1970s, much of cancer research was focused on the viral theory of cancer and the identification of virally encoded oncogenes, otherwise known as viral tumor antigens, that contributed to cellular transformation. In 1979, while studying Simian virus 40 (SV40) induced tumors, several research groups simultaneously discovered a non-viral protein approximately 50-55 kDa in size that associated with the SV40 large T-antigen (Kress et al., 1979; Lane and Crawford, 1979; Linzer and Levine, 1979; Melero et al., 1979; Smith et al., 1979). High levels of this protein and antibodies that target it were also found in other viral and non-virally transformed cells (Deleo et al., 1979;

Linzer and Levine, 1979; Rotter et al., 1980). By 1983, researchers agreed they were studying the same protein and adopted the name “p53” because it migrated at approximately 53 kDa by SDS-polyacrylamide gel electrophoresis (SDS-PAGE). However, its actual size was later determined to be only 43.7 kDa (Levine and Oren, 2009).

Following the discovery of p53, researchers in the 1980s raced to clone the encoding murine and human gene for experimental study of its function in cells. Several labs successfully generated p53 complementary DNA (cDNA) clones, allowing for transfection and overexpression of the protein in experimental model systems. Three articles published in 1984 showed that transfected p53 could cooperate with other oncogenes to transform cells (Eliyahu et al., 1984; Jenkins et al., 1984a; Parada et al., 1984). In addition, many tumors but not normal tissue produced high amounts of p53 (Rotter, 1983), in alignment with earlier findings showing that increased p53 levels correlated with SV40 T-antigen functionality (Linzer et al., 1979).

These early observations led researchers to believe that p53 was an oncogene; however, this classification was challenged by several articles published in the late 1980s. These studies found that p53 alleles were often inactivated through viral or genomic alterations, including rearrangements and deletions (Chandar et al., 1992; Masuda et al., 1987; Mowat et al., 1985; Wolf and Rotter, 1984, 1985), suggesting that p53 loss also promotes cancer. Finally, in 1989 the Levine lab could not reproduce earlier findings showing the transforming and oncogenic activity of p53 when using a new cDNA clone (Finlay et al., 1989). Comparing the genetic sequences of the p53 clones revealed that many of the previously used cDNA clones contained mutations in

the p53 coding region. When the wild-type p53 sequence was finally established (Eliyahu et al., 1988; Finlay et al., 1988), it became clear that early studies showing oncogenic p53 function were conducted with mutated versions of p53 which had been cloned from tumor-derived cell lines.

While mutant forms of p53 displayed oncogenic properties, the wild-type p53 protein quickly became re-classified as a tumor suppressor. Work out of the Vogelstein lab demonstrated that p53 showed hallmarks of a tumor suppressor as both wild-type p53 alleles were typically mutated or deleted in colorectal cancers (Baker et al., 1989). Further, overexpression of wild-type p53 was sufficient to suppress the oncogenic transformation of cultured cells (Eliyahu et al., 1989; Finlay et al., 1989). In a seminal discovery, germline mutations in p53 were found to be responsible for Li-Fraumeni syndrome, a dominantly inherited and highly penetrant familial predisposition to a diverse array of cancers that often present early in life (Malkin et al., 1990; Srivastava et al., 1990). Finally, while murine models engineered to be deficient for p53 initially appear normal, they develop spontaneous cancers, typically lymphomas and sarcomas, within six months of age (Donehower et al., 1992). These last two pieces of evidence firmly established wild-type p53 as a bona fide tumor suppressor.

Structure and Function

Following the recognition of p53 as a tumor suppressor, research in the p53 field grew exponentially. After four decades of research, it is now well established that p53 is a sequence-specific DNA binding transcription factor, and this activity is essential for its tumor suppressive function (Bargonetti et al., 1991; El-Deiry et al., 1992; Farmer et al.,

1992; Pietenpol et al., 1994). In addition to the central DNA binding domain (amino acids 102-292), the protein consists of two N-terminal transactivation domains (amino acids ~1-40 and ~41-61), a proline-rich domain (amino acids ~61-94), an oligomerization domain (amino acids ~323-356), and an unstructured C-terminal domain (amino acids ~364-393). Oligomerization is essential for the function of p53. p53 binds DNA as a tetramer, and each dimer of the tetrameric complex binds a 10 base pair response element with the consensus sequence RRCWWGYY (R=A/G, W=A/T, Y=C/T) (El-Deiry et al., 1992; Kitayner et al., 2006).

Through transcriptional activation, p53 has been shown to govern a complex and diverse array of biological processes. The primary function of p53 is to maintain genomic stability in response to cellular stress and upon DNA damage, p53 has been shown to induce cell cycle arrest (Kastan et al., 1991), apoptosis (Clarke et al., 1993; Lowe et al., 1993), and senescence (Shay et al., 1991). Many other non-canonical functions for p53 have been described, including but not limited to modulation of cellular metabolism (Kruiswijk et al., 2015; Morris et al., 2019) and autophagy (Eby et al., 2010; Tasdemir et al., 2008); regulation of cellular plasticity and stemness (Chang et al., 2011); and stimulation of DNA repair (Williams and Schumacher, 2016).

Numerous downstream target genes have been discovered which contribute to the heterogenous biological functions of p53. One of the first identified and most ubiquitous target genes of p53 is the cyclin-dependent kinase inhibitor CDKN1A, encoding the protein p21, which functions to stop cell cycle progression by binding and inhibiting cyclin/cyclin-dependent kinase (CDK) complexes (El-Deiry et al., 1993; Harper et al., 1993). MDM2, an E3 ligase and the primary negative regulator of p53, was also

identified as a p53 target gene (Juven et al., 1993). By inducing genes like BAX and BBC3, which belong to the BCL-2 family, p53 promotes caspase activation and apoptosis (Miyashita et al., 1994). While attempts to identify universal target genes have been made (Allen et al., 2014; Fischer, 2017), the expression of many genes remains context- and cell-type dependent.

Activation and Regulation

p53 activation prevents the accumulation of DNA damage and the propagation of oncogenic alterations to daughter cells. However, even after over forty years of research, there are still many unknowns concerning the cellular functions of p53. Adding to the complexity, p53 is activated in response to a variety of cellular stress signals including but not limited to; genotoxic damage, telomere erosion, hypoxia, nutritional starvation, mitochondrial stress, temperature changes, and oncogene activation (Lane and Levine, 2010). Because unrestricted activation of p53 can be detrimental to a cell, timely and precise regulation of p53 is critical. This regulation occurs mainly through post-translational modification (PTM) of the protein. Early studies identified p53 as a phosphoprotein (Jenkins et al., 1984b). After DNA damage or replication stress, p53 is phosphorylated by several different kinases (e.g., ATM and ATR), primarily in the N-terminal transactivation domains (Meek and Anderson, 2009). Phosphorylation at Ser15 activates p53 by blocking the binding, ubiquitination and degradation of p53 by its primary negative regulator and E3 ligase MDM2 (Shieh et al., 1997). Phosphorylation at Ser15 has also been shown to catalyze the binding of modifying enzymes and the addition of other PTMs, many of which contribute to the recruitment of transcriptional

machinery and further protein activation (Dumaz and Meek, 1999; Lambert et al., 1998; Saito et al., 2002, 2003; Sakaguchi et al., 1998, 2000).

Ubiquitination is another PTM that is critical for p53 function and negative regulation. In the absence of cellular stress, p53 protein has a short half-life (~30 minutes) and is maintained at low steady-state levels through MDM2-mediated ubiquitination and proteasomal degradation so that it exerts a minimal effect on cell fate. As mentioned above, MDM2 is a transcriptional target of p53, so stabilization of p53 results in an autoregulatory feedback loop. PTM and activation of p53 stimulate the production of MDM2, which in turn functions to ubiquitinate and induce proteasomal degradation of the p53 protein (Haupt et al., 1997; Momand et al., 1992) (Fig. 1). In addition to facilitating p53 degradation, MDM2 binding to the N-terminal transactivation domain of p53 inhibits its transcriptional activity (Haupt et al., 1997). The importance of this relationship is highlighted by the embryonic lethality in murine models with MDM2 deletion, which is rescued by simultaneous deletion of p53 (Jones et al., 1995; de Oca Luna et al., 1995). Because the p53/MDM2 feedback loop is critical, it is also highly regulated (Lu, 2010).

p53 can also be stabilized and activated through other mechanisms, such as the genetic deletion of MDM2 or other alterations like the activation of ARF that suppress MDM2 function (Zhang et al., 1998). In addition to MDM2, several other ubiquitin ligases have been shown to contribute to p53 degradation, including Pirh2, COP1, CHIP, ARF-BP1, E6-AP, TOPORS, TRIM24, and MKRN1 (Meek and Anderson, 2009). The main sites of p53 ubiquitination are six carboxy-terminal lysines (K370, K372, K373, K381,

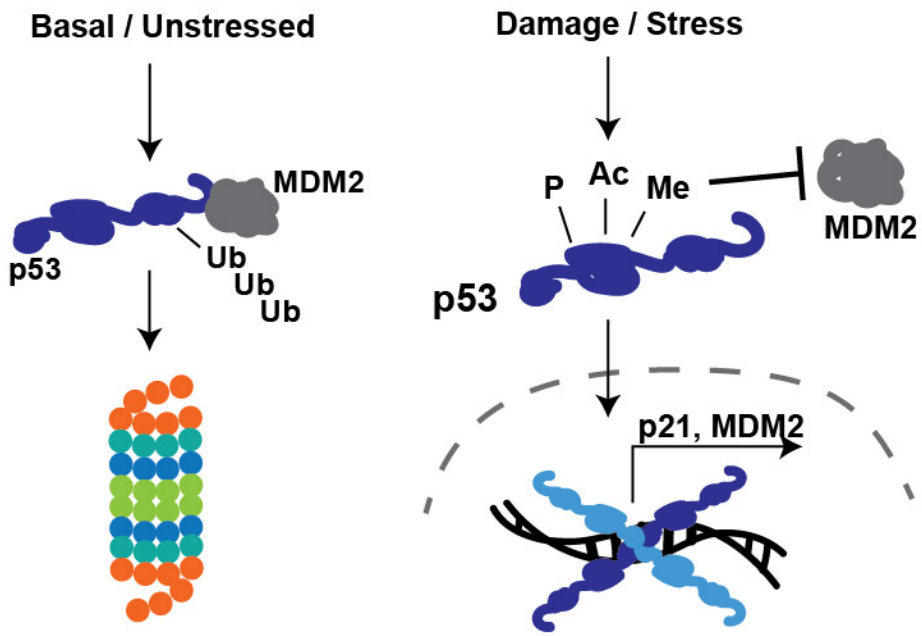

Figure 1. MDM2 autoregulatory feedback loop.
Schematic showing the regulation of p53 levels by MDM2. In unstressed conditions (left), p53 is ubiquitinated by MDM2 and degraded by the proteasome. Upon cellular stress (right), post-translational modification of the p53 protein inhibits the interaction and ubiquitination by MDM2, leading to stabilization of the protein. This stabilization results in increased transactivation of p53 target genes, including MDM2, which in turn functions to negatively regulate p53 activity.

K382, and K386) (Rodriguez et al., 2000). Acetylation of these lysine residues by the transcriptional coactivators CBP/P300 has been shown to inhibit MDM2 ubiquitination, also contributing to p53 stabilization (Gu and Roeder, 1997; Sakaguchi et al., 1998). However, much work remains to elucidate the complex and heterogeneous mechanisms contributing to p53 stabilization and regulation necessary for the protein's cellular function.

Other p53 PTMs such as acetylation, methylation, ubiquitination, neddylation, sumoylation, and others have been reported to contribute to the regulation and transcriptional activation of the protein. However, the complex nature of these modifications and their role in p53 function are still not completely understood. As these various PTMs are reversible, demodifying enzymes also play a critical role in regulating p53 activity. Phosphatases, deacetylases, and deubiquitinating enzymes like PPMID, HDAC1 and HAUSP, respectively, that negatively regulate p53 have been identified and are often overexpressed in human cancers (Bulavin et al., 2002; Ito et al., 2002; Li et al., 2002).

The p53 Family

Since the discovery of p53, two additional p53 family members, p63 and p73, have been identified. Evolutionary studies have identified an ancestral gene of all three p53 family members in the modern-day sea anemone that resembles a combined p63/p73 gene and functions to protect germ-line gametes from DNA damage (Belyi et al., 2010). The gene most closely related to *TP53* appeared in the early vertebrate lineage characterized by cartilaginous fish, evolving to protect the germ-line and

somatic stem cells from genomic instability (Belyi et al., 2010). Genes encoding all three p53 family members appear in bony fish. While p53 has generally sustained functions in maintaining genomic stability, p63 and p73 have diversified with the evolution of higher vertebrates (Belyi et al., 2010).

In 1997, p73 was identified and found to share 63% amino acid identity with p53 in the DNA-binding domain, as well as a shared ability to induce p21 expression and regulate cell cycle checkpoints (Kaghad et al., 1997). However, distinct from p53 knockout mice, p73 knockout mice do not have spontaneous tumor formation but instead display developmental defects (Yang et al., 2000) that have been explained by a loss of ciliated cell formation (Marshall et al., 2016; Nemajerova et al., 2016). For years, researchers have been attempting to find evidence that p73 also functions as a tumor suppressor, however, this remains controversial (Rosenbluth and Pietenpol, 2008).

One year after the discovery of p73, p63 was identified and reported to have 60% amino acid identity with the p53 DNA-binding domain and 85% identity with the p73 DNA-binding domain (Yang et al., 1998). p63 knockout mice have major developmental defects in epithelial tissues and die shortly after birth (Mills et al., 1999; Yang et al., 1999). Although the functions of the p53 family members have diverged, the members share a high degree of sequence homology and structural conservation in their DNA-binding domains. A shared ability to transcriptionally activate overlapping target genes is thought to serve as a fail-safe mechanism to initiate cell cycle arrest or apoptosis upon p53 inactivation (Flores et al., 2002; Jost et al., 1997; Kaghad et al., 1997).

TP53: The Most Frequently Altered Gene in Human Cancer

The Spectrum of *TP53* Mutations

The mutation of *TP53* is the most common gene alteration in human cancer. Genomic sequencing has revealed that p53 is mutated in approximately half of all human cancers (Campbell et al., 2020; Kandoth et al., 2013), although the frequency, distribution, and type of p53 mutations that occur vary considerably by cancer type (Kastenhuber and Lowe, 2017). Mutations in p53 appear at a much higher frequency in epithelial and advanced-stage cancers, such as the basal-like and HER2-enriched breast cancers (Fig. 2). The vast majority of mutations (~86%) occur in the DNA binding domain of the protein (exons 5 – 8) (Olivier et al., 2010). These mutations are typically single amino acid missense mutations. However, nonsense, frameshift, and splice-site mutations generating truncated proteins account for approximately 25% of cases (Shirole et al., 2016). Nearly 25% of missense mutations occur at “hotspot” residues, the most frequent at residues R175, R248, and R273. p53 missense mutations can be classified into those that directly disrupt DNA binding (contact mutants like the R248W and R273H mutations) or those that alter the structure of the DNA-binding domain (structural mutants like the R175H mutation).

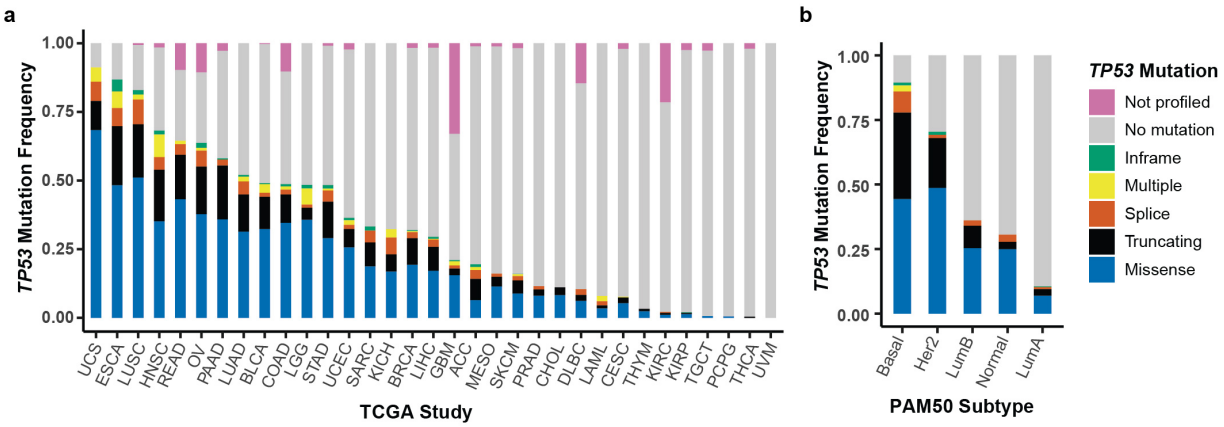

Figure 2. *TP53* mutation frequency in human cancer.
Stacked bar plots showing *TP53* mutation type and frequency across cancer types (a) or intrinsic breast cancer subtypes (b). Source: The Cancer Genome Atlas (TCGA). Cohort acronyms can be found in Table 3. Colors represent the different types of *TP53* mutations: missense mutations (blue), truncating mutations (black), splice-site mutations (orange), multiple mutations (yellow), in-frame mutations (green), no mutation (gray), or not profiled for *TP53* mutational status (pink).

Molecular Consequences of *TP53* Mutation

Loss of p53 Function

In general p53 mutations, both truncating and missense, lead to a loss-of-function (LOF) in DNA binding and regulation of gene expression (Cho et al., 1994; Kern et al., 1992). Somatic mutation of *TP53* tends to be an early event in most cancers (Gerstung et al., 2020), although this can vary by cancer type. For example, mutation of p53 has been found in premalignant cells of high-grade serous ovarian cancer (Kuhn et al., 2012), but is a late-occurring event in colorectal cancers (Fearon and Vogelstein, 1990). The field has yet to agree on which p53 function is the most important for tumor suppression, however, separation-of-function mutants have been utilized to address this question. For example, the use of p53 mutants that can transactivate only a subset of canonical target genes has been shown to retain tumor-suppressive abilities (Jiang et al., 2011). The human R175P p53 mutation has defects in apoptotic function but retains the ability to initiate cell cycle arrest (Rowan et al., 1996). In a separate study, genetically engineered mice containing the murine equivalent R172P display suppressed tumorigenesis and increased survival compared to p53 null controls (Liu et al., 2004). These data suggest that maintaining genomic stability through cell cycle arrest but not the ability to induce apoptosis is critical for p53 tumor suppressor function.

Development of Aneuploidy

When cell cycle control is lost, cells accumulate genomic and chromosomal alterations. Aneuploidy, or a state of non-euploid chromosome number, has been

shown to promote tumorigenesis (Chunduri and Storchová, 2019; Orr et al., 2015; Sheltzer and Amon, 2011; Vasudevan et al., 2021; Zhu et al., 2018). Aneuploidy can present as either gains or losses of entire chromosomes, termed whole-chromosome aneuploidy, or as more complex alterations that include deletions, amplifications, or translocations in large regions of chromosomes, termed structural aneuploidy (Chunduri and Storchová, 2019; Orr et al., 2015). Several mechanisms associated with cell cycle defects have been identified that contribute to aneuploidy and the resulting genomic alterations. For example, whole chromosome aneuploidies can be generated through whole-genome doubling (WGD) or defects in chromosomal segregation. In contrast, structural aneuploidies are often the consequence of unrepaired DNA damage leading to chromosomal breakage (Orr et al., 2015).

Aneuploidy is rarely found in normal cells and typically causes embryonic lethality, except for certain conditions like Down's syndrome, in which patients are born with a trisomy of chromosome 21 (Santaguida and Amon, 2015). Aneuploidy is a nearly ubiquitous feature of human cancers: it is estimated to occur in approximately 90% of solid human tumors and 50% of hematological malignancies (Beroukhim et al., 2010; Weaver and Cleveland, 2006). Aneuploidy is also a common feature of cells that contain mutated p53 (Bischoff et al., 1990; Boyle et al., 1998), and several studies have shown that mutations in *TP53* significantly correlate with aneuploidy in human tumors (Ciriello et al., 2013; Davoli et al., 2017; Taylor et al., 2018; Zack et al., 2013). Recent work has highlighted the importance of p53 LOF and the development of aneuploidy in tumorigenesis, as the clonal divergence from a diploid karyotype following p53 loss conferred fitness advantages to cells (Salehi et al., 2021).

Loss of Heterozygosity and Dominant-Negative Effects

Acquisition of aneuploidy can also contribute to the further inactivation of p53. During tumor progression, germline and somatic *TP53* mutations are almost always followed by loss of heterozygosity (LOH), a form of structural aneuploidy where segmental deletions in the chromosome 17 *TP53* locus occur to inactivate the remaining wild-type allele (Baker et al., 1989; Campbell et al., 2020; Donehower et al., 2019; Liu et al., 2016). In cases where LOH does not occur, p53 mutation can confer dominant-negative activity against the wild-type p53 protein: mutant p53 proteins can hetero-oligomerize with the wild-type protein, reducing DNA binding affinity for p53 response elements and attenuating p53 transcriptional activity (Milner and Medcalf, 1991; Milner et al., 1991). Mutant p53 proteins exert dominant-negative effects in cancer cell lines and mice (Boettcher et al., 2019; Giacomelli et al., 2018; Harvey et al., 1995). The accumulation of mutant p53 proteins in transformed cells has also been shown to enhance dominant-negative effects seen in mice (Lang et al., 2004).

There is likely some context specificity to dominant-negative p53 functions, as studies using murine models report differing results. Some reports have shown that mutant p53 proteins do not exert complete dominant-negative effects over the wild-type protein (Olive et al., 2004; Song et al., 2007). However, in Li-Fraumeni patients, dominant-negative p53 mutations in the DNA binding domain are associated with the highest risk of cancer development (Kratz et al., 2017).

Mutant p53 Gain-of-Function

Early studies of putative wild-type p53 revealed that mutated forms of p53 could facilitate the immortalization of cells when transfected alone and cooperate with established oncogenes to initiate cellular transformation (Eliyahu et al., 1984; Jenkins et al., 1984a; Parada et al., 1984). In addition to mutant p53 loss-of-function and dominant-negative activities, the concept of mutant p53 having gain-of-function (GOF) activities was introduced over 30 years ago when expression of mutant p53 proteins was shown to confer cells lacking endogenous protein with novel phenotypes (Dittmer et al., 1993; Halevy et al., 1990). Since then, numerous publications using *in vitro* cell model systems and mouse models of various p53 mutations have reported a dizzying array of mutant p53 GOF phenotypes (Muller and Vousden, 2014) (Fig 3).

While p53 LOF promotes genomic instability, mutant p53 proteins have also been reported to have GOF activities that result in increased genomic and chromosomal instability. For example, fibroblasts from Li-Fraumeni syndrome (LFS) patients containing the R175H mutation were shown to become polyploid while cells with truncated p53 did not, suggesting that mutant p53 disrupts the mitotic checkpoint (Gualberto et al., 1998). Mutant p53 has also been implicated in aberrant centrosome amplification resulting in aneuploidy (Murphy et al., 2000; Noll et al., 2012) and in facilitating structural aneuploidy through inhibitory interactions with DNA repair proteins like MRE11 (Song et al., 2007).

Studies *in vivo* with mice harboring germline knock-in alleles homologous to the human R175H (structural) or R273H (contact) mutants displayed altered tumor spectrums with increased incidence of carcinomas when compared to p53-null mice

(Olive et al., 2004). Separate murine models containing R248W and R273H mutations introduced into the humanized p53 knock-in allele also developed a more complex array of tumors (Song et al., 2007). Some murine models of p53 mutations have displayed increased metastasis (Lang et al., 2004) or metastatic features such as enhanced cellular migration and cellular survival (Adorno et al., 2009; Muller et al., 2009; Nakayama et al., 2020; Yeudall et al., 2012). Several reports have even ascribed chemotherapeutic resistance to mutant p53 GOF activity. For example, mutant p53 in breast cancer cells has been associated with resistance to anthracyclines such as doxorubicin (Aas et al., 1996; Blandino et al., 1999; Li et al., 1998).

Numerous publications have reported that cells containing mutant p53 proteins display altered cellular growth and metabolism. Cells containing mutant p53 have enhanced xenograft growth (Dittmer et al., 1993; Liu et al., 2011; Shaulsky et al.) and have also displayed increased proliferation (Lang et al., 2004) and colony formation (Kalo et al., 2012; Liu et al., 2011). Changes to cellular metabolism are often necessary to sustain proliferative demands of cancer cells and have also been associated with mutant p53 proteins (Eriksson et al., 2017; Freed-Pastor et al., 2012; Zhang et al., 2013). More recent studies have attributed enhanced proteasome activity, altered transcript splicing, and cancer cell immune evasion to mutant p53 GOF activities (Escobar-Hoyos et al., 2020; Ghosh et al., 2021; Walerych et al., 2016). Many other GOF phenotypes have been identified and ascribed to mutant p53 proteins, making the discovery of molecular mechanisms that contribute to these wide-ranging phenotypes challenging.

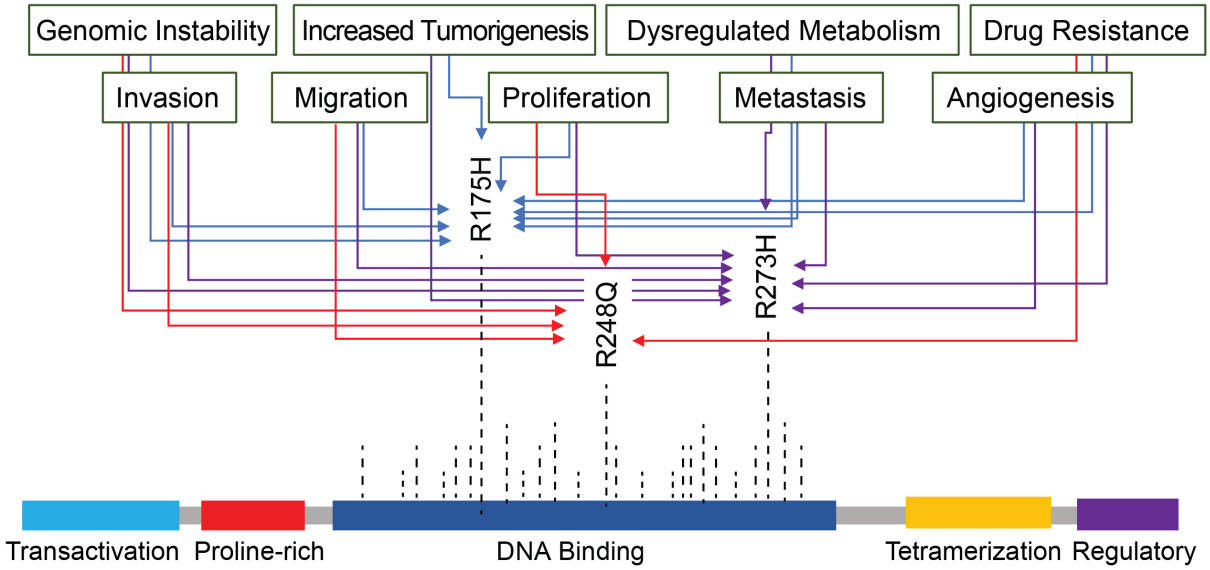

Figure 3. Mutant p53 gain-of-function phenotypes.
Schematic depicting the gene structure of *TP53* and the three most frequently occurring hotspot mutations. These p53 mutations have been widely studied and have been associated with a spectrum of gain-of-function phenotypes.

Transcriptional Mechanisms Described for Mutant p53 GOF

Consensus on the molecular basis for these mutant p53 GOF activities does not exist. However, several mechanisms have been proposed and are primarily related to mutant p53 modulation of transcription and altered binding partners. In addition, although the DNA binding and gene transactivating activities of most p53 hotspot mutant proteins are severely impaired (Kern et al., 1992), some mutant p53 proteins have been reported to bind mutant p53-specific response elements and activate gene expression in a mutant p53-dependent manner (Strano et al., 2007; Zhu et al., 2015).

The most commonly identified mechanism for altered gene expression by mutant p53 proteins embraces novel interactions between mutant p53 and other transcription factors, which results in either activation or repression of transcriptional activity. For example, studies have report novel interactions occurring between mutant p53 and the p53 family members p63 and p73 that inhibit their transcriptional activity (Di Agostino et al., 2006; Di Como et al., 1999; Lang et al., 2004; Muller and Vousden, 2013; Strano et al., 2000; Subramanian et al., 2015). Several studies have identified altered transcriptional targets of mutant p53 proteins (Strano et al., 2007; Turrell et al., 2017; Vogiatzi et al., 2016; Weisz et al., 2007; Zalcenstein et al., 2003; Zhu et al., 2015), and while several attempts have been made to develop a mutant p53 gene expression signature (Boettcher et al., 2019; Donehower et al., 2019; Freed-Pastor et al., 2012; O'Farrell et al., 2004; Scian et al., 2004a; Walerych et al., 2016), a validated list of mutant p53 target genes has not yet come to fruition.

Non-Transcriptional Mechanisms Described for Mutant p53 GOF

Mutant p53 has also been reported to bind and modulate the function of proteins not involved in transcriptional processes. For example, mutant p53 proteins have been shown to interact with and inhibit proteins that facilitate DNA repair, thereby inducing genomic instability (Liu et al., 2010; Song et al., 2007). Recent work has shown mutant p53 to promote cancer cell immune evasion by interacting with and inhibiting components of the cytoplasmic DNA sensing machinery and the innate immune response (Ghosh et al., 2021). Proteomic studies of mutant p53 interactomes through mass spectrometry analyses are scarce, however, one such study identified binding proteins for the R273H p53 mutant with known roles in cellular invasion (Coffill et al., 2012). Also, the accumulation of mutant p53 protein has been proposed to enhance and contribute to these altered cellular interactions and will be reviewed further below in Chapter IV. Altogether, these GOF mechanisms and phenotypes vary greatly according to the specific p53 mutation, the model system used for experimentation and the cell type analyzed.

The Controversy of Mutant p53 GOF

The question of whether mutant p53 GOF activities exist is a controversy within the field. Many of the phenotypes reported have been identified using overexpression model systems that lack regulation by the endogenous p53 promoter. Evidence supporting the mutant p53 GOF hypothesis includes the high frequency of missense mutations that occur and the accumulation of mutations at specific hotspot amino acids, suggesting that GOF activities confer a fitness advantage to select for these alterations.

However, many hotspot mutations, including R273 and R175, contain methylated CpG dinucleotides, rendering them more likely to mutate by spontaneous deamination (Rideout et al., 1990). The incidence of missense mutations in *TP53* is comparable to the frequency of missense mutations found in tumors (87% observed versus 72.9% expected). In contrast, nonsense mutations are overrepresented two-fold (8% versus 3.6%), suggesting that p53 LOF is a factor promoting this selection (Olivier et al., 2010; Petitjean et al., 2007). Recent findings have confirmed this, revealing that natural mutational processes combined with LOF and dominant-negative activities select for the spectrum of p53 mutations (Giacomelli et al., 2018). These findings were further corroborated by a study utilizing mutant p53 isogenic models of myeloid malignancies, which show no evidence of GOF, but instead LOF and dominant-negative activities over wild-type p53 protein (Boettcher et al., 2019).

Perhaps the best evidence for mutant p53 GOF is from two concurrent studies of mouse models harboring knock-in p53 mutations equivalent to the human R175H and R273H mutations. The mice expressing these mutant p53 proteins displayed altered tumor spectrums and increased metastasis compared to p53-null mice (Lang et al., 2004; Olive et al., 2004). While this work was persuasive, careful comparison of these models revealed conflicting evidence for GOF *in vivo*, with an increased incidence of carcinomas in R175H/- (Olive et al., 2004) but not R175H/R175H (Lang et al., 2004) mice. The latter inconsistency was attributed to differing murine genetic backgrounds. Further, some studies of mutant p53 murine models are plagued by a lack of discrimination between dominant-negative and GOF activities (Morton et al., 2010). The distinction of dominant-negative versus GOF activities is important to determine given

the evidence for dominant-negative but not GOF tumorigenic effects exerted by the mutant p53 in mice (Boettcher et al., 2019; Harvey et al., 1995).

Mutant p53 proteins constitute a complex family of hundreds of proteins with varying DNA binding and transactivation activity (Kato et al., 2003; Soussi and Lozano, 2005). In addition to the issues described above, the heterogeneity among p53 mutations complicates the current understanding of mutant p53 GOF activities (Soussi, 2007). Finally, GOF activities observed *in vitro* are not always recapitulated *in vivo*, and GOF phenotypes observed in mice are not substantiated clinically in LFS patients. Recent analyses with improved sequencing technology and increased power have shown LFS patients with p53 missense mutations have nearly the same lifetime penetrance as those with nonsense and frameshift mutations and only a slightly decreased age of tumor onset (Bougeard et al., 2015; Xu et al., 2015). Thus, mutant p53 GOF may not be an intrinsic property of mutant p53, which in fact, we demonstrate in Chapter III through the use of isogenic epithelial models of *TP53* mutation.

Stabilization of Mutant p53

Although wild-type p53 is maintained at low levels, mutant p53 proteins often accumulate in transformed cells and human tumors (Bártek et al., 1991; Rotter, 1983). This feature is so predominant that immunohistochemical staining of p53 was used as a proxy for the identification of p53 mutations and determination of prognosis in multiple cancer types (Alsner et al., 2008; Dowell et al., 1994; Hall and Lane, 1994; Silvestrini et al., 1996; Yemelyanova et al., 2011). Mutation and accumulation of p53 have also been correlated with circulating p53 antibodies in human cancer patients, and mice with SV40

transformed tumors (Crawford et al., 1982; Rotter et al., 1980; Soussi, 2000). Thus, the accumulation of p53 in transformed cells and tissues supported early arguments that p53 had oncogenic activities. It continues to be argued that increased stabilization and accumulation of the mutant protein is necessary for mutant p53 to exert its oncogenic GOF effects; however, there is very little evidence to support this claim fundamentally.

Mechanisms for mutant p53 accumulation are not well defined. Wild-type and mutant p53 proteins appear to be stabilized similarly in response to cellular stress such as DNA damage and ionizing radiation (Boettcher et al., 2019; Midgley and Lane, 1997; Suh et al., 2011; Terzian et al., 2008). However, mutant p53 proteins have lost some form of regulation, as they have an increased protein half-life compared to the wild-type protein (Giaccia and Kastan, 1998; Oren et al., 1981). One explanation for cellular accumulation is the inability of mutant p53 proteins to upregulate transcription of MDM2, leading to a lack of MDM2-mediated degradation (Momand et al., 1992; Vijayakumaran et al., 2015). However, mice lacking MDM2 expression do not display p53 accumulation in normal tissues (Terzian et al., 2008) and many cancer cell lines display high levels of mutant p53 while also having expression of MDM2 (Gudas et al., 1995; Li et al., 2011a). It has been suggested that p53 mutants alter the binding of MDM2 and thus degradation of the mutant p53 protein (Midgley and Lane, 1997) although others have shown mutant proteins are still bound by MDM2, ubiquitinated, and degraded (Lukashchuk and Vousden, 2007). Study of mutant p53 stabilization has primarily been focused on post-translational processes, however, recent work using RNA *in situ* hybridization approaches has indicated that active transcription of *TP53* mRNA does contribute to p53 stabilization (Xue et al., 2019).

The stabilization of mutant p53 can be mediated by other factors, such as defects in the retinoblastoma (RB) pathway and the presence of proteins that bind and inhibit MDM2 such as ARF (Terzian et al., 2008). In addition, MDM2-independent factors such as the downregulation of other E3 ligases which can ubiquitinate mutant p53, like CHIP or Pirh2, can contribute to mutant p53 stabilization (Lukashchuk and Vousden, 2007; Parrales et al., 2016). Additional E3 ligases such as COP1 (Dornan et al., 2004) and TRIM24 (Allton et al., 2009) can regulate wild-type p53 stability, although their ability to ubiquitinate mutant p53 is unclear. The role of p53 deubiquitinating enzymes like HAUSP/USP7 in stabilization of mutant p53 protein has not been determined.

Alterations commonly found in cancer cells like the increased expression of c-Myc, PTEN, and activated Ras, as well as increased levels of oxidative stress, have been implicated in the stabilization of mutant p53 (Fuchs et al., 1998; Li et al., 2008; Liu et al., 2017; Suh et al., 2011). The association of mutant p53 with histone deacetylases (HDACs) and chaperone proteins like HSP90 and HSP70 have also been shown to play an important role in protein accumulation (Li et al., 2011a). Finally, other cellular factors like cellular stiffness, localization of the mutant protein, and alterations to non-proteasomal degradation pathways may contribute to mutant p53 accumulation (Ingallina et al., 2018; Lukashchuk and Vousden, 2007; Morselli et al., 2008).

The accumulation of mutant p53 in human tumor cells is surprisingly heterogeneous. Mutant p53 protein is unstable in most normal tissues of mice with engineered *TP53* mutations (Lang et al., 2004; Olive et al., 2004; Terzian et al., 2008), and the same has been observed in normal cells of LFS patients (Soussi, 2007). Mutant p53 has been observed to accumulate in some normal tissues of mutant p53 knock-in

mice, such as crypts of the small intestine and hair follicles of the skin, however this accumulation was dependent on *TP53* gene dosage and confined to rapidly proliferating cells (Goh et al., 2015).

Across cell lines and tumors, mutant p53 stabilization is varied and is likely dependent on the other alterations present (Bouchalova et al., 2014; Xue et al., 2019). Furthermore, p53 stabilization is detected in some but not all tumors formed in mutant p53 murine models (Terzian et al., 2008). LOH has been correlated with mutant p53 protein stability and tumor onset in mice (Alexandrova et al., 2015) and may play an important role in mutant p53 stabilization. There is much to learn about the contexts in which mutant p53 protein becomes stabilized, especially as this represents a potentially targetable phenomenon in cancer cells. Attempts to destabilize mutant p53 for clinical utility will be described further below. Chapter IV will describe isogenic model systems of *TP53* mutations used to study mechanisms contributing to the heterogeneous accumulation of mutant p53 proteins.

Clinical Significance of p53 Alterations

Prognostic Relevance of *TP53* Alteration

The clinical significance and prognostic relevance of p53 status continue to be controversial due to disparate results among studies (Robles and Harris, 2010; Roth, 1999). It has been shown that p53 mutational status predicts poor outcomes in multiple cancer types (Petitjean et al., 2007). In breast cancer, missense mutations that affect DNA binding were shown to be associated with unfavorable survival outcomes than

truncating mutations or missense mutations in non-DNA binding motifs (Olivier et al., 2006). Other studies have contradictory results, finding *TP53* mutations associated with both negative and positive survival outcomes in patients (Langerød et al., 2007; Olivier et al., 2006; Ozcelik et al., 2007; Silwal-Pandit et al., 2014). Studies using more advanced sequencing technologies and larger cohort sizes have failed to identify statistically significant differences in patient survival based on the *TP53* genotype alone (Donehower et al., 2019). These disparate findings can be traced to the suboptimal methods used to classify mutation status, the existence of other alterations within the p53 pathway, and the lack of clarification on if *TP53* mutation is a prognostic factor independent of other clinical features such as stage, hormone receptor status for breast cancers, or prior treatment (Shahbandi et al., 2020; Ungerleider et al., 2018).

Many studies have identified correlations between p53 accumulation and prognosis across multiple cancer types (Alsner et al., 2008; Dowell et al., 1994; Hall and Lane, 1994; Quinlan et al., 1992; Silvestrini et al., 1996; Yemelyanova et al., 2011). However, the fact that p53 accumulation is heterogeneous and depends mainly on the type of mutation that occurs has severely limited the clinical relevance of p53 protein accumulation and immunohistochemical (IHC) analysis. For example, prognostic associations with *TP53* mutation and protein accumulation in breast cancer are subtype specific and highly dependent on the biological features of the tumor and clinical treatment regimens used (Bouchalova et al., 2014; Silwal-Pandit et al., 2014; Ungerleider et al., 2018). p53 accumulation is a strong predictor of recurrence in ER-positive breast cancers treated with aromatase inhibitors (Yamamoto et al., 2014), although mutation status was not confirmed in this study. The presence of p53 auto-

antibodies identified in the sera of cancer patients has also been investigated for clinical value. These antibodies are predominantly associated with p53 missense mutation and accumulation of the protein and have been associated with high-grade tumors and poor survival. Only 20-40% of patients with p53 mutations will display p53 antibodies in their sera, however this is limited by the sensitivity of ELISA assays typically used for detection (Soussi, 2000). The detection of p53 antibodies could have clinical utility for early detection or disease monitoring following treatment and will be an interesting area for further study.

The clinical significance of *TP53* mutations is still debated. Germline detection of *TP53* mutations is important for the identification and monitoring of LFS patients. However, detection of somatic *TP53* mutations is currently only recommended for treatment decision making in chronic lymphocytic leukemia, as chromosome 17p deletion or *TP53* mutation is predictive of resistance to chemoimmunotherapy and disease progression (Hallek, 2019; Stilgenbauer et al., 2014). p53 alterations may still prove to be clinically relevant in some cancer types. For example, in oncogene-driven cancer types with intermediate frequencies of *TP53* mutation, such as in HER2-enriched breast cancers and EGFR mutated lung adenocarcinomas, *TP53* mutation is an indicator of poor prognosis (Clinical Lung Cancer Genome Project (CLCGP) and Network Genomic Medicine (NGM), 2013; Hainaut and Pfeifer, 2016; Silwal-Pandit et al., 2014). *TP53* alteration encompasses a diverse array of cellular changes (e.g., mutation position, type, and effect on protein structure; allelic alterations and LOH; and alterations to the p53 pathway like MDM2 amplification). Improved assessment of these complex alterations and their functional impacts will be needed to accurately determine

clinical significance of *TP53* alterations. In Chapter 3, we describe the clinical utility of assessment of the type p53 mutation (truncating versus missense) on patient outcomes. Further, we will show that prognostic relevance is largely dependent on p53 LOF and other clinical factors, but not the specific type of p53 mutation in cancer types with high frequency of p53 mutation.

Targeting Mutant p53 in Human Cancers

In the cancer field, targeting mutant p53 is much like the quest for the holy grail. Because mutant p53 is altered in a majority of human cancers, the targeting of mutant p53 would be a substantial clinical advancement. There are three main strategies for targeting mutant p53; restoration of wild-type activity, degradation of the mutant protein, and inhibition of downstream pathways or protein-interacting partners (Bykov et al., 2017; Muller and Vousden, 2014). Other emerging mechanisms for targeting mutant p53 include identifying synthetically lethal targets and developing agents that elicit a targeted immune response to mutant p53 containing cells.

Restoration of Wild-Type p53 Activity

So far, attempts to restore wild-type p53 activity have been limited to the use of small molecules or synthetic peptides. Reactivating compounds like PRIMA-1 or APR-246 (a methylated PRIMA-1 analog) bind covalently to p53 core domain thiols or cysteine residues respectively, to stabilize the structure of specific p53 mutants (Lambert et al., 2009; Zhang et al., 2018). While some compounds have shown promise in inducing apoptosis and inhibiting cell proliferation, most have not advanced to clinical

trials (Bykov et al., 2002; Kim et al., 1999; Lehmann and Pietenpol, 2012). Only APR-246 has seen success, advancing through Phase I and II clinical trials with acceptable safety profiles and anti-tumor activity, primarily in ovarian and hematologic malignancies (Gourley et al., 2016; Lehmann et al., 2012; Sallman et al., 2021). However, many of these compounds show off-target effects, such as the induction of oxidative stress which may at least partially account for their anti-tumor activity (Bykov et al., 2017).

Other efforts have been made to target tumors containing wild-type p53, most notably through the use of MDM2 agonists. Peptide and non-peptide inhibitors such as the drug Nutlin have been designed to inhibit the interaction between p53 and MDM2. Pre-clinical testing has shown MDM2 inhibition with nutlin can stabilize p53, activate target gene expression, and preferentially inhibit the growth of cancer cell lines containing wild-type p53 (Vassilev et al., 2004). Derivatives of nutlin have been tested in phase I clinical trials and shown some therapeutic promise; however, further clinical testing has been limited because patients often develop severe adverse hematological toxicities such as neutropenia and thrombocytopenia (Andreeff et al., 2016; Wang et al., 2017).

Targeting Downstream Pathways and Synthetic Lethality

Attempts to exploit synthetic lethality or target downstream pathways regulated by mutant p53 are complicated by the lack of reproducibility and context specificity of reported GOF phenotypes. One example of this is the use of statins to destabilize mutant p53 protein and target the mevalonate pathway, which has been reported to be dysregulated by mutant p53 (Freed-Pastor et al., 2012; Parrales et al., 2016; Turrell et

al., 2017). Other studies have shown that using proteasome inhibitors or drugs that target alternative splicing has therapeutic potential in reducing tumor growth of mutant p53 containing cells (Escobar-Hoyos et al., 2020; Walerych et al., 2016). In an attempt to take advantage of the genomic instability often seen in mutant p53 containing cells, inhibitors targeting the proteins involved in cell cycle checkpoints and DNA damage response such as PARP, ATR and CHK1 are also being investigated (Polotskaia et al., 2015; Singh et al., 2017), however, these strategies have not moved forward to clinical testing.

Destabilizing Mutant p53

Attempts to degrade or destabilize mutant p53 have also seen progress even though mechanisms underlying protein accumulation are poorly understood. Studies have shown that knockdown of mutant p53 leads to cell death, suggesting that some cancers rely on and become “addicted” to mutant p53 (Braicu et al., 2013; Lim et al., 2009). In mouse models, the conditional ablation of the R248Q mutant p53 protein inhibits tumor growth and extends animal survival (Alexandrova et al., 2015; Schulz-Heddergott et al., 2018), although this dependence may be unique to the R248Q mutation. It is unclear if long-term depletion of mutant p53 would be an effective therapeutic strategy.

Use of HSP90 inhibitors (like 17-AAG or ganetespib) or the HDAC inhibitor SAHA used alone or in combination has been shown to destabilize mutant p53 protein and be preferentially cytotoxic to mutant p53 containing cell lines and mutant p53 xenografts (Alexandrova et al., 2015; Li et al., 2011b). However, not all cells appear to be

dependent on mutant p53 protein. For example, the growth of an extensive panel of cancer cell lines was not dependent on mutant p53 protein expression (Giacomelli et al., 2018), so it remains uncertain if destabilization of mutant p53 protein as an anti-cancer treatment approach will be successful.

Many tumors show variable mutant p53 stabilization, but in others like triple-negative breast cancers where *TP53* mutation occurs in nearly 80% of tumors (Shah et al., 2012; The Cancer Genome Atlas Network, 2012), accumulation of p53 demonstrated prognostic relevance and was less variable than in hormone receptor-positive breast cancers (Bouchalova et al., 2014). Thus, accumulated mutant p53 protein may represent an actionable therapeutic target in specific cancer types, however, further pre-clinical studies are needed to improve mechanistic understanding of mutant p53 stabilization. Elucidation of mechanisms contributing to p53 stabilization that are shared or unique to the mutant protein are especially important, as strategies designed to destabilize mutant p53 may also affect the wild-type protein, potentially leading to unintended consequences in normal tissues.

New and Emerging Therapeutic Opportunities

The newest approach to targeting mutant p53 protein in human cancers stems from recent advances in cancer immunotherapies. Several groups have attempted to utilize immune-based strategies to trigger immune responses against mutant p53 tumor-associated antigens. Immune targeting of p53 has been attempted by developing peptide-based cancer vaccines or adoptive transfer of mutant p53-specific cytotoxic T cells. Results from clinical trials have indicated that although p53-specific immune

responses were observed, reduced tumor-burden in metastatic colorectal cancer patients was not evident and clinical studies have not progressed past phase I/II clinical trials (Vermeij et al., 2011).

A recent study has shown that bi-specific antibodies can be generated to target T cell-based immune responses against cancer cells which present an R175H mutant p53 peptide on the cell surface (Hsiue et al., 2021). Although efficacy is limited to one specific p53 mutation (R175H) and HLA allele, this represents a new era of harnessing the immune system to identify cancer-promoting alterations such as p53 mutations. However, more work is needed to identify mechanisms through which cancer cells containing mutant p53 evade the immune system, especially those that accumulate high protein levels, and whether off-target toxicities of these immune-modulating agents will limit their clinical use.

Summary

The tumor suppressor protein p53 is critical for the maintenance of genomic stability and the prevention of tumorigenesis. Mutations in p53 most notably lead to loss of p53 transcription factor function, which is often followed by the heterogeneous acquisition of genomic and chromosomal alterations. Specific high-frequency missense mutant p53 proteins have been proposed to acquire novel oncogenic activities leading to diverse cellular phenotypes. Accumulation of the mutant protein, and *de novo* activities or altered protein-protein interactions have been proposed as mechanisms for these novel phenotypes. However, many studies of mutant p53 “gain-of-function” activity have been conducted using cellular models that rely on unregulated and

overexpressed mutant protein and have contributed to disparate and context-specific results.

Given the therapeutic interest in targeting mutant p53 proteins, the experiments presented in this dissertation evaluate mechanisms underlying (i) tumor cell phenotypes associated with mutant p53 (Chapter III) and (ii) mutant p53 protein accumulation in aneuploid tumor cells (Chapter IV). The collective results provide significant insight to the controversy of whether mutant p53 GOF activities exist and if mutant p53 protein represents a sound target for therapeutic development in the oncology field.

CHAPTER II

MATERIALS AND METHODS

Cultured Cells and *in vitro* Experiments

Cell Culture

The CAL-51, CAL-51 isogenic clonal cell lines, and 293FT cells were cultured in DMEM with 10% (v/v) FBS. The MCF10A cell line and isogenic clonal cell lines were cultured in DMEM:F12 with 5% horse serum, 100 ng/mL cholera toxin, 500 ng/mL hydrocortisone, 20 ng/mL human epidermal growth factor, and 10 µg/mL insulin. All cell lines were maintained in the described media with 1% penicillin and streptomycin in a 37°C incubator at 5% carbon dioxide. Cells were routinely tested to be negative for mycoplasma. DNA fingerprinting analysis was performed on CAL-51 and several isogenic clones in March 2016. MCF10A and CAL-51 parental isogenic clonal cell lines were also validated against known karyotypes.

CRISPR/Cas-Mediated Genome Editing

Genome editing using the CRISPR/Cas9 system was performed in close adherence to the Zhang lab's protocol (Ran et al., 2013). Guide RNAs (gRNAs) were designed in the Benchling web tool (https://www.benchling.com/); 20-nucleotide (nt) gRNAs were selected (3-5 per desired mutation site) with the highest target specificity score that cut within at least 15 nt of the desired mutant base for screening.

Complementary guide oligos were ordered with an initial 5' guanine (if not already present) and BbsI overhangs for cloning into pSpCas9(BB)-2A-GFP (PX458) (Addgene #48138). Guide oligos were resuspended at 100 μM, phosphorylated, and annealed through incubation with T4 PNK and ligation buffer. Cloning into PX458 was conducted by incubating the plasmid and diluted oligo duplexes with Tango buffer, DTT, ATP, FastDigest BbsI, and T7 ligase. The ligation products were subsequently treated with PlasmidSafe ATP-dependent DNase to digest residual linear DNA. Cloned plasmids were transformed into DH5α competent cells and selected on LB agar plates containing 100 μg/mL ampicillin. Plasmid DNA was isolated from the resulting colonies using a QIAprep Spin Miniprep Kit (Qiagen), and sequence verified by Sanger sequencing.

The following was performed to assess gRNA activity. Cloned plasmids were transfected into 293FT cells using Lipofectamine 3000; and, 72 h later, DNA was isolated from the transfected cells using QuickExtract DNA extraction solution (Epicentre) per manufacturer's recommendations. Genomic DNA was amplified with primers (R175H & Null: FWD CACTTGTGCCCTGACTTTCA, REV TTGCACATCTCATGGGGTTA; R273H: FWD CCTCTGCTTGCCTCTGACCCCT, REV TGCACCCTTGGTCTCCTCCACC) designed to generate an asymmetric ~500 bp PCR product around the gRNA cut site using Platinum Taq DNA Polymerase High Fidelity. PCR products were purified using a QIAQuick PCR Purification Kit (Qiagen) and annealed by a gradual reduction in temperature from 95°C, followed by SURVEYOR digestion using SURVEYOR nuclease S and enhancer S with supplemented magnesium chloride. SURVEYOR digestion products were run on a 5% polyacrylamide TBE gel and visualized using SYBR Gold. gRNAs producing a prominent asymmetric

digestion product were selected for further use (R175H & null (amino acid position 181): CACCGTATCTGAGCAGCGCTCATGG; null (amino acid position 196): CACCGTCCTCAGCATCTTATCCGAG; R273H: CACCGTGCGTGTTTGTGCCTGTCC). A negative control (no transfected plasmid) was included to rule out digestion products generated by endogenous single nucleotide polymorphism (SNP) mismatches.

Once a gRNA was selected for a specific mutant site, homology-directed repair (HDR) templates were designed using the Benchling web tool. HDR templates were designed to contain mutant bases corresponding to clinically observed hotspot mutations, along with a synonymous mutation in the protospacer adjacent motif (PAM) to prevent CRISPR/Cas9-mediated cleavage of the HDR-recombined alleles and ~75 bp of flanking homologous sequence on each side. For the following HDR templates, nucleotides surrounded by brackets indicate the clinically observed missense mutation, and lower-case nucleotides depict synonymous mutations designed to disrupt the PAM site or reduce guide RNA complementarity.

R175H:CACCCCCGCCCGGCACCCGCGTCCGCGCCATGGCCATCTACAAGC AGTCACAGCACATGACGGAGGTTGTGAGGC[A]CTGCCCaCACCATGAGCGCTGCT CAGATAGCGATGGTGAGCAGCTGGGGCTGGAGAGACGACAGGGCTGGTTGCC;

R273H:TCCTTACTGCCTCTTGCTTCTCTTTTCCTATCCTGAGTAGTGGTAATC TACTGGGACGGAACAGCTTTGAGGTGC[A]TGTTTGcGCtTGTCCTGGGAGAGACCG GCGCACAGAGGAAGAGAATCTCCGCAAGAAAGGGGAGCCTCACCACGA.

When the engineering of a synonymous PAM mutant was not possible due to codon position, two additional synonymous mutations were engineered into the gRNA

target region to reduce complementarity. HDR templates were ordered as Ultramer oligos (IDT).

CRISPR/Cas9-mediated editing of cells was conducted by incubating 2.5 μg of cloned PX458 plasmid, 5 μL of P3000 reagent, 7.5 μL of Lipofectamine 3000, and if attempting knock-in mutagenesis rather than frameshift knockout, an additional 5 μL of 10 μM single-stranded HDR template in 250 μL of Opti-MEM. The resulting DNA-lipid complexes were added to one well of a subconfluent 6-well plate, with the number of wells scaled as necessary. After 48 h, transfected cells were trypsinized, washed in PBS, resuspended in 4% (v/v) FBS in PBS, and stained with 0.5 μg/mL propidium iodide for live/dead discrimination. GFP-positive live cells were gated using lipofectamine-only negative control cells with and without propidium iodide along with transfected cells lacking propidium iodide. Fluorescence-activated cell sorting was performed by the Vanderbilt Flow Cytometry Shared Resource. GFP+/PI- cells were sorted into 96-well plates containing complete culture medium for isolation of single-cell clones.

Clonal populations were expanded 21-28 d after sorting, and DNA was isolated using QuickExtract DNA extraction solution (Epicentre) to determine the *TP53* genotype. Genomic DNA was amplified with primers designed to generate an asymmetric 500 bp PCR product around the gRNA cut site using Platinum Taq DNA Polymerase High Fidelity. PCR products were purified using a QIAQuick PCR Purification Kit (Qiagen) and screened using restriction enzyme cut sites present only in HDR recombined sequences (BtsI for R175H, NlaIII for R273H). Cells that passed the restriction digest check were further verified by Sanger sequencing. When mixed

sequencing traces were present due to heterozygous frameshift alleles, allele cloning was conducted by amplifying genomic DNA using primers described above with EcoRI or BamHI restriction site overhangs, followed by digestion and cloning into the pUC19 vector (New England BioLabs) for transformation. Once bacterial colonies were selected and expanded, DNA isolation was performed using a QIAprep Spin Miniprep Kit (Qiagen), and individual clones were Sanger sequenced to identify single trace alleles. All clonal cell line genotypes were further validated through the analysis of variants from whole-exome sequencing and RNA sequencing (see details below).

shRNA-Mediated Gene Knockdown

TP53 (Mission TRCN0000003753 or TRCN0000342259) or non-targeting negative control (MISSION pLKO.1-puro Non-Mammalian shRNA Control, SCH002; Mission pLKO.5-puro TRC2 Non-Mammalian, SHC202) shRNAs were purchased from Sigma Aldrich. Lentivirus was produced by co-transfection of shRNA-expressing viral vectors (10 μg) with packaging plasmids PMD2.G (2.5 μg, Addgene, 12259) and pxPAX2 (7.5 μg; Addgene, 12260) into 293FT cells. Viral supernatant was harvested 48 h after transfection and passed through a 0.45 μm syringe filter to clear cellular debris. Viral aliquots were stored at -80°C prior to infection and limited to one freeze-thaw cycle before use. Target cells were infected with a 1:10 dilution of the virus in the presence of 10 μg/mL polybrene for 24 h. After fresh media were added, cells were grown for 48 h until antibiotic selection with puromycin (CAL-51, 0.625μg/mL; MCF10A, 1 μg/mL). Knockdown was verified through immunoblotting and RNA-sequencing.

Immunoblotting

All cells were lysed in RIPA buffer (pH 7.4) buffer (150mM NaCl, 50mM Tris-HCl [pH 7.5], 0.1% SDS, 1.0% NP-40, 0.5% Deoxycholic Acid, 5mM EDTA) supplemented with 1 mM DTT, phosphatase inhibitors (50 mM NaF, 0.2 mM Na_3VO_4) and protease inhibitors (10 mg/mL CLAP, 200 mg/mL AEBSF). Protein concentration was determined (Modified Lowry Protein Assay Kit, ThermoFisher), and equal amounts of protein separated by SDS polyacrylamide gel electrophoresis (SDS-PAGE) and transferred to PVDF membrane. Western blots were incubated with primary antibodies (Table 1) overnight at 4°C. Membranes were washed and incubated in HRP-conjugated secondary antibodies (goat anti-Mouse or goat anti-Rabbit, Thermo Fischer Scientific, 31432 and 31462) for one h at room temperature. Membranes were again washed and developed using ECL kits and digitally imaged (Amersham Imager 600, GE Healthcare Life Sciences). Western blots were quantified relative to loading controls with Fiji (Schindelin et al., 2012).

Immunoprecipitation

Whole-cell protein extracts were prepared by scraping and lysing cells in EBC buffer (50 mM Tris-HCL [pH 7.5], 100 mM NaCl, 0.5% NP-40, supplemented with 1 mM DTT, phosphatase inhibitors [50 mM NaF, 0.2 mM Na_3VO_4] and protease inhibitors [10 mg/mL CLAP, 200 mg/mL AEBSF]). Cell lysates were cleared of cellular debris by centrifugation at 14,000 rpm for 10 min on a table top microcentrifuge at 4°C, and protein concentration was determined as described above. Co-immunoprecipitation was performed by overnight incubation of 1 mg whole-cell lysate with 1 µg/sample of anti-

Epitope	Company	Catalog #	Species	IB	IF	IHC
p53 (DO-1)	Santa Cruz	sc-126	mouse	1:1000	1:2500*	
p53 (DO-7)	Santa Cruz	sc-47698	mouse			1:2500
p73 (EP436Y)	Abcam	ab40658	rabbit		1:1500*	
GAPDH	Merck Millipore	MAB374	mouse	1:1000		
actin	Santa Cruz	sc-47778	mouse	1:1000		
vinculin	Invitrogen	700062	mouse	1:1000		
p21 (F-5)	Santa Cruz	sc-6246	mouse	1:200		
MDM2 (SMP14)	Santa Cruz	sc-965	mouse	1:200		
α-tubulin (B-7)	Santa Cruz	sc-5286	mouse		1:200	
PARP	Cell Signaling	9542	rabbit	1:1000		
anti-HA	Sigma-Aldrich	H6908	rabbit	1:1000		

Table 1. Antibodies used in this dissertation.
This table lists the epitope, company, catalog number (#), and species of each antibody, as well as the antibody dilution used for the following applications: immunoblotting (IB), immunofluorescence (IF), and immunohistochemistry (IHC). IF dilutions with an asterisk indicate the dilution used for tyramide signal-amplification immunofluorescence (TSA-IF).

p53 (Santa Cruz, DO-1), anti-p73 (Abcam, EP436Y) or the appropriate mouse or rabbit control IgGs pre-bound to 25 µL Dynabeads Protein G magnetic beads (Invitrogen, 10003D). The immunoprecipitates were washed four times with 1 mL of EBC buffer using a magnetic stand. Samples were eluted using 30µL 1X Laemmli sample buffer diluted in EBC lysis buffer, followed by a five-minute incubation at 95°C. Immunoprecipitates, as well as 5% of the whole-cell lysate input were resolved by SDS-PAGE and western blotting was conducted as described above. For detection, PVDF membranes were incubated with primary antibodies against p53 DO-1 (1:1000, Santa Cruz, sc-126), p73 EP436Y (1:1000, Abcam ab40658), and GAPDH (1:1000, Merck Millipore, MAB374), and visualized following 1 h room temperature incubation with TrueBlot HRP-conjugated secondary antibodies (Rockland, 18-8817-30 and 18-8816-31).

Immunofluorescence

Cells were seeded in 96 well plates at 10,000 cells per well. After 24 h, cells were fixed with 100% methanol for 10 min at room temperature and subsequently washed with PBS. Cells were permeabilized with 0.1% tween-20 in PBS for 10 min and blocked with 5% Goat Serum/0.3% Triton X in PBS for 60 min at room temperature. Following a 10 minute peroxidase inactivation with 3% hydrogen peroxide, cells were blocked with Image-it FX Signal Enhancer for 30 min and then incubated with primary antibody overnight at 4°C (p53 DO-1, 1:2500) diluted in PBS with 5% goat serum. HRP-conjugated secondary antibody (ThermoFisher Scientific, 31462) was applied for 1 h at room temperature and cells were incubated with Tyramide Signal Amplification (TSA)

reagent (PerkinElmer, NEL741B001KT (fluorescein) or NEL744B001KT (cyanine 3) plus 0.0015% H_2O_2) according to manufacturer's recommendations. Additional rounds of blocking steps were performed prior to incubation with a second primary antibody (p73 EP436Y or α-tubulin B-7 as described in Table 1), HRP- or fluorophore-conjugated secondary antibody, and TSA reagent for dual-immunofluorescence staining. Lastly, cells were incubated in Hoechst 33342 (5 µg/µL) for at least 30 min before imaging using the ImageXpress instrument in the Vanderbilt High-Throughput Screening core and quantified using the MetaXpress Multi-Wavelength Cell Scoring Module (Molecular Devices).

Subcellular Localization Assay

Subcellular fractionation was conducted using a Subcellular Protein Fractionation Kit for Cultured Cells (Thermo Fisher Scientific, 78840) according to the manufacturer's protocol. Protein lysates were resolved by SDS-PAGE and immunoblotting as described in the "immunoblotting" section above. For detection of specific proteins, western blots were incubated with primary antibodies for p53 (DO-1), as well as GAPDH and PARP (described in Table 1) as cytoplasmic and nuclear controls, respectively.

Ubiquitination Assay

CAL-51 cells were seeded in 100 mm dishes to be 60-80% confluent the following day. Prior to transfection, medium was replaced with antibiotic-free medium. Cells were transfected with 6 µg of HA-tagged Ubiquitin (HA-Ubiquitin was a gift from Edward Yeh; Addgene #18712) or empty vector control (pcDNA3) using Lipofectamine

3000 diluted in Opti-mem (Invitrogen) at a 1:2 DNA/lipid ratio. Cells were transfected overnight after which cell media was refreshed. Forty-eight h after transfection, cells were treated with MG132 (10 μM, 5h), harvested by scraping and lysing in EBC buffer. Cell lysate (1mg) was immunoprecipitated using p53 DO-1 antibody as described in the "immunoprecipitation" section above. Immunoblotting was conducted as described above in the "immunoblotting" section and proteins were visualized using anti-HA (Sigma-Aldrich, H6908), p53 DO-1 (Santa Cruz, sc-126) and GAPDH (Merck Millipore, MAB374) antibodies.

DNA Content Analysis Using Flow Cytometry

One million cells were prepared for cell cycle analysis by trypsinization and washing with PBS, followed by fixation in 70% ethanol. Cells were stained in a solution consisting of 0.1% (v/v) Triton X-100 and 20 μg/mL propidium iodide. Samples were analyzed at the Vanderbilt Flow Cytometry Shared Resource on a 3-laser LSRSII. Single cells were selected by pulse processing and visualized using FlowJo (10.0.7).

DNA Content Analysis Using Metaphase Spreads

Sub-confluent cells (~75%) in a 10-cm culture dish were treated for 1 h with 0.5 μg/mL KaryoMAX colcemid pre-warmed at 37°C. Media were removed and reserved, and cells were trypsinized and resuspended in the reserved media. After centrifugation (300g, 5 min, 4°C), cells were gently resuspended with 0.2 mL media and combined with 5 mL of 0.075M potassium chloride dropwise while vortexing gently. Cells were incubated at 37°C for 25 min, with gentle inversion every 5 min to keep cells in solution.

Cells were then pre-fixed with 0.5 mL pre-chilled methanol:glacial acetic acid (3:1) fixative solution dropwise while vortexing gently. Cells were centrifuged (300g, 5 min, 4°C) and gently resuspended with 5 mL fixative solution. After storage at 4°C, cells were dropped onto pre-chilled Superfrost Plus microscope slides and air-dried at a slant for a minimum of 1 h in the dark. Cells were then mounted with ProLong Gold Antifade Reagent with DAPI and coverslipped. Metaphase spreads were imaged (> 15 individual cells per cell line) using fluorescence microscopy with an oil-immersion 100x objective, and individual chromosomes counted manually using Fiji.

Drug Sensitivity Assays

For adherent viability assays, cells were seeded at 1500 cells per well in quadruplicate in 96-well plates and treated with a six-point, three-fold dose-escalation alongside untreated controls for 72 h. AlamarBlue (ThermoFisher Scientific) was used according to manufacturer recommendations, and fluorescence measured and analyzed with microplate data collection and analysis software Gen5 (Biotek). Viability and IC_{50} were analyzed in Prism (Graphpad, 8.4.3) by performing a non-linear fit to log-transformed normalized fluorescence values.

Doubling Time Analysis

For doubling time experiments, cells were seeded at 1,500 cells per well in quadruplicate into five 96 well plates. Every 24 h over five days, plates were fixed with 100% methanol for 10 min and stored in PBS at 4˚C until imaging. Hoechst 33342 was added to cells (5 µg/µL), and nuclei were counted using the ImageXpress instrument in

the Vanderbilt High Throughput Screening core. Nuclei were counted using MetaXpress Multi-Wavelength Cell Scoring Module V6.6.3.733 (Molecular Devices), and doubling time was calculated using the following formula:

$$Doubling\ Time = \frac{duration * \log(2)}{\log(Final\ Concentration) - \log(Initial\ Concentration)}$$

Colony Formation Assay

Cell lines were seeded onto twelve-well plates (Corning) (MCF10A, 500; CAL-51, 1,000 cells per well) and incubated for seven days. Colonies were fixed with 100% methanol for 10 min and stained with a 1:1 mixture of methanol and crystal violet aqueous solution (Electron Microscopy Sciences) at room temperature for 1 h. Cells were washed three times with dH_2O before places inverted to dry. Images were taken using the Odyssey infrared imaging system (Li-COR) and colonies counted using CellProfiler(Carpenter et al., 2006).

Metabolic Staining

To measure mitochondrial membrane potential and mass, cells were stained with TMRE and MitoTracker Green (each at 0.2 μM), respectively. Cellular ROS was measured with DCFDA reagent (2.9 μg/mL). Mitochondrial ROS was measured with MitoSOX Red Reagent (3.85 μg/mL). After incubating for 30 min at 37°C, DCFDA and MitoTracker Green staining were visualized by flow cytometry with the MACSQuant Analyzer 10 FITC channel, while TMRE and MitoSOX staining was visualized with the PE channel (Miltenyi Biotec). Data were analyzed using FlowJo version 10.5.3. For resazurin staining, cells were seeded at 5,000 cells per well in quadruplicate in 96-well

plates. After 48 h, AlamarBlue was applied at a 1X concentration, and cells were incubated for 6 h. Fluorescence was analyzed with microplate data collection and analysis software Gen5 (Biotek). Cells were then fixed and counted as described for doubling time assay.

Transwell Migration Assay

MCF10A (1.5×10^5) or CAL-51 (2×10^5) cells were plated in triplicate onto transwells with 8-μm pore polycarbonate membrane inserts (Corning) with serum-free medium. Complete medium was used as a chemoattractant in the lower chamber. After 18 h, cells were fixed with 100% methanol for 10 min and stained with a 1:1 mix of crystal violet in 100% methanol. Non-migrated cells on the upper side of the insert were removed with a cotton swab. In parallel, cells were separately plated onto 24 well plates without transwell inserts to determine the total number of attached cells by fixing, imaging, and counting Hoechst 33342 stained nuclei as described for resazurin metabolic assay. The relative migration was calculated as the number of migrated cells normalized to the total number of cells. For each experiment, the number of cells from each image (CAL-51, crystal violet stained 4X magnification; MCF10A, Hoechst stained, 20X magnification) was counted using CellProfiler (Carpenter et al., 2006).

Murine Model and *in vivo* Experiments

Xenograft Tumor Studies

Mice were housed and treated in accordance with NIH guidelines and protocols approved by the Institutional Animal Care and Use Committee at the Vanderbilt University Medical Center. Mice were maintained on a 12 h light-dark cycle at 20-26°C and 30-70% humidity, and housed in ventilated cages with constant access to food and water. For cell line xenograft studies, female 6-8 week-old athymic nude mice (The Jackson Laboratory, #002019) were anesthetized using isoflurane and injected subcutaneously in the left and right flank with 5×10^6 MCF10A or 2.5×10^6 CAL-51 cells suspended in 200μL PBS. Mice were monitored weekly and palpable tumors measured with digital calipers every three days until the experimental endpoint, at which time mice were euthanized by isoflurane overdose and cervical dislocation. Tumor volumes were calculated as $\text{width}^2 \times \text{length}/2$. Replicate mice injected with the same cell line were removed from the study when a single mouse had a tumor volume exceeding 1500 mm^3. Tumors used for subsequent molecular analysis were fixed overnight in 10% neutral buffered formalin (NBF), followed by 70% ethanol until further processing or flash-frozen in liquid nitrogen and stored at -80°C. All analyses were performed blinded to *TP53* genotype or aneuploidy status.

Immunohistochemistry

Xenograft tumors were formalin-fixed and paraffin-embedded (FFPE) at the Vanderbilt University Medical Center Tissue Pathology Shared Resource (VUMC

TPSR). Three 1 mm cores were punched from each FFPE block in regions selected by a pathologist to construct a tissue microarray (TMA). Five-micron sections were deparaffinized with xylene and rehydrated with graded alcohol incubations. Pressurized antigen retrieval was performed at 125°C for 4 min (Dako, S2367), followed by a 20 minute depressurization and cooling period prior to peroxidase inactivation by incubation with 3% hydrogen peroxide for 15 min. Sections were permeabilized with 0.1% Tween-20 in PBS for 20 min, blocked with 5% Goat Serum, 0.3% Triton X 100 in PBS for 1 h, followed by M.O.M. (Mouse on Mouse) blocking (Vector Laboratories, MKB-2213-1) for 1 h and incubation with antibody (p53 DO-7, 1:2500) overnight at 4°C in 5% Goat Serum with PBS. HRP-conjugated secondary antibody (SignalStain Boost HRP Mouse, Cell Signaling, Catalog #8125) was incubated with tissue for 30 min, followed by DAB reagent (Dako, K3468) for 90 seconds. Hematoxylin was used as a counterstain and all washes were conducted with PBS or PBS with 0.25% Goat Serum, 0.015% Triton X-100.

Genomics: DNA/RNA Sequencing and Microarray Analysis

RNA Sequencing and Gene Set Enrichment Analysis

Cell lines were harvested by scraping, and pellets were frozen at -80°C. RNA was extracted using ZYMO Quick-RNA MiniPrep Kits (Zymo Research) or with Aurum Total RNA Mini kit for p53 knockdown RNA-seq experiments according to the manufacturer's instructions. RNA concentration and purity were measured on a NanoDrop spectrophotometer, and 2 μg RNA (A260/280 > 2) were sent for sequencing

(VANTAGE core at Vanderbilt University Medical Center or Novogene Co. Ltd., Beijing, China). Sequencing libraries were generated using Illumina TruSeq or NEBnext Ultra RNA Library Prep Kits following the manufacturer's recommendations. Sample quality control to test for RNA integrity and contamination was performed using Agarose Gel electrophoresis and the Agilent 2100 Bioanalyzer System. Library preparations were sequenced by the Novaseq 6000 platform, generating unstranded 150bp paired-end reads, and resulting in ~19-30 million reads per sample. Raw RNA-seq reads (FASTQ files) were trimmed to remove adapter sequences using Flexbar v3.4.0(Dodt et al., 2012), and quality was evaluated using FastQC v0.11.7(Andrews, 2010) and MultiQC v1.5(Ewels et al., 2016). Reads were quantified against GENCODE v28 transcripts using Salmon v0.12.0(Patro et al., 2017) correcting for sequence-specific bias and fragment-level GC bias. Transcript abundances were imported into R v3.6.1 and summarized to the gene level using tximport 1.12.3 (Soneson et al., 2016). DESeq2 v1.24.0(Love et al., 2014) was used for differential gene expression and PCA analysis with independent hypothesis weighting IHW_1.12.0 (Ignatiadis et al., 2016). Shrunken log-fold changes were generated using ashr_2.2-47 (Stephens, 2016). Genes were classified as differentially expressed if they had a false discovery rate (FDR) adjusted p-value less than 0.1 and a Log2 fold change of ≥ 1 or ≤ -1. Gene set enrichment analysis (GSEA v4.0.3) (Subramanian et al., 2005) was conducted with the MSigDB 7.0 gene sets using GSEA Preranked in the default parameters. Genes were ranked according to the Wald statistic output from DESeq2.

Cytogenomic Microarray and Copy Number Analysis

Whole-genome cytogenomic microarray and copy number analysis were performed at the VUMC Cytogenetics Laboratory using the CytoScan HD SNP microarray platform (Thermo Fisher). Briefly, 250 ng of whole genomic DNA isolated from cultured cell lines was digested with NspI, ligated with NspI adapter primers, and amplified using Platinum Taq with a GeneAmp PCR System 9700. PCR products were purified, fragmented, labeled with biotin, and hybridized to the microarray chip. Chips were washed, stained, and scanned on an Affymetrix scanner. Raw CEL files were analyzed using the Rawcopy R package (http://rawcopy.org)(Mayrhofer et al., 2016). Segmented log ratios and frequency plots were generated using the copynumber R package (v_1.24.0)(Nilsen et al., 2012). Differential chromosome regions were analyzed with CNApp (Franch-Expósito et al., 2020). Aneuploidy scores were generated relative to the WT parental clone and calculated as the sum of the absolute value of the segmented log ratios for each profiled cell line. Cell lines were classified by AS quantile as aneuploid-high (upper quantile, MCF10A AS > 198.5, lines M1-33, M1-19, M1-12 and M2-9; CAL-51 AS $\geq$ 128.3, lines CN-81, C2-56, C2-22, C2-42, C2-09 and C1-06) or aneuploid-low (lower quantile, MCF10A AS < 114.1, lines MW-04, MW-27, MN-37 and M2-13; CAL-51 AS $\leq$ 43.7, lines CW-08, CW-23, CW-64, C1-18, C1-10 and C2-38).

Whole Exome Sequencing

Cell lines were harvested by scraping and pellets frozen at -80˚C. Genomic DNA was extracted using Qiagen DNeasy Blood and Tissue kit, according to the manufacturer's instructions. DNA concentration and purity were measured on a

NanoDrop spectrophotometer, and 500ng were submitted for sequencing at the Vanderbilt Technologies for Advanced Genomics (VANTAGE). Library preparation and capture were performed using the Twist Exome library prep and capture kit (Twist Bioscience). Sequencing was performed at 150 bp Paired-end on Illumina NovaSeq 6000, targeting an average of 20M reads per sample for 50x coverage. Data analysis was performed using an NGSPERL based custom pipeline (Sheng et al., 2015). Demultiplexed raw sequencing files were trimmed with Cutadapt (2.10) (Martin, 2011) and read quality was evaluated using FastQC before and after adapter trimming. All trimmed reads were aligned using BWA (0.7.17-r1188) (Li and Durbin, 2010) to the human genome (v38). The mapped result was refined by local realignment and base quality recalibration using GATK3, and all reads containing soft clip were discarded. Single nucleotide variants were called using GATK4 (McKenna et al., 2010) with Variant Quality Score Recalibration (VQSR) mode. The SNVs with inbreeding coefficient less than -0.2, a depth less than 10 in any sample, or genotype quality less than 20 in any sample were discarded. SNVs with a minor allele frequency of less than 0.3 in more than 90% of the samples were also discarded. Valid SNVs were annotated by ANNOVAR (20180416) (Wang et al., 2010). All SNVs with minor allele frequencies larger than 0.001 in any of ExAC, 1000G, gnoMad, or TOPMed databases were treated as high-frequency SNVs in population and removed. Copy number variations were also called based on GATK4 germline best practice (McKenna et al., 2010). Mutation analysis was conducted using the R maftools package (Mayakonda et al., 2018).

Analyses of Publicly Available Datasets

Cancer Cell Line Aneuploidy Analysis

Cancer cell line encyclopedia (Barretina et al., 2012) (CCLE) and *TP53* alteration data were acquired from Memorial Sloan Kettering Cancer Center cBioPortal (http://www.cbioportal.org) (Cerami et al., 2012; Gao et al., 2013). MCF10A SNP6 copy number data were acquired from https://www.synapse.org/#!Synapse:syn2346643/wiki/62255 (Daemen et al., 2013). The FGA by aneuploidy was calculated as the length of Log_2 ratio segments > |0.2|, divided by the length of all segments measured. MCF10A and CAL-51 copy number heatmaps were visualized using the Integrative Genomics Viewer (IGV 2.3.97) (Robinson et al., 2011).

Analysis of Cancer Cell Line Metastasis

Metastasis map (MetMap) (Jin et al., 2020) data was acquired from https://depmap.org/metmap/data/index.html. CCLE annotation and *TP53* mutation data (21Q1) were downloaded from the depmap portal (https://depmap.org/portal/download/). WT *TP53* samples were defined as cell lines that had silent mutations or no mutation in *TP53*. Missense cell lines were defined as those that contained a single *TP53* missense mutation. Cell lines with truncating mutations were defined as those containing nonsense, frameshift, or splice-site mutations in *TP53*.

TCGA Aneuploidy and Clinical Analysis

TCGA MC3 mutation data (mc3.v0.2.8.CONTROLLED.maf.gz) (Ellrott et al., 2018) was used to determine the *TP53* genotype and was downloaded from the NCI Genomic Data Commons. WT *TP53* samples were defined as individuals that had DNA sequencing data but no mutation calls, silent or non-coding mutations. Samples with multiple alterations or in-frame mutations in *TP53* were removed from the analysis. Missense tumors were defined as those that contained a single *TP53* missense mutation. Tumors with truncating mutations were defined as those containing nonsense, frameshift, stop-gain, or splice-site mutations. The FGA by aneuploidy for TCGA samples was acquired from cBioPortal (http://www.cbioportal.org). Progression-free survival data were obtained from the TCGA Pan-Cancer Clinical Data Resource(Liu et al., 2018). TCGA cohorts with low frequency (<10%) or fewer than 20 individuals with *TP53* missense mutations were excluded. Survival curves were constructed with the R survival package (Therneau, 2020) using the Kaplan-Meier method, and the difference between groups was assessed by the Log-rank test. Individuals with multiple tumors were excluded from the analysis. Survival was compared by *TP53* genotype or between individuals with aneuploid-low (lower quantile FGA) and aneuploid-high (upper quantile FGA) tumors with either WT, missense, or truncating *TP53* mutations.

CHAPTER III

ACQUISITION OF ANEUPLOIDY DRIVES MUTANT P53 GOF PHENOTYPES

Introduction

Mutation of *TP53* is one of the most frequent genomic alterations in human tumors. Mutations in p53 lead to a loss of p53 function (LOF), and certain high-frequency "hotspot" mutations have also been proposed to confer oncogenic gain-of-function (GOF) properties (Dittmer et al., 1993; Muller and Vousden, 2014). Many p53 GOF phenotypes have been described using *in vitro* cell model systems and mouse models, including increased proliferation (Lang et al., 2004); colony formation (Kalo et al., 2012; Liu et al., 2011); genomic instability (Agapova et al., 1996; Gualberto et al., 1998; Noll et al., 2012); metastasis (Lang et al., 2004); xenograft growth (Dittmer et al., 1993; Liu et al., 2011); metabolic dysregulation (Eriksson et al., 2017; Freed-Pastor et al., 2012; Zhang et al., 2013); enhanced migration (Adorno et al., 2009; Muller et al., 2009; Sun et al., 2020; Yeudall et al., 2012); and development of distinct tumor spectra (Olive et al., 2004).

Understanding mutant p53 GOF activities is complicated by the diversity and context-specific nature of reported GOF phenotypes. The study of mutant p53 GOF activities is made even more challenging because mutations in p53 are positively correlated with the development of aneuploidy (Ciriello et al., 2013; Davoli et al., 2017; Taylor et al., 2018), which can increase heterogeneity through diverse chromosomal alterations and contribute to tumorigenesis (Ben-David and Amon, 2020; Chunduri and

Storchová, 2019; Orr et al., 2015; Zhu et al., 2018). Recent advances in genome editing enable the generation of model systems that can circumvent confounding experimental limitations of overexpression models, including non-physiological protein expression lacking regulation by the endogenous promoter. Use of the CRISPR/Cas9 system allows for the study of mutant p53 function in a controlled context and has led to observations that challenged the mutant p53 GOF hypothesis in myeloid malignancies (Boettcher et al., 2019). Given the potential of using mutant p53 protein as a therapeutic target in many cancer types, and the longstanding debate of whether GOF activities exist, there is a critical need to study mutant p53 GOF activities in models of epithelial malignancies controlled for the confounding effects of exogenous protein expression and chromosomal alterations that occur following p53 LOF.

In this Chapter we describe the characterization of two isogenic epithelial cell line models (one non-transformed and one tumor-derived) developed using CRISPR/Cas9-mediated genome editing. In these models, parental cells were modified to express either of the most frequently occurring p53 missense mutations (R175H or R273H), to be deficient for p53 protein (null), or to retain the wild-type (WT) protein. Endogenous p53 expression is regulated by the native p53 promoter in these engineered models, providing a biologically relevant system for rigorous functional experimentation across different p53 states. Additionally, the use of clonally derived cell lines originating from the same near-diploid parental genetic background allows for assessment of the genomic alterations and resulting molecular heterogeneity following mutation of *TP53*. Through our comparative analyses of isogenic epithelial cells, which initially differed only by *TP53* genotype, we discovered that increased aneuploidy is consistently

observed in our mutant p53-expressing cell lines. Further, we discovered that *in vitro* GOF phenotypes are only present in mutant p53-expressing cell lines that display increased aneuploidy and that these phenotypes are not dependent on mutant p53 protein expression. Mutant p53-containing cell lines did not have increased tumorigenicity or metastasis *in vivo*, and analysis of human tumors revealed that loss of p53 function and increased aneuploidy were associated with unfavorable prognoses. Importantly, our results reveal aneuploidy as a mechanism contributing to the diversity of reported mutant p53 GOF phenotypes.

Results

Generation and characterization of genetically-engineered cell line models to study potential mutant p53 GOF activities

To select cell lines that would provide controlled model systems for the study of p53 mutation, we evaluated p53 status and the fraction of the genome altered (FGA) across cancer cell lines (Cancer Cell Line Encyclopedia, n=957). We selected two *TP53* WT lines derived from breast epithelium that are near-diploid and have a low FGA (MCF10A=13%, CAL-51=3%) compared to pan- or breast cancer cell lines (Fig. 4a and Fig. 6a). MCF10A is a non-transformed cell line derived from normal human mammary epithelium (Soule et al., 1990). CAL-51 is a metastatic breast cancer cell line derived from a pleural effusion (Gioanni et al., 1990). Both lines are considered “triple-negative” since they lack estrogen and progesterone receptor expression and *HER2* amplification (Lehmann et al., 2011; Neve et al., 2006). To minimize genomic heterogeneity, we

performed single-cell selection and clonal expansion to generate a parental clonal line for each model. Using CRISPR/Cas9-mediated gene editing (Ran et al., 2013), we generated mutations in *TP53* using homology-directed repair (HDR) templates containing mutant bases corresponding to hotspot *TP53* mutations, R175H and R273H, along with synonymous mutations to prevent CRISPR/Cas9-mediated cleavage of the HDR-recombined alleles (Fig. 4b). As controls for CRISPR-mediated off-target effects, we identified WT cell lines that underwent incomplete HDR (containing engineered synonymous mutations but not the missense mutation). *TP53* null cell lines were generated from frameshift insertions or deletions in both alleles, resulting in cells deficient for full-length p53 protein. Through single-cell isolation, clonal expansion, and genotyping, we derived independent biological replicates for each model and *TP53* genotype; WT (R/R), null (-/-), and the two p53 mutants, R175H and R273H (H/-, or H/H) (Fig. 4b, Fig. 5). In total, we generated 15 clonally derived isogenic MCF10A cell lines (2 WT, 4 null, 4 R175H, and 5 R273H) and 21 clonally derived isogenic CAL-51 cell lines (4 WT, 5 null, 4 R175H, and 8 R273H) (Fig. 5).

To analyze p53 activity in the engineered *TP53* lines, we performed RNA-sequencing (RNA-seq) on all cell lines derived from MCF10A and CAL-51 models. Both models displayed decreased p53 target gene expression in the *TP53* null, R175H, and R273H mutant cell lines compared to WT cell lines (Fischer, 2017) (Fig. 4c). Gene set enrichment analysis (GSEA) showed significant negative enrichment of p53 target gene expression in R175H and R273H mutant and null cell lines (all comparisons: NES < -2.8, FDR < 0.0001) (Fig. 4d), demonstrating p53 LOF as a sequence-specific transcription factor in the null, R175H and R273H cell lines. We also analyzed protein

expression after exposure of the MCF10A and CAL-51 models to the anthracycline doxorubicin. Doxorubicin treatment resulted in increased p53 protein levels and downstream targets, MDM2 and p21, in cell lines expressing WT p53. p53 protein levels also increased after doxorubicin treatment in mutant cell lines in the transformed CAL-51 model, similar to previous reports (Boettcher et al., 2019; Terzian et al., 2008). However, no changes in MDM2 or p21 expression were observed, further indicating p53 LOF in null, R175H, and R273H p53 mutant cell lines (Fig. 4e). To further analyze p53 activity, we treated all cell lines with the small molecule Nutlin-3a, which inhibits the interaction between p53 and MDM2, the primary p53 negative regulator (Vassilev et al., 2004). Comparison of half-maximal inhibitory concentrations (IC_{50}) revealed that only WT cell lines were sensitive to Nutlin-3a, while all null, R175H, and R273H cell lines showed a significant increase in IC_{50} (null, R175H, and R273H compared to WT: MCF10A, $P < 0.0015$; CAL51, $P < 0.0001$) (Fig. 4f). Therefore, genome editing of WT *TP53* to null, R175H, or R273H mutations abrogated canonical p53 function and resulted in a loss of sensitivity to Nutlin-3a, consistent with previously reported results (Boettcher et al., 2019; Humpton et al., 2018).

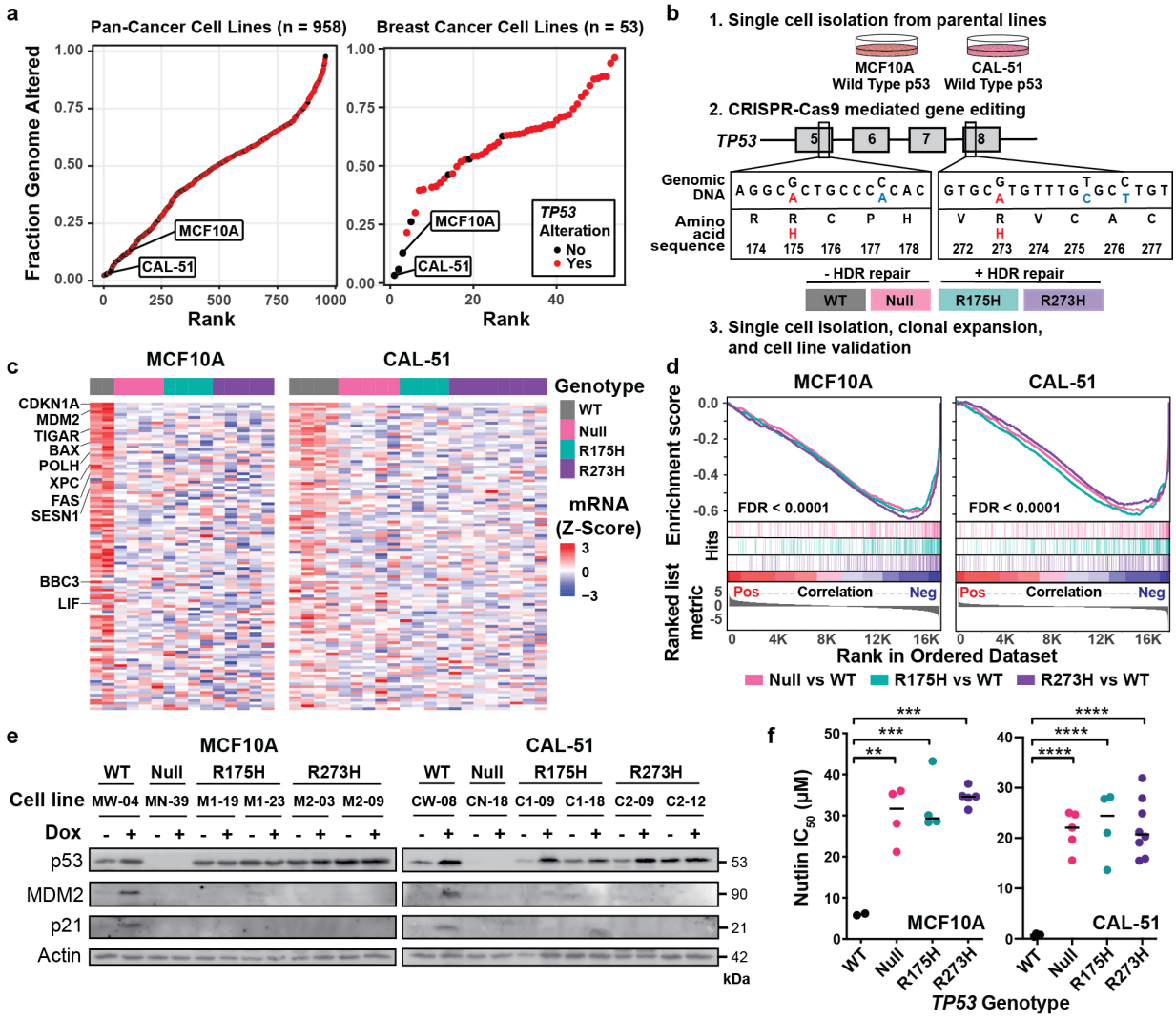

Figure 4: Generation and characterization of genetically-engineered epithelial cell line models to study potential mutant p53 GOF activities.

a Fraction of the genome altered across pan-cancer (*n* = 958, left panel) and breast cancer cell lines (*n* = 53, right panel) from the Cancer Cell Line Encyclopedia, with (red) and without (black) *TP53* alterations (mutation or deletion); including the non-transformed MCF10A cell line. **b** Experimental workflow for CRISPR-Cas9 genetic engineering of isogenic cell line models with *TP53* missense (red) and synonymous (blue) mutations and the resulting isogenic cell lines that either did (R175H and R273H, +HDR) or did not undergo complete homology-directed repair (WT and Null, -HDR). HDR, homology-directed repair. **c** Heat map of normalized gene expression for the top 116 p53 target genes(Fischer, 2017) for all cell lines at passage five after clonal expansion. **d** GSEA plot showing negative enrichment of p53 target genes from RNA-seq differential gene expression analyses between *TP53* Null (pink), R175H (teal), and R273H (purple) clones compared to the MCF10A and CAL-51 WT cell lines. **e** Western blots of relative p53, MDM2, p21, and actin protein levels in the indicated cell lines after 6 h of doxorubicin treatment (dox, 0.2 μM). **f** IC_{50} values for Nutlin-3a in the MCF10A and CAL-51 cell lines after treatment for 72 h. Dots represent the mean IC_{50} per cell line calculated from at least two independent experiments and black lines indicate median IC_{50} per *TP53* genotype. One-way ANOVA with Dunnett's multiple comparison test, $^{**}P < 0.01$, $^{***}P < 0.001$, $^{****}P < 0.0001$. Isogenic cell lines were generated by Timothy Shaver and Hailing Jin.

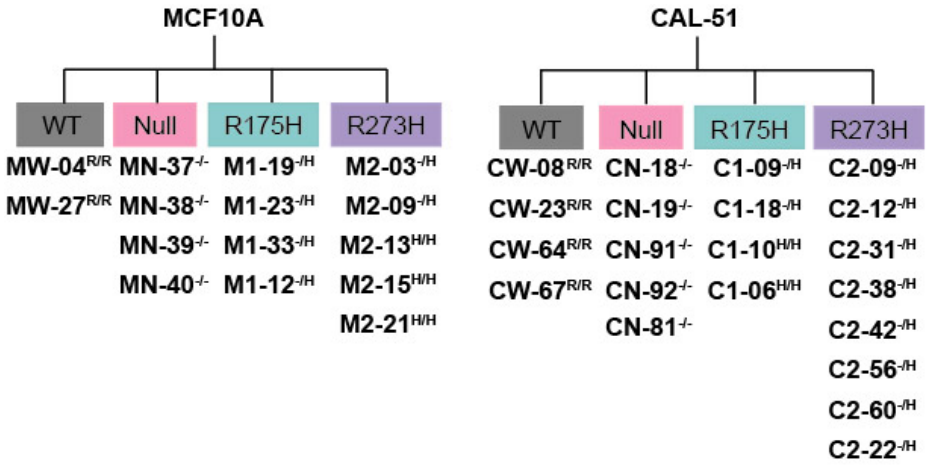

Figure 5. Genetically-engineered epithelial isogenic cell line models to study potential mutant p53 GOF activities.
Diagram of clonally-derived CRISPR-Cas9 isogenic MCF10A (left) and CAL-51 (right) cell lines grouped by *TP53* genotype (WT, Null, R175H, or R273H). Genotypes of each clone are indicated as homozygous wild-type (R/R), homozygous mutant (H/H), heterozygous null/mutant (-/H) and homozygous null (-/-).

p53 mutant isogenic cell lines display increased frequency of aneuploidy

Mutation of p53 is associated with development of aneuploidy (Gualberto et al., 1998; Hanel and Moll, 2012). To evaluate the relationship between p53 mutations and the development of aneuploidy, we assessed DNA content in our MCF10A and CAL-51 models early (passage five) after clonal expansion. Analysis of metaphase spreads and flow cytometry of propidium iodide (PI)-stained cells revealed that while the MCF10A derived lines maintained a near-diploid median number of chromosomes, five of the CAL-51 lines (three R273H, one R175H, and one null) contained a median number of chromosomes >2N (Fig. 6b, c). Four of these five were nearly tetraploid, suggesting that whole-genome doubling (WGD) likely occurred in these cells. Since metaphase spreads and PI staining detect gross chromosomal alterations, we also examined DNA copy number by cytogenomic microarray analysis (CMA) after 30 passages in culture. All MCF10A cell lines showed aneuploidy, with chromosomal gains (1q, a portion of 5q and 8q, and 20) consistent with known parental MCF10A cell line karyotypes (Fig. 7a and Fig. 6a). Additional whole-chromosome or arm-level alterations were identified in chromosomes 4, 5, 13, 15, and 18 (Fig. 7a). Structural alterations, including gain or loss of chromosomal regions, were evident in all MCF10A cell lines. Chromothripsis, a chromosome shattering and rearrangement event that manifests as alternating patterns of gains and losses, was also detected in several MCF10A R273H mutant clones (M2-09, M2-03, and M2-13, Fig. 7a; chromosomes 6, 7 and 15, Fig. 8). In contrast, the CAL-51 cells displayed mostly whole-chromosome alterations, such as gains in chromosomes 6 and X and losses in chromosomes 3, 13, and 16 in both the *TP53*

mutant and null genotypes (Fig. 7a), consistent with other analyses of tetraploid cells (Fujiwara et al., 2005).

To identify chromosomal alterations common to each genotype, we generated frequency plots to show the percentage of cell lines with a given chromosomal alteration for each *TP53* genotype relative to the parental WT cell line. Compared to null cells, mutant cell lines in both models appeared to have increased frequency of chromosomal gains and losses (Fig. 7b). Statistical analysis to compare differentiated chromosomal arm regions between mutant and null cells revealed that chromosome 18q in the R175H mutant MCF10A cells was the only region significantly altered (adjusted $P < 0.1$). To quantify the degree of copy number alterations within each cell line, we generated an integrative aneuploidy score (AS) from the CMA data that reflects the sum of segmented copy number alterations (Log_2 ratios) in the clonal lines relative to the respective parental WT clone. In both models, mutant and null cell lines showed an increased median AS compared to WT (MCF10A R175H $P = 0.011$). Compared to null lines, there was a significant increase in AS in MCF10A R175H lines ($P = 0.046$) (Fig. 7c). The median AS was higher in the R273H mutant compared to null lines in both models, although not reaching statistical significance (Fig. 7c). For use in subsequent comparative analyses of the models, AS quantiles were used to classify cell lines in each model as aneuploid-high (upper quantile AS) or aneuploid-low (lower quantile AS) (Fig. 7c).

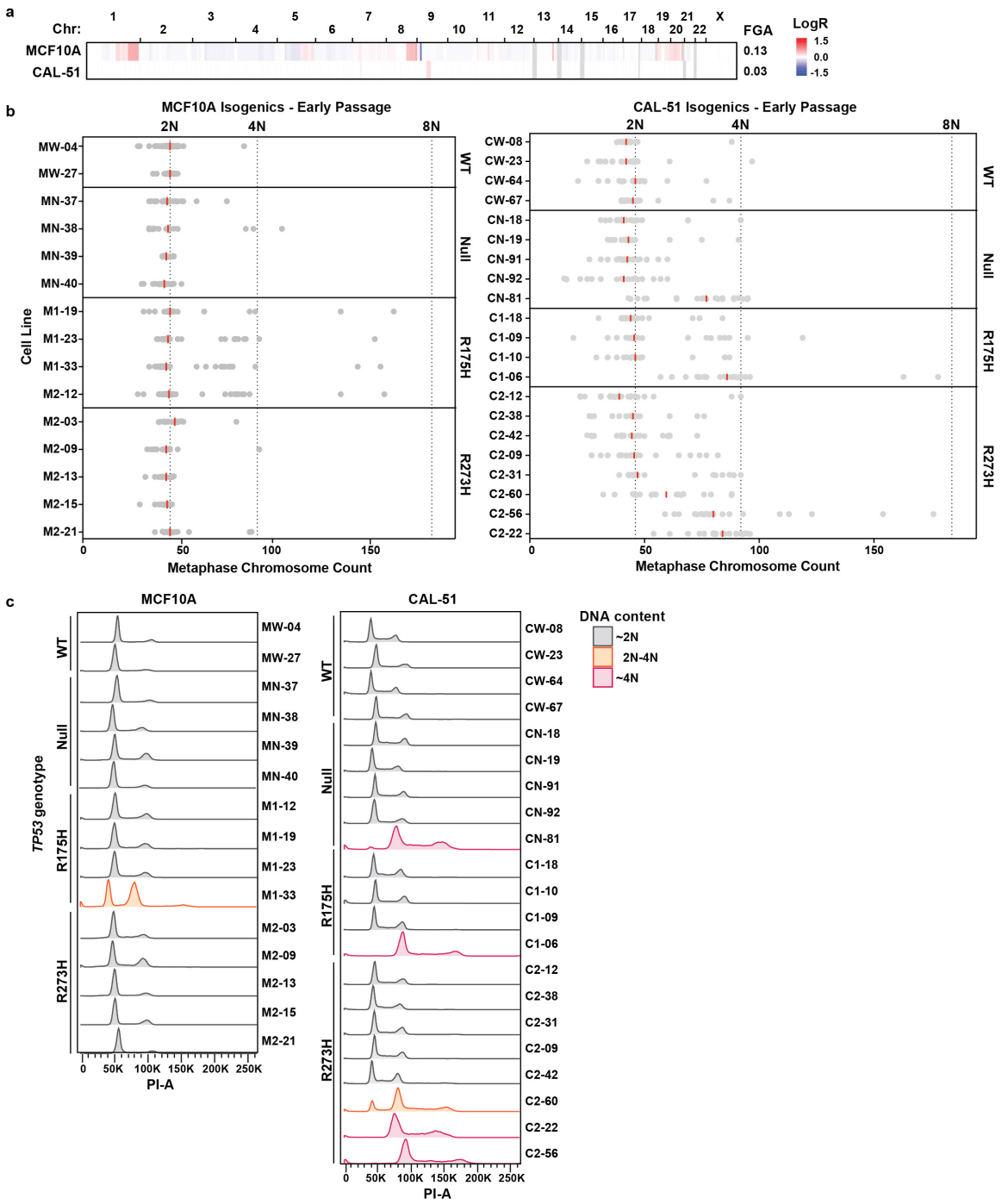

Figure 6. DNA content analysis of MCF10A and CAL-51 early passage cell lines.
a Heat map of chromosomal alterations (Log_2 ratios, LogR), either gain (red) or loss (blue) across the genomes of MCF10A and CAL-51 cell lines and the corresponding fraction of the genome altered (FGA). **b** Quantification of chromosomes using metaphase spreads (≥15 cells per clonal cell line) for the indicated MCF10A or CAL-51 cell lines at passage five after clonal expansion. Red bars indicate the median chromosome number. Outliers with >200 chromosomes were removed for visualization. **c** Histograms showing DNA content of MCF10A (left) and CAL-51 (right) isogenic cell line populations by flow cytometry of propidium iodide (PI) stained cells at passage five after clonal expansion. Colors represent DNA content (gray = ~2N, orange = 2N-4N, pink = ~4N). All analyses were conducted with the help of Hailing Jin.

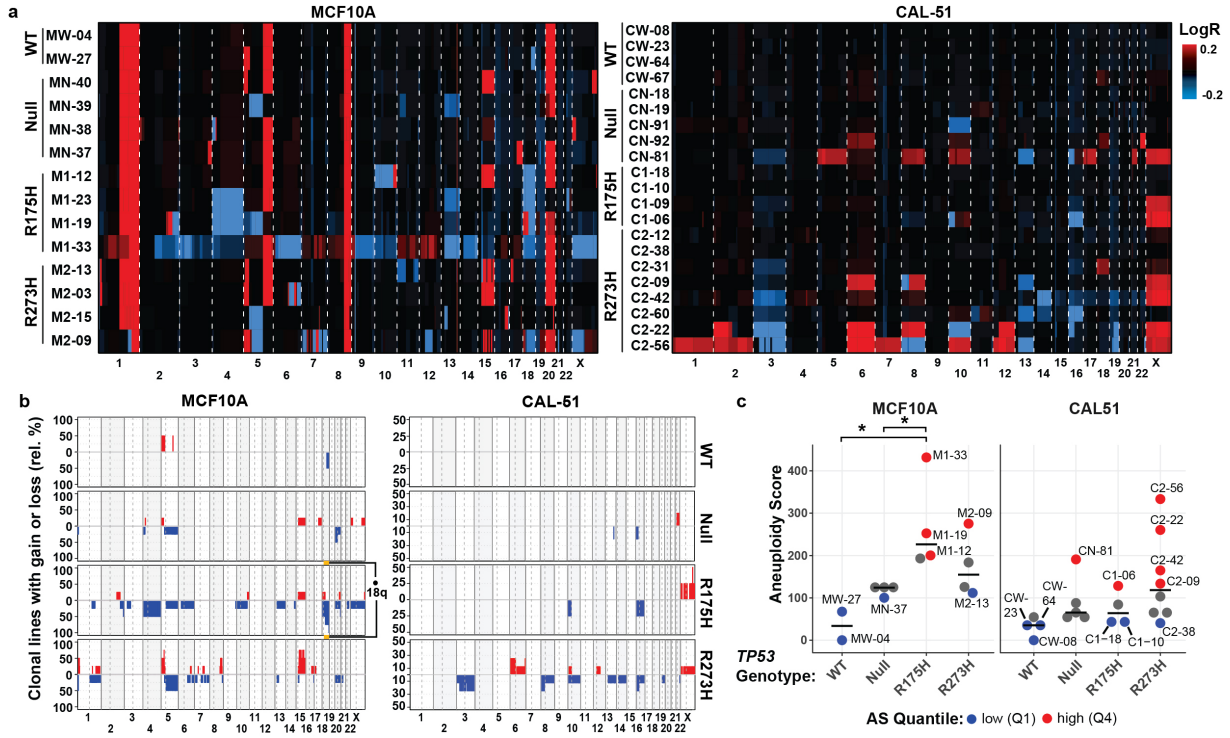

Figure 7: p53 mutant isogenic cell lines display increased frequency of aneuploidy.
a Copy number alterations (Log_2 ratios, LogR) in MCF10A (left) and CAL-51 (right) isogenic cell lines grouped by *TP53* genotype. Chromosomal gain (red) and loss (blue). **b** Frequency plots of the proportion of clonal lines from each genotype containing the indicated chromosomal copy number gains (red) or losses (blue). Chromosomal alterations were calculated relative to the parental WT clone in the MCF10A (left) and CAL-51 (right) cell lines from (**a**). Chromosome 18q in the R175H mutant MCF10A cells was the only region significantly altered; • adjusted $P < 0.1$, two-sided student's *t*-test comparing chromosome arms between *TP53* genotypes. **c** Aneuploidy score (AS) in each MCF10A (left) and CAL-51 (right) cell line by *TP53* genotype (MCF10A $n = 2$ WT, 4 Null, 4 R175H and 4 R273H cell lines; CAL-51 $n = 4$ WT, 5 Null, 4 R175H and 8 R273H cell lines). Colors indicate cell lines classified as aneuploid-low (lower quantile AS [Q1], blue), and aneuploid-high (upper quantile AS [Q4], red). Cell lines colored in gray indicate an intermediate AS (quantiles 2 and 3). *$P < 0.05$ (WT vs R175H, $P = 0.011$; Null vs R175H, $P = 0.046$), one-way ANOVA with Dunnett's multiple comparison test.

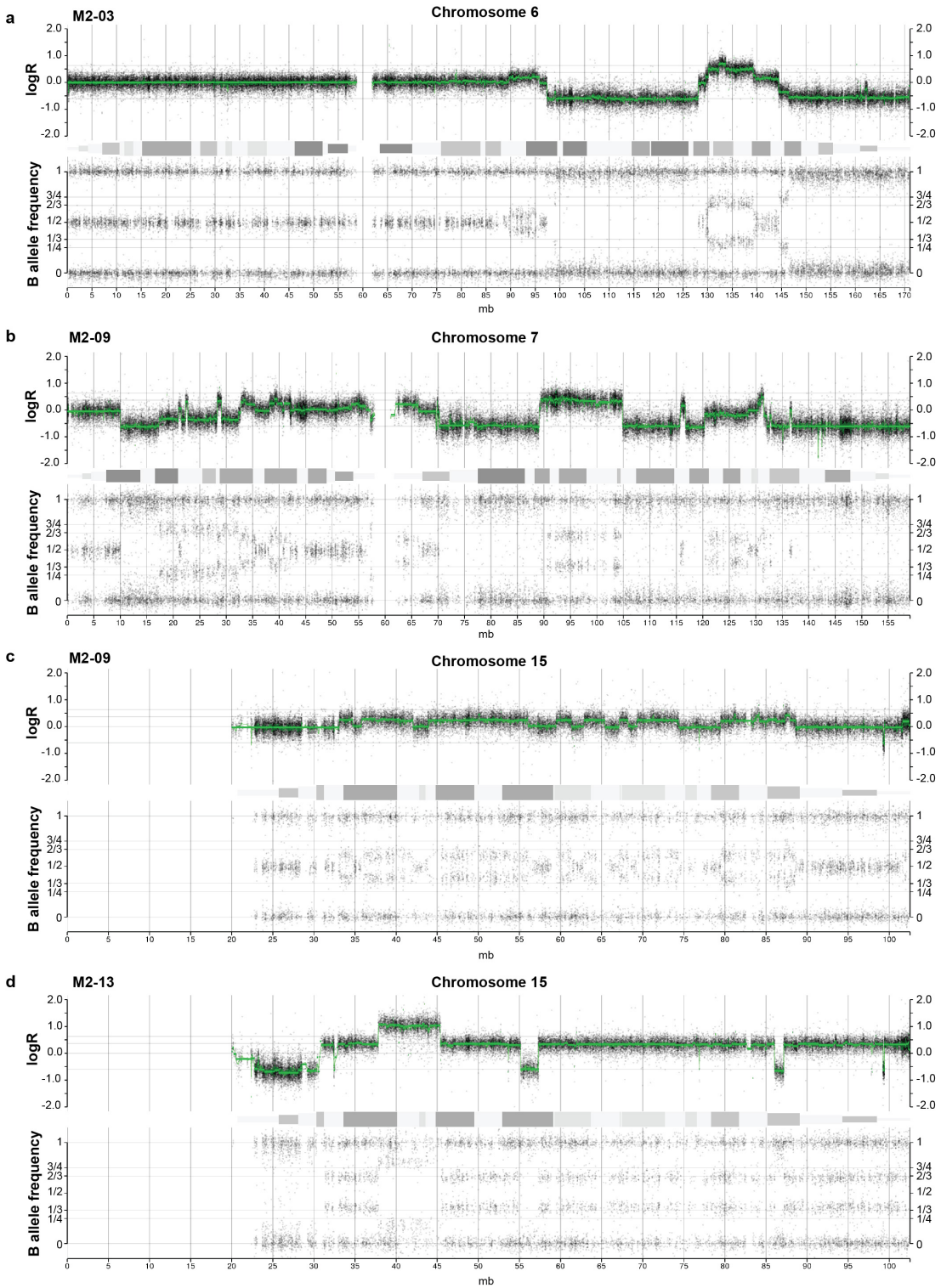

Figure 8. Analysis of chromothripsis in MCF10A *TP53* R273H mutant clonal cell lines.
a - d Visualization of cytogenomic microarray analysis (CMA) segmented copy number (Log_2 ratios, LogR) and B-allele frequency for the MCF10A clonal cell lines M2-03 (**a**) M2-09 (**b - c**) and M2-13 (**d**), which displayed chromothripsis or alternating segments of chromosomal gain and loss in chromosome 6 (**a**), chromosome 7 (**b**), and chromosome 15 (**c - d**).

To examine the possibility that acquired mutations in other genes could account for the observed increased aneuploidy in our models, we conducted whole-exome sequencing (WES) in tandem with CMA. No gene mutations were significantly enriched in aneuploid-high cell lines in either model (Table 2). Further, no significant enrichment in mutations was observed for a set of genes known to be associated with hereditary cancers (Fig. 9a) (Invitae Corporation, 2018). However, the MCF10A cell line with the highest AS (M1-33) displayed deletions in *BRCA2* and *RB1* (Fig. 9a). There was not a significant difference in the total number of mutations in either model relative to *TP53* genotype (Fig. 9b). In sum, these results show that aneuploidy occurs at an increased frequency after *TP53* mutation in both isogenic models.

Symbol	Aneuploid High (n)	Aneuploid Low (n)	P-value	Adj P-value	Model	Cell Lines Altered
TP53	4	2	0.42857	1	MCF10A	MN-37, MN-38, MN-39, MN-40, M1-12, M1-19, M1-23, M1-33, M2-03, M2-09, M2-13, M2-15, M2-21
HKDC1	4	2	0.42857	1	MCF10A	MW-04, MN-37, MN-38, M1-12, M1-19, M1-23, M1-33, M2-09, M2-21
HTT	2	4	0.42857	1	MCF10A	MW-04, MW-27, MN-37, MN-39, MN-40, M1-19, M2-03, M2-09, M2-13, M2-21
NCSTN	0	2	0.42857	1	MCF10A	MW-04, MN-37, MN-38, M2-21
RYR2	0	2	0.42857	1	MCF10A	MW-04, MN-37, MN-38, M2-21
WNK3	0	2	0.42857	1	MCF10A	MW-04, MN-37, MN-38, M2-21
SYN2	3	1	0.48571	1	MCF10A	MN-37, MN-40, M1-12, M1-19, M1-23, M1-33, M2-21
TP53	5	2	0.16667	1	CAL-51	CN-18, CN-19, CN-91, CN-92, CN-81, C1-09, C1-18, C1-10, C1-06, C2-09, C2-12, C2-31, C2-38, C2-42, C2-56, C2-60, C2-22
PXDN	0	3	0.16667	1	CAL-51	CW-08, CW-64, CN-19, C1-18
BICRA	1	3	0.52381	1	CAL-51	CW-08 CW-64, CN-18, CN-19, C1-18, C2-12, C2-22
KCNN3	3	1	0.52381	1	CAL-51	CN-92, C1-06,C2-38, C2-42, C2-56, C2-22
TTN	3	1	0.52381	1	CAL-51	CN-18, CN-81, C2-12, C2-38, C2-42, C2-56, C2-22
VCX3B	4	2	0.52381	1	CAL-51	CW-08, CW-23, CW-67, CN-18 CN-19, C1-10, C1-06, C2-09, C2-12, C2-31, C2-42, C2-56, C2-22

Table 2. Analysis of mutations common to aneuploid high isogenic cell lines. Analysis of whole-exome sequencing and two-sided Fischer's Exact Test between mutations in aneuploid-high (upper quartile AS) and aneuploid-low (lower quartile AS) cell lines in MCF10A and CAL-51 isogenic cell line models.

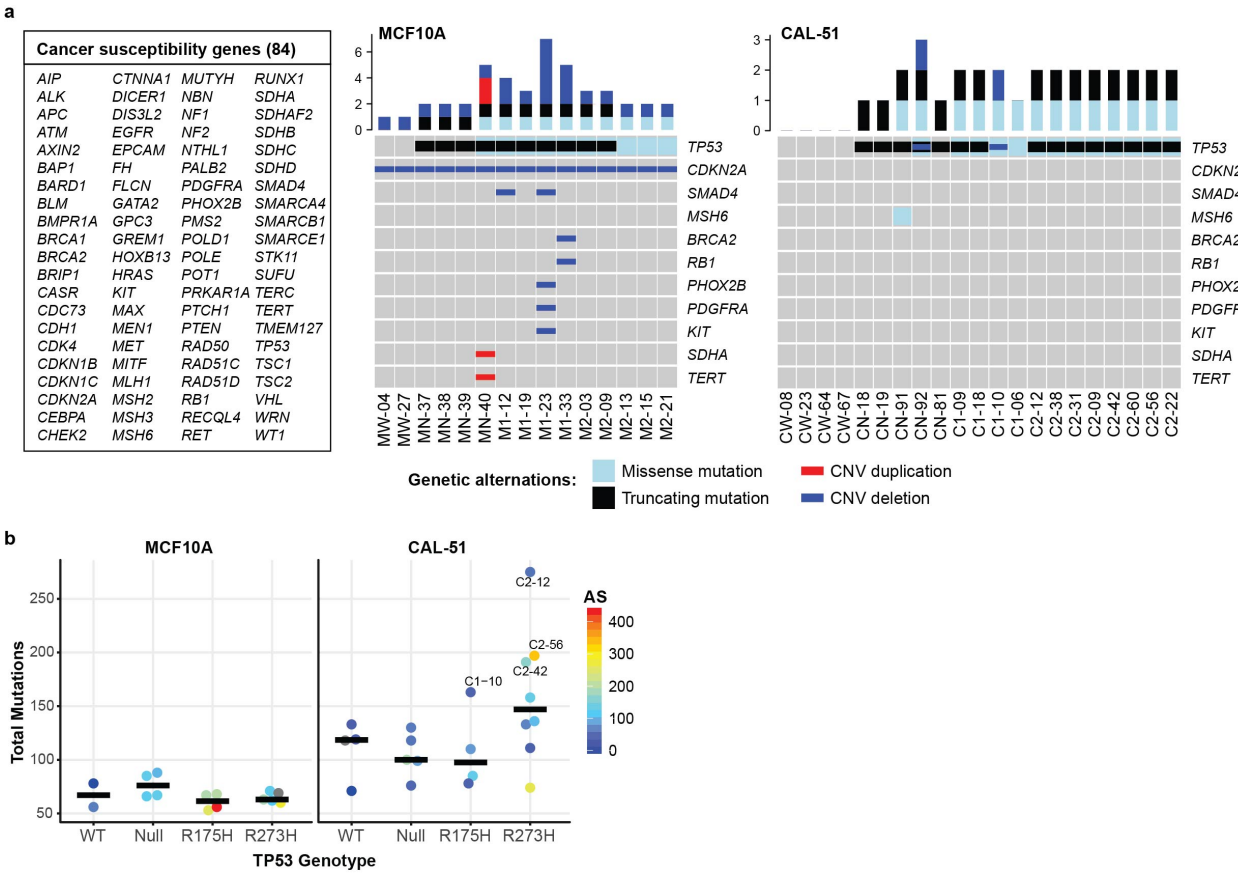

Figure 9. Acquisition of aneuploidy in *TP53* mutant lines is not associated with other cancer driver gene mutations.

a Mutation or copy number alterations in 84 common cancer susceptibility genes (left panel) within indicated clonal cell lines from MCF10A (middle panel) and CAL-51 (right panel). Bar graphs on top of the two right panels indicate the total number of alterations within each cell line. Missense and truncating mutations are shown as light blue and black bars, respectively, in the grid below. Copy number duplication and deletion are shown as smaller red and blue bars, respectively. If a gene is not shown, no alterations were detected. **b** Dot plots comparing total number of mutations in clonal cell lines with the indicated *TP53* genotype in MCF10A (left, *n* = 2 WT, 4 Null, 4 R175H and 4 R273H) and CAL-51 (right, *n* = 4 WT, 5 Null, 4 R175H and 8 R273H) cells. Cell lines are colored by their calculated aneuploidy score (AS). Black lines indicate the median number of mutations across all clonal lines grouped according to *TP53* genotype. One-way ANOVA with Dunnett's multiple comparison test. Whole exome sequencing analysis was conducted with the help of Tiger Sheng.

Mutant p53 does not contribute to the development of aneuploidy through modulation of p73 activity

Because of the significant overlap in DNA binding sites and transcriptional activities of p73 and p53 (Yang and McKeon, 2000), it has been hypothesized that p73 can have compensatory transcriptional activity in the absence of WT p53 (Talos et al., 2007; Tomasini et al., 2008; Tsuchihara et al., 2018). Both p53 and p73 have been implicated in controlling cellular ploidy through transcriptional regulation of cell cycle checkpoints, and loss of p73 in a p53-deficient background results in increased aneuploidy (Talos et al., 2007). Additionally, p73 has been shown to play an important role in the spindle assembly checkpoint by binding and inhibiting key centrosome maintenance proteins (Tsuchihara et al., 2018). Certain p53 mutants, like the R175H mutant, have been shown to bind the p53 family member p73 and inactivate p73 transcriptional activity, although many of these observations have been made using exogenously expressed or tagged protein (Di Como et al., 1999; Gaiddon et al., 2001; Strano et al., 2000).

To determine if protein-protein interactions between mutant p53 and p73 influence the development of aneuploidy, we conducted co-immunoprecipitation (IP)-Western analyses using the isogenic MCF10A and CAL-51 cell line models. No significant interactions were identified relative to control cell lines containing no p53 protein (Null) or IgG controls (Fig. 10a-b). Co-immunoprecipitation experiments were also conducted in additional cancer cell lines containing endogenous mutant p53 and p73 protein or a control cell line with no p53 protein (Null). Again, we found no evidence of interactions relative to control cell lines (Fig. 10c).

To determine if p73 transcriptional activity differs in the context of differing *TP53* genotypes, we evaluated known p73 target gene expression in our isogenic models (Marshall et al., 2016; Rosenbluth et al., 2011) using RNA-seq in our isogenic models. Unsupervised hierarchical clustering of p73-target genes did not separate cell lines by *TP53* genotype (Fig. 10d), indicating that p73 transcriptional activity is not modulated by mutant p53.

Finally, dual-immunofluorescence experiments were performed in CAL-51 cell lines. Analysis of p53 and p73 staining revealed that p53 and p73 protein are expressed in separate cells regardless of the *TP53* genotype (Fig. 11). Co-localization of mutant p53 and p73 was seen only in a small fraction of aneuploid cell lines. Therefore, given the lack of evidence for a physical interaction between mutant p53 and p73 proteins in our models, we conclude that mutant p53 does not promote aneuploidy through modulation of p73, contradictory to previous reports (Gaiddon et al., 2001; Strano et al., 2000; Talos et al., 2007).

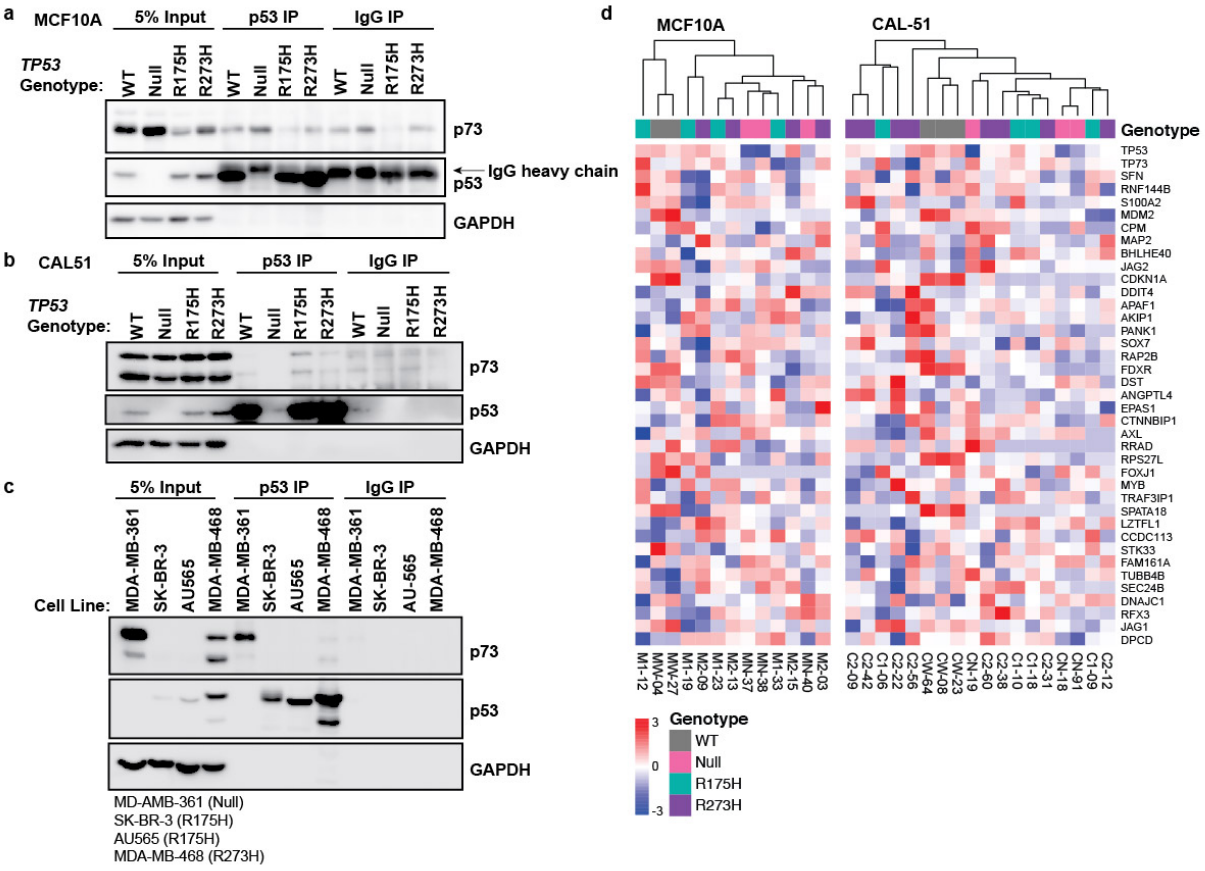

Figure 10. Mutant p53 does not interact with or alter p73 gene transactivation.
a – c Immunoprecipitation (IP) of protein lysates with p53 antibody (DO-1) or control IgG, from MCF10A (**a**) or CAL-51 isogenic cell lines (**b**), or cancer cell lines containing endogenous mutant p53 and p73 proteins (**c**). Immunoblots showing input and immunoprecipitated p53, p73 with loading control (GAPDH). **d** Hierarchical clustering of curated p73 target genes from MCF10A (left) and CAL-51 (right) cell lines. Immunoprecipitation experiments were conducted with the help of Hailing Jin.

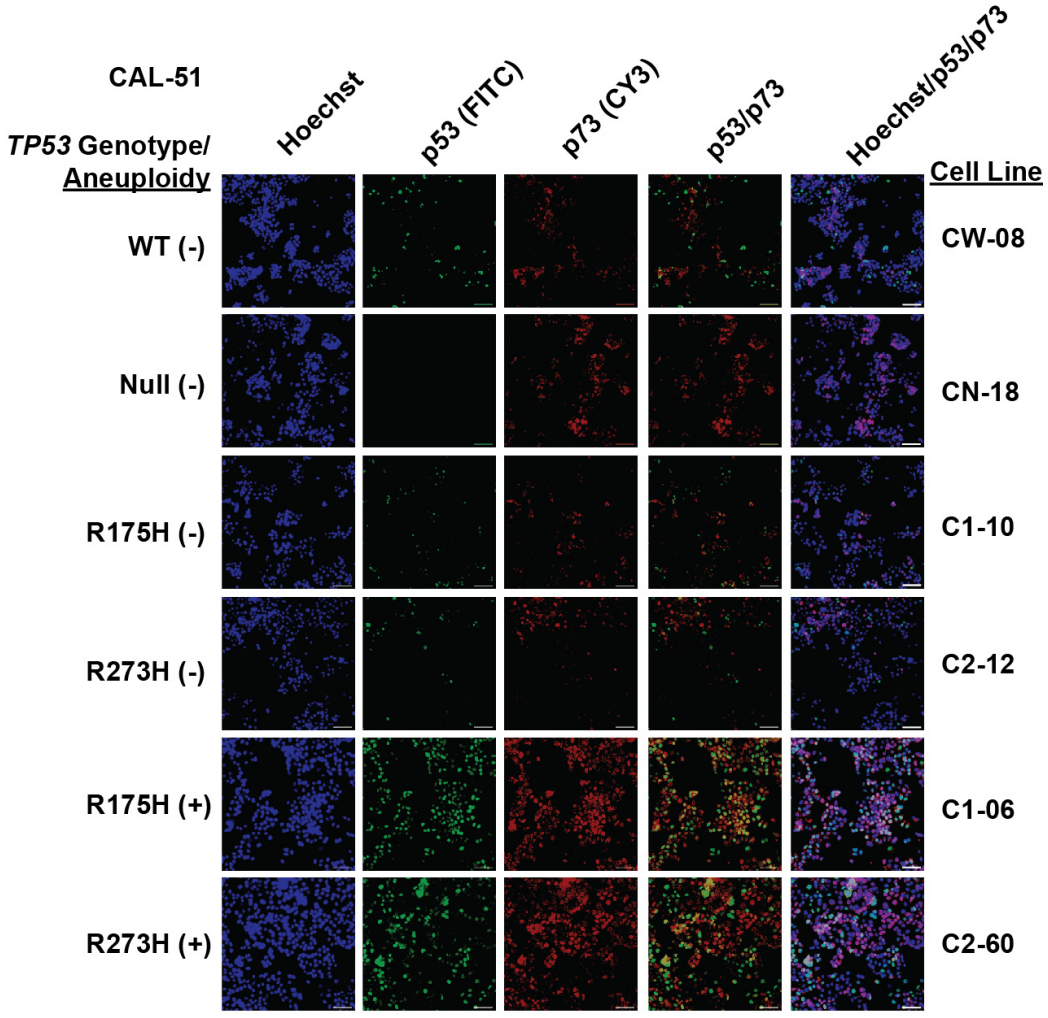

Figure 11. Mutant p53 and p73 do not co-localize in a majority of CAL-51 cells.
Representative tyramide signal-amplified (TSA) immunofluorescence images of isogenic CAL-51 cell lines with varying *TP53* genotypes dual stained for p53 (FITC), p73(CY3) and nuclear stain Hoechst (blue). Cell lines were identified as aneuploid (+) or non-aneuploid (-) through DNA content analysis by flow cytometry and propidium iodide staining. Scale bars, 100 μM.

Gene expression changes are associated with aneuploidy and not mutant p53 expression

Previously, mutant p53 GOF phenotypes were ascribed to the acquisition of a mutant p53-dependent transcriptional program (Scian et al., 2004a, 2004b; Turrell et al., 2017). To investigate this possibility in our models, we performed RNA-seq in parallel with CMA and WES experiments on MCF10A and CAL-51 cell lines cultured under normal conditions or with doxorubicin to induce genotoxic stress (Fig. 13a). Principal component analyses (PCA) of all genes revealed differences in global gene expression patterns, with cell lines clustering independent of *TP53* genotype or doxorubicin treatment in both models (Fig. 12a and Fig. 13b). Further, we found that the most significant degree of variance in the PCA could be attributed to cell lines with higher levels of aneuploidy (Compare Fig. 12a to Fig. 7c). We conducted differential gene expression analyses comparing R175H or R273H mutants to null cells in MCF10A and CAL-51 models. Comparison of differentially expressed genes (DEGs) revealed almost no shared genes between R175H or R273H mutants in both MCF10A and CAL-51 models, except for *TP53* and a gene encoding for Histone H2A (Fig. 12b). R175H mutant cells in the MCF10A cell line had a larger number of DEGs; however, GSEA revealed that the most significantly altered pathway between MCF10A R175H and null cells was the chromosome positional pathway CHR18Q21 (Fig. 13c), indicating that increased DEGs are related to chromosomal changes in those cells (Fig. 7b).

To further assess the impact of aneuploidy on the number of DEGs, we conducted differential gene expression analysis between CAL-51 R273H mutants with varying levels of aneuploidy (high, medium, or low AS) and two aneuploid-low null cell

lines (Fig. 13d). Mutant clones with the greatest aneuploidy showed the greatest number of DEGs, whereas comparison of R273H AS-low versus null AS-low cells revealed only 17 significantly DEGs (Fig. 13e). To test if mutant p53 expression affected the number of DEGs, we generated stable p53 knockdown cell lines from our isogenic models with shRNAs targeting *TP53* or a non-targeting control (NT) (Fig. 14a). We validated knockdown of p53 by RNA-seq or western blot (Fig. 14b, c). RNA-seq comparing aneuploid-high CAL-51 R273H cell lines (C2-22 and C2-56) with NT control to those with p53 knockdown revealed only six DEGs (Fig. 14d), and there were no differences in global gene expression patterns by PCA between the p53 knockdown and NT control cells (Fig. 14e). These data suggest that DEGs in our isogenic p53 mutant cell lines result from genetic variation and not a novel transcriptional program induced by mutant p53.

Distinct transcriptional programs have been reported to be transactivated by mutant p53 (Scian et al., 2004a). However, we did not observe genotype-specific patterns for these reported genes, with heterogeneous expression observed across cell lines in both models (Fig. 12c). In the CAL-51 model, unsupervised hierarchical clustering revealed that cell lines with a higher AS clustered together and had increased expression of most of these reported mutant p53-upregulated genes (Fig. 12c, right). To determine if our cell lines displayed gene expression patterns consistent with those previously found in aneuploid cells, we analyzed expression of the HET70 gene set, which consists of genes upregulated in cells displaying karyotype heterogeneity (Sheltzer, 2013). Unsupervised hierarchical clustering revealed that cell lines with a higher AS clustered together in both MCF10A and CAL-51 models and had increased

expression of HET70 genes (Fig. 12d). These data suggest transcriptional changes are associated with karyotype heterogeneity and are not driven by the p53 mutations analyzed herein.

We hypothesized that aneuploidy and the resulting stochastic genetic variation led to the altered gene expression profiles in *TP53*-mutated cells. To test this hypothesis, we determined if gene dosage effects resulting from chromosomal alterations aligned with the changes in gene expression observed in the PCA (Fig. 12a). For each untreated cell line, we compared the average transcriptome expression per chromosome to the average chromosomal copy number and observed a significant correlation in highly altered chromosomes across cells from both models (MCF10A, chromosome (chr) 5: r = 0.96, chr18: r = 0.99; CAL-51, chr10: r = 0.94, chr6: r = 0.84; all $P < 0.0001$), but not in chromosomes lacking copy number changes (Fig. 12d). These data indicate that chromosomal imbalances, rather than mutant p53 expression, significantly correlate with transcriptional changes in our isogenic models.

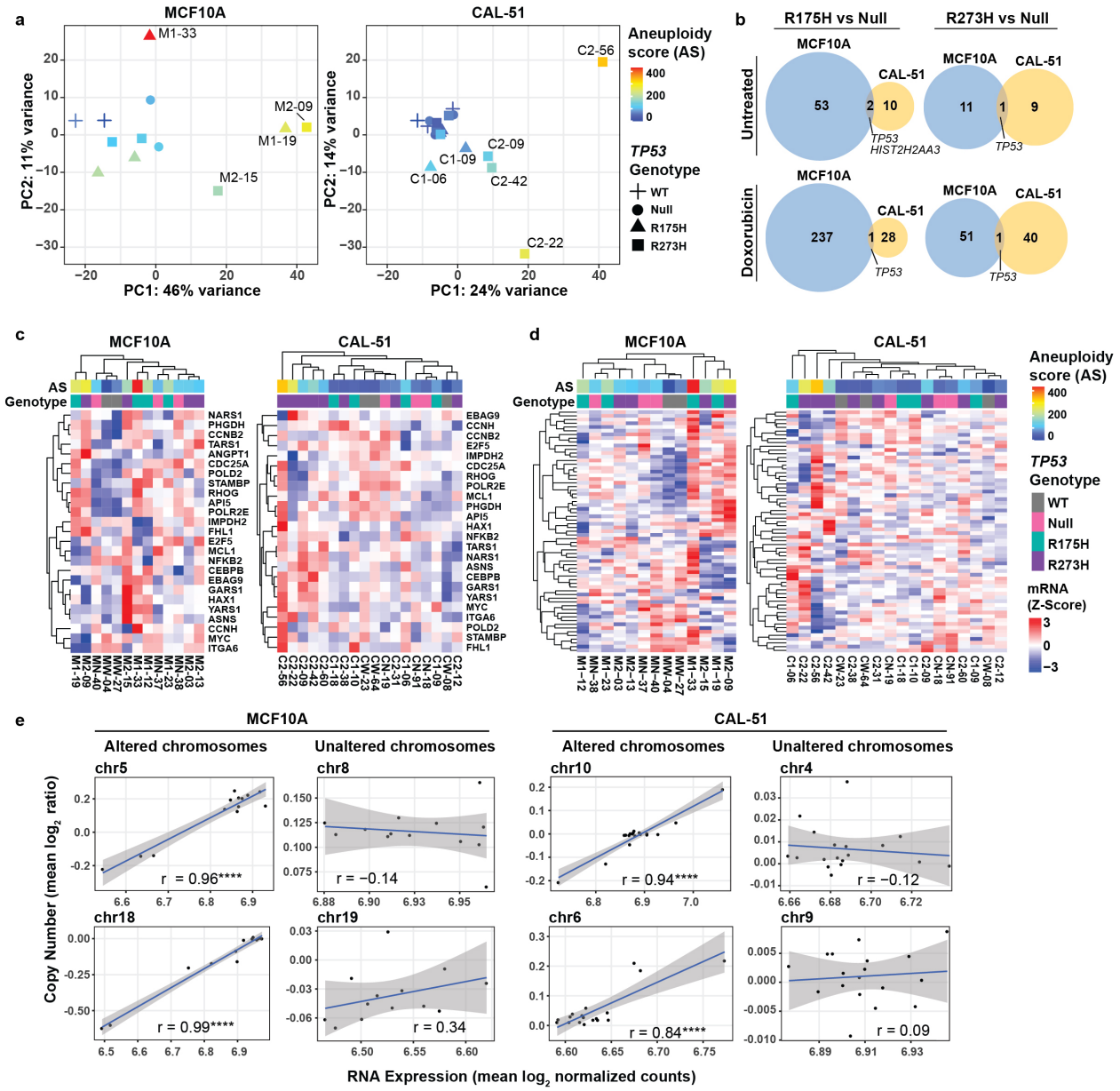

Figure 12: Gene expression changes are associated with aneuploidy and not mutant p53 expression.

a Principal component (PC) analysis of gene expression values for untreated MCF10A (left panel) and CAL-51 (right panel) isogenic cell lines. **b** Venn diagrams showing the overlap between differentially expressed genes in R175H (left) and R273H (right) cell lines compared to null cells in MCF10A (blue) and CAL-51 (yellow) models. Cells were either untreated (top) or treated with doxorubicin (0.2 μM, 6 h) (bottom). Cell lines used in RNA-seq analyses are shown in Supplementary Fig. 5a. **c** Hierarchical clustering and comparison of gene expression for previously reported mutant p53-associated upregulated genes(Scian et al., 2004a) from the indicated MCF10A (left panel) and CAL-51 (right panel) cell lines. **d** Hierarchical clustering and comparison of gene expression for the karyotype heterogeneity associated HET70 gene signature[43] from the indicated MCF10A (left panel) and CAL-51 (right panel) cell lines. **e** Scatter plots comparing average chromosomal copy number with chromosomal RNA expression for MCF10A (left panel, n = 13) and CAL-51 (right panel, n = 18) cell lines across frequently altered or unaltered chromosomes. Each point represents the mean per cell line. The blue line represents a linear model of the best fit, with the gray area representing the 95% confidence intervals. r = Pearson correlation coefficient, ****P < 0.0001.

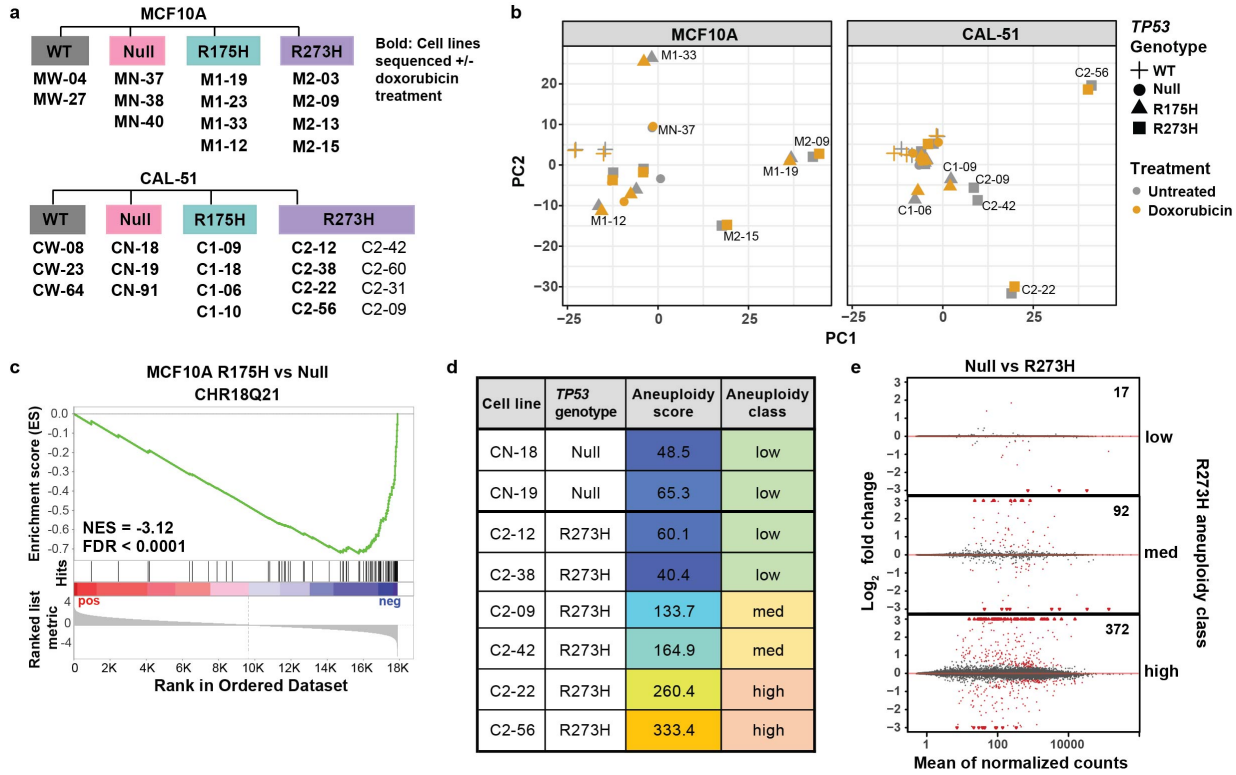

Figure 13. Gene expression changes are associated with aneuploidy and not mutant p53 expression.

a Diagram shows MCF10A (top) and CAL-51 (bottom) cell lines used for RNA-seq analyses grown under the indicated control (all cell lines) or treated (bold font; doxorubicin, 0.2 μM) conditions for 6 h. **b** PCA plot for MCF10A (left panel) and CAL-51 (right panel) clonal cell lines. Data point shapes represent the indicated *TP53* genotype (cross = WT, circle = Null, triangle = R175H, square = R273H) and treatment as described in Part A (untreated = gray, doxorubicin treated = orange). PC1, principal component 1. PC2, principal component 2. **c** GSEA plot showing negative enrichment of CHR18Q21 positional pathway genes from RNA-seq differential gene expression analysis between MCF10A *TP53* R175H and null cells. pos, positive. neg, negative. **d** Table showing CAL-51 Null and R273H cell lines separated into low, medium, or high aneuploidy classes based on their calculated aneuploidy score. **e** MA plots showing the shrunken Log_2 fold changes of all genes in CAL-51 aneuploid low, p53 null clones compared to p53 R273H mutant clones classified as having either low, medium, or high aneuploidy as described in (**d**). The number of differentially expressed genes ($P < 0.1$, $Log_2fc > |1|$) are shown in the upper right-hand corner of each plot. Genes with $P < 0.1$ are depicted in red. *P* values are adjusted for false discovery rate.

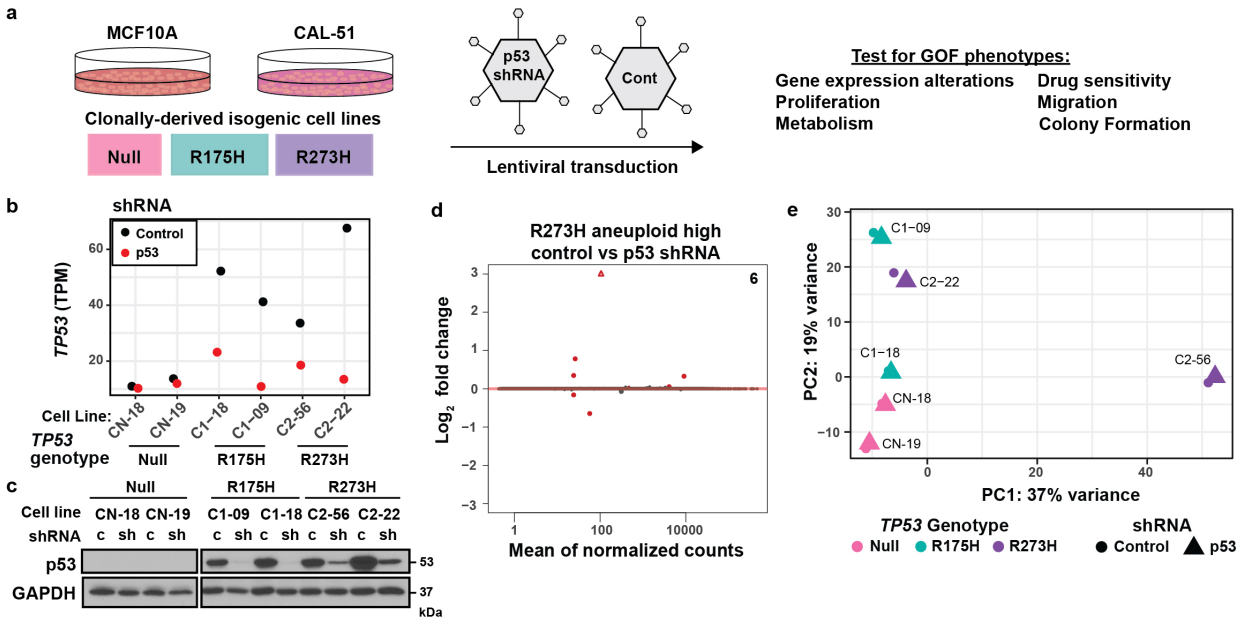

Figure 14. Generation of clonal lines with stable knockdown of p53 and characterization for gene expression analyses.

a Diagram demonstrating workflow of lentiviral-mediated shRNA knockdown of p53 or non-targeting control (cont) in isogenic MCF10A and CAL-51 null and *TP53* mutant (R175H and R273H) cell lines and phenotypic gain-of-function (GOF) characterization. **b** RNA-seq transcript per million (TPM) values for *TP53* in CAL-51 cells of the indicated genotype expressing p53 shRNA (p53, red) or non-targeting shRNA controls (control, black). **c** Western blot analysis of p53 and GAPDH protein in CAL-51 cells with p53 shRNA (sh) or non-targeting control shRNA (c). Blots are representative of at least two independent experiments. **d** MA plot showing the shrunken Log_2 fold change of all genes in CAL-51 R273H aneuploid high cells (C2-56 and C2-22) containing stable expression of p53 shRNA compared to the same cells containing non-targeting shRNA controls. The number of differentially expressed genes (False Discovery Rate adjusted $P < 0.1$, $Log_2fc > |1|$) are shown in the upper right-hand corner of each plot. Genes with $P < 0.1$ are depicted in red. **e** PCA plot for CAL-51 cells containing p53 shRNA (triangle) or non-targeting shRNA controls (control, circle).

Clonal *in vitro* gain-of-function phenotypes are associated with aneuploidy and not mutant p53 expression

Cancer cells with mutant p53 have been reported to have neomorphic activities leading to oncogenic phenotypes such as increased cellular proliferation rates (Lang et al., 2004), increased colony formation (Kalo et al., 2012; Liu et al., 2011), altered cellular and mitochondrial metabolism (Cordani et al., 2018; Eriksson et al., 2017; Kalo et al., 2012; Liu et al., 2015), and chemotherapeutic resistance (Aas et al., 1996; Blandino et al., 1999; Li et al., 1998). To determine if our mutant p53 cell lines displayed evidence of GOF activities *in vitro*, we performed a variety of functional assays using our full panel of MCF10A and CAL-51 cell lines. Assessment of proliferation through cell growth assays revealed no significant differences in doubling time for MCF10A and CAL-51 cells by *TP53* genotype (Fig. 15a) or upon stable p53 knockdown (Fig. 15b, Fig. 16a, b). Decreased proliferation has been associated with aneuploid states (Williams et al., 2008). Similarly, in both MCF10A and CAL-51 models, the average doubling time for aneuploid-high cells was higher than that of aneuploid-low cells (MCF10A $P = 0.035$, CAL-51 $P = 0.047$) (Fig. 17a). Colony formation assays also revealed no significant differences for MCF10A and CAL-51 cells by *TP53* genotype or with p53 knockdown; however, cell lines with the most colonies formed were among those with the highest AS (M1-33, C2-56, Fig. 15c, d), indicating that changes in cell growth in our clonal cell lines can be attributed to genetic variation caused by aneuploidy rather than *TP53* genotype.

We evaluated our cell lines for changes in cellular metabolism but observed no significant differences in the level of reactive oxygen species (ROS), mitochondrial

superoxides, mitochondrial mass, or mitochondrial membrane potential in MCF10A cells by *TP53* genotype (Fig. 17b-e). We did observe a significant difference in mitochondrial metabolism when measuring the reduction of resazurin in MCF10A R175H clonal lines; however, this increase was most notable in the cell line with the highest AS (M1-33) and did not change upon p53 knockdown (Fig. 15e, f, Fig. 17a). In the CAL-51 lines, there was not a significant difference in resazurin reduction relative to *TP53* genotypes or upon p53 knockdown (Fig. 15e, f and Fig. 16b). However, similar to the MCF10A model, cell lines with the highest metabolic activity were among those with the highest AS (CN-81, C1-06 and C2-56, Fig. 7a), and we observed a significant correlation between this metabolic activity and the AS calculated for each clone ($P = 0.0001$, Fig. 17f). In CAL-51 R273H mutant cells with varying aneuploidy (Fig. 17g), we observed that mitochondrial membrane potential was increased in three aneuploid R273H mutant lines compared to three non-aneuploid R273H mutant lines (Fig. 17h). Previous reports have shown that mutant p53 upregulates the mevalonate pathway (Freed-Pastor et al., 2012); however, analysis of RNA-seq data for mevalonate pathway gene expression revealed that expression was clonal, and not associated with the *TP53* genotype or AS, except in the CAL-51 model in which highly aneuploid samples showed increased expression of the gene NAD(P) Dependent Steroid Dehydrogenase-Like (*NSDHL)* (Fig. 17i). These data indicate that altered cellular metabolism is associated with aneuploidy and independent of *TP53* genotype.

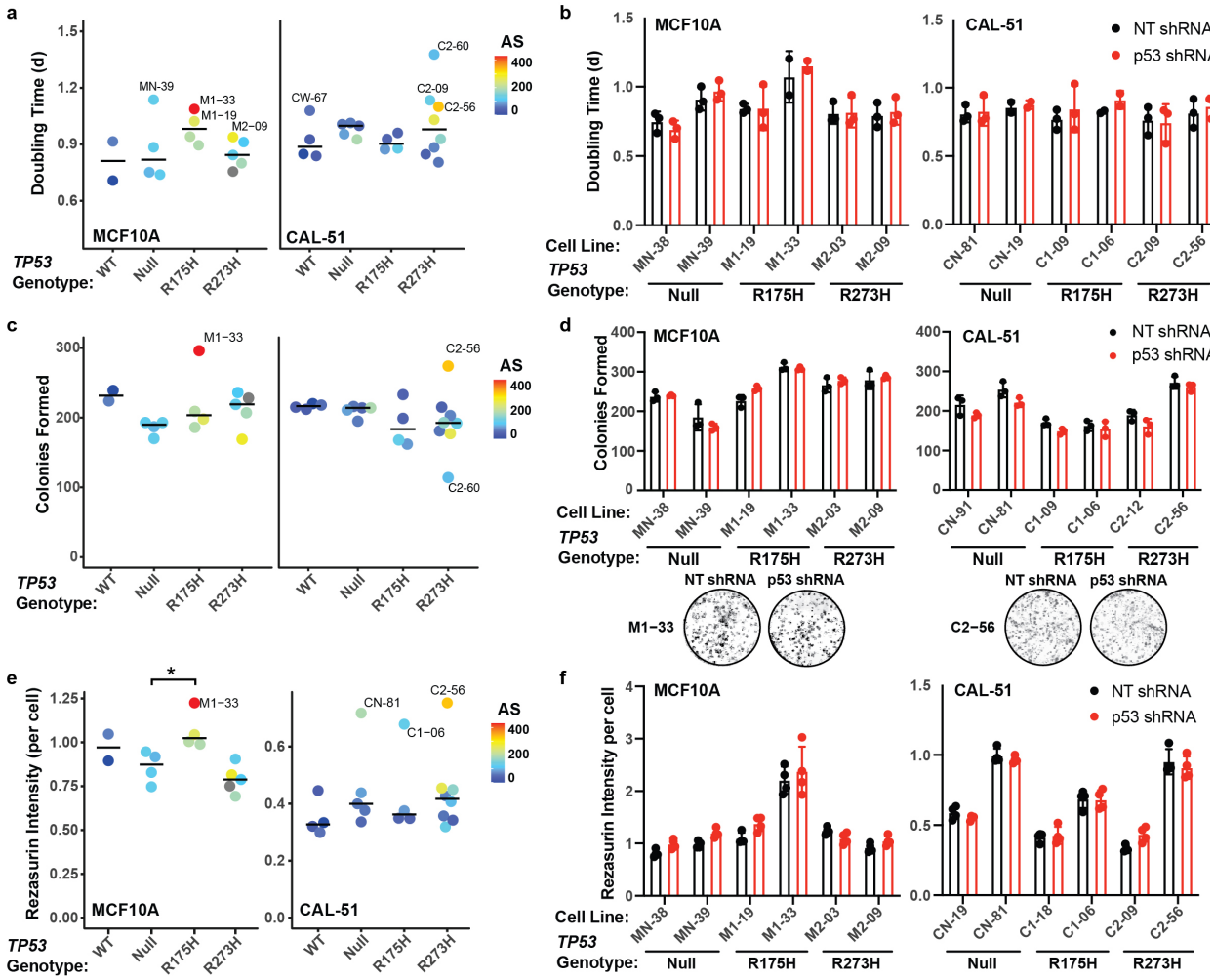

Figure 15: Differences in proliferation, colony formation and metabolism are associated with aneuploidy and not mutant p53 expression.
a Average doubling time in all MCF10A (left) and CAL-51 (right) clonal cell lines by *TP53* genotype. **b** Doubling time in MCF10A (left) and CAL-51 (right) cell lines of the indicated *TP53* genotype expressing either a non-targeting (NT, black) or p53 targeting shRNA (red). Mean ± standard deviation (s.d.) from *n* = 3 independent experiments per cell line (except M1-33, CN-19, and C1-06 cell lines, *n* = 2). **c** Average number of colonies formed in all MCF10A (left) and CAL-51 (right) cell lines by *TP53* genotype. **d** Average number of colonies formed in MCF10A (left) and CAL-51 (right) cell lines of the indicated *TP53* genotype expressing either a non-targeting (NT, black) or p53 targeting shRNA (red). Bottom, representative images. Mean ± s.d. of *n* = 3 technical replicates representative of at least two independent experiments per cell line. **e** Resazurin intensity per cell, in all MCF10A (left) and CAL51 (right) cell lines by *TP53* genotype. **f** Resazurin intensity per cell in MCF10A (left) and CAL-51 (right) non-targeting (NT, black) or p53 shRNA (red) containing cell lines. Mean + s.d. of *n* = 4 technical replicates, representative of at least two independent experiments per cell line. (**a, c, e)** Dots represent the mean per cell line (MCF10A *n* = 2 WT, 4 Null, 4 R175H, and 5 R273H cell lines; CAL-51 *n* = 4 WT, 5 Null, 4 R175H and 8 R273H cell lines) from at least two independent experiments. Bars indicate the median per genotype. Dots are colored by their calculated aneuploidy score (AS), and those colored in gray were not profiled in cytogenomic microarray experiments. One-way ANOVA with Dunnett's multiple comparison test, *$P <$ 0.026. (**b, d, f)** Significance tested using two-way analysis of variance with Sidak's multiple comparisons test. Western blots showing knockdown of p53 are shown in Fig. 16a, b. All analyses were conducted with the help of Hailing Jin. Colony formation images were quantified with the help of Johanna Schafer.

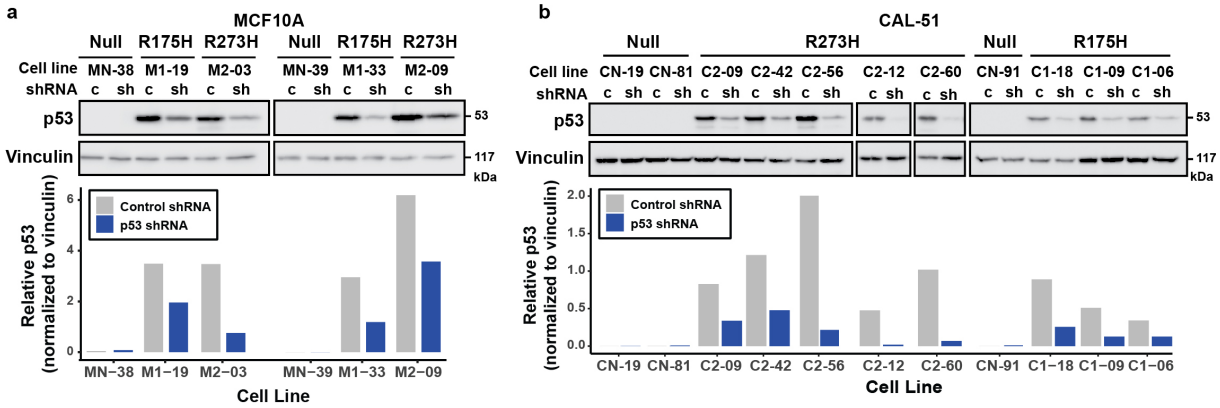

Figure 16. Analysis of p53 protein in MCF10A and CAL-51 clonal lines with stable p53 knockdown. **a - b** Western blot analyses of the indicated proteins in the indicated MCF10A (**a**) and CAL-51 (**b**) cells with p53 shRNA (sh) or non-targeting control shRNA (c). Lower panels display quantification of p53 protein levels (normalized to the loading control vinculin) and correspond to upper panels (**a – b**). Blots are representative of at least two independent experiments.

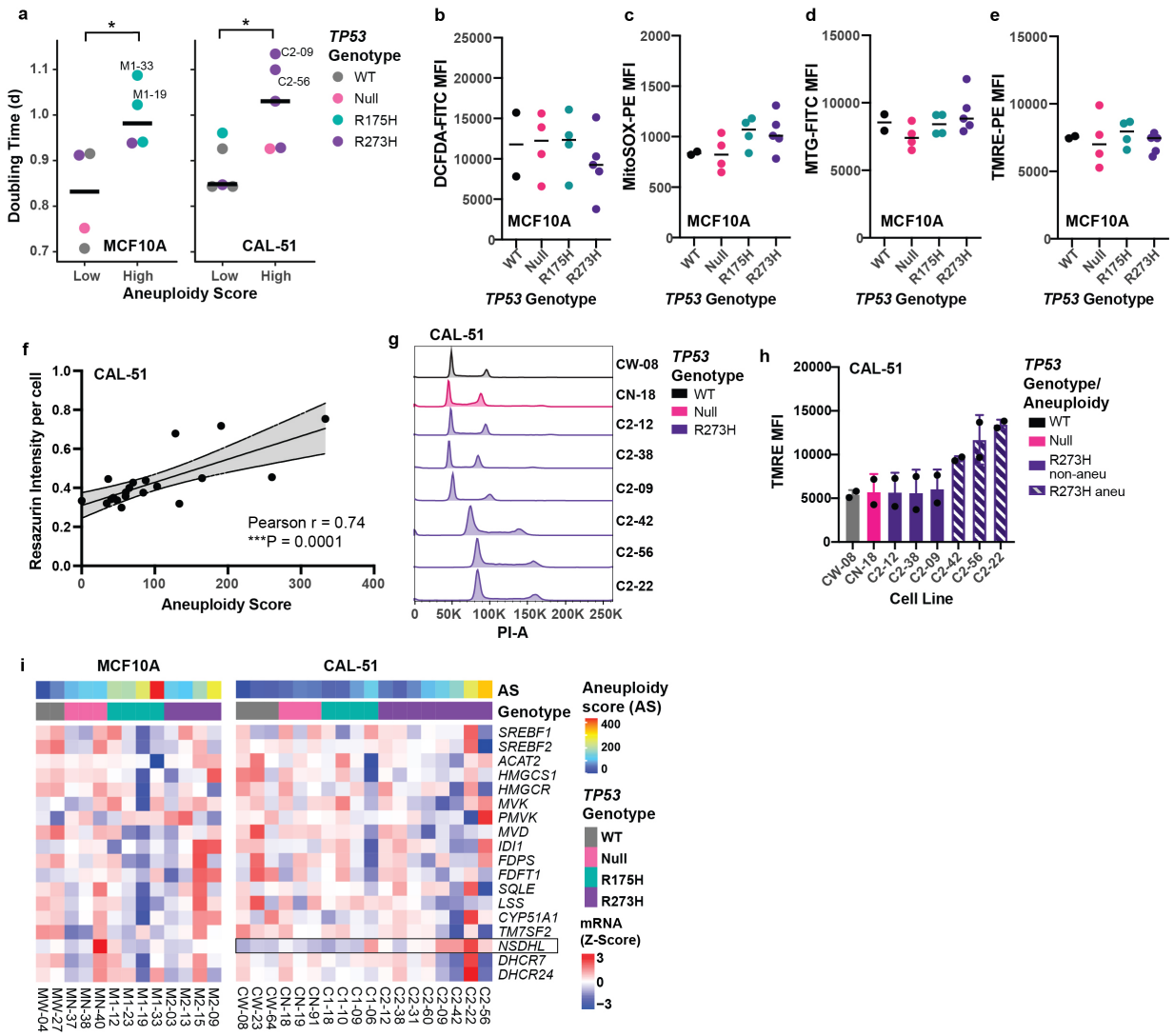

Figure 17. Analysis of proliferation and metabolic activity in isogenic clonally-derived lines.
a Doubling time in MCF10A (left) and CAL-51 (right) cells classified by aneuploidy score (AS) as either aneuploid-low (lower quartile AS) or aneuploid-high (upper quartile AS). Dots represent the mean for each cell line from at least two independent experiments. Bar indicates median value per group. **P* = 0.0348, 0.0469, from left to right, Two-tailed student's t-test. **b - e** Dot plots showing intensity of the metabolic indicators (**b**) DCFDA (reactive oxygen species) (**c**) MitoSOX (mitochondrial superoxides) (**d**) MTG (mitochondrial mass) and (**e**) TMRE (mitochondrial membrane potential), across all MCF10A cell lines with the indicated *TP53* genotype (*n* = 2 WT, 4 Null, 4 R175H, and 5 R273H). Each point represents the average geometric mean fluorescent intensity (MFI). Bars indicate the median staining for each genotype from two independent experiments. **f** Scatter plot showing aneuploidy score versus the average resazurin staining intensity for all CAL-51 cell lines. The black line represents a linear model of the best fit, with the gray area representing the 95% confidence intervals. Significance was determined using Pearson correlation, ****P* = 0.0001. **g** Cell cycle distributions showing DNA content of cells in (**h**) by propidium iodide (PI) staining and flow cytometry in the CAL-51 isogenic model. Colors represent *TP53* genotype (black = WT, pink = Null, purple = R273H). **h** Bar graph showing TMRE mean fluorescent intensity of CAL-51 non-aneuploid (solid purple) and aneuploid (dashed purple) R273H cell lines. Mean + s.d. from n = 2 independent experiments. **i** Heatmaps comparing gene expression for mevalonate pathway transcription factors and genes encoding for pathway enzymes in MCF10A (left) and CAL-51 (right) cell lines. Metabolic analyses shown in **b - e** were conducted with the help of Rachel Hongo and Katy Beckermann.

To determine if R175H or R273H *TP53* mutations confer resistance to commonly used cancer chemotherapeutic agents, we treated all clonal lines in both models with increasing concentrations of doxorubicin or paclitaxel for 72 h. Significant changes in drug sensitivity were observed when comparing cells with p53 LOF (null, R175H, or R273H) to WT cells (MCF10A, doxorubicin [$P = 0.027$]; CAL-51, doxorubicin [$P = 0.009$] and paclitaxel [$P < 0.0001$]) (Fig. 18a, b). However, there was no significant difference in sensitivity when comparing either R175H or R273H mutant lines to *TP53* null cells in either model or with knockdown of p53 (Fig. 18a-d, Fig. 16a, b). The heat shock protein 90 (Hsp90) inhibitor 17-AAG and histone deacetylase (HDAC) inhibitor SAHA (Vorinostat) have been reported to decrease cell viability in mutant p53-containing cancer cells (Li et al., 2011a, 2011b). However, CAL-51 cells showed no significant differences in 17-AAG or SAHA IC_{50} values by *TP53* genotype (Fig. 18e, f) or after p53 knockdown (Fig. 18g, Fig. 16b). Compared to aneuploid-low cells, aneuploid-high cells had significantly increased sensitivity to SAHA ($P = 0.0006$) (Fig. 18h). Altogether, these data indicate that *in vitro* GOF phenotypes are not associated with mutant p53 expression but can be associated with genomic alterations such as aneuploidy that occur following the loss of p53 function.

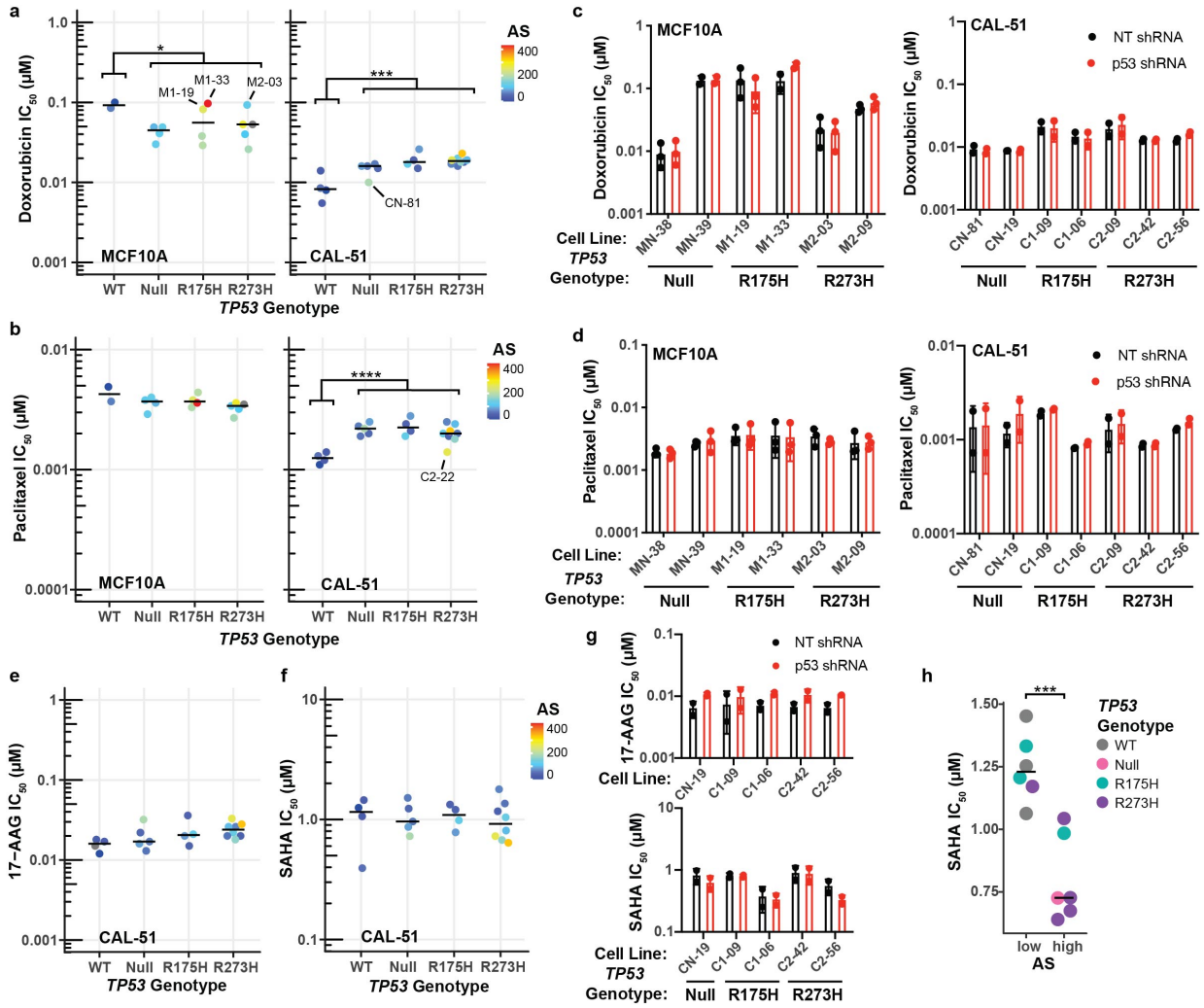

Figure 18: Clonal differences in drug sensitivity are associated with aneuploidy and not mutant p53 expression.

a, b IC_{50} values for MCF10A (left) and CAL-51 (right) cell lines treated for 72 h with increasing concentrations of either doxorubicin (**a**) or paclitaxel (**b**). **c, d** IC_{50} values in MCF10A (left) and CAL-51 (right) cell lines containing non-targeting control (NT, black) or p53 shRNAs (red) after treatment with doxorubicin (**c**) or paclitaxel (**d**). Mean ± s.d. from *n* = 2 two independent experiments per CAL-51 cell line, or *n* = 3 for MCF10A cell lines (except for MN-39, and M1-33 in (**c**), *n* = 2). **e, f** IC_{50} values for CAL-51 cell lines treated for 72 h with increasing concentrations of either 17-AAG (**e**) or SAHA (**f**). **g** Mean 17-AAG (top) and SAHA (bottom) IC_{50} values in CAL-51 cell lines containing non-targeting (NT, black) or p53 shRNAs (red). Mean ± s.d. from *n* = 2 independent experiments per cell line. **h** Mean SAHA IC_{50} values for *n* = 6 high-aneuploid and *n* = 6 low-aneuploid (upper and lower quartile AS, respectively) CAL-51 cell lines. Colors indicate *TP53* genotype. Two-tailed student's t-test, ***$P = 0.0005$. (**a, b, e, f**) Dots represent the mean for each cell line from at least two independent experiments. Bars represent the median per *TP53* genotype. Dots are colored by their calculated aneuploidy score (AS), and those colored in gray were not profiled in cytogenomic microarray experiments. *$P < 0.05$, ***$P < 0.001$, ****$P < 0.0001$, Two-tailed student's t-tests. Significance between *TP53* genotypes tested using one-way ANOVA with Dunnett's multiple comparison test. (**c, d, g**) Significance tested using two-way analysis of variance with Sidak's multiple comparisons test. Western blots showing knockdown of p53 are shown in Fig. 16a, b. All analyses were conducted with the help of Hailing Jin.

Clonal differences in tumorigenicity are associated with aneuploidy and not p53 genotype

It has been reported that tumor cells with *TP53* mutations display more aggressive features in murine models (Dittmer et al., 1993; Liu et al., 2011). To investigate if our p53 mutant-containing cell lines displayed gain-of-function activities that would lead to increased tumorigenesis *in vivo*, we evaluated xenograft tumor growth of our MCF10A and CAL-51 cell lines after subcutaneous injection (Fig. 19a and Fig. 20a). MCF10A cell lines did not form tumors in mice, regardless of *TP53* genotype or DNA content (Fig. 20b, c). CAL-51 cell lines showed significant differences in tumor growth by *TP53* genotype, with *TP53* null cell lines having significantly increased tumor growth compared to *TP53* WT, R175H or R273H mutant cells (WT vs Null, $P = 0.035$; R175H vs Null, $P = 0.008$; R273H vs Null, $P = 0.022$; Fig. 21b). While tumor growth was variable across CAL-51 cells regardless of *TP53* genotype, we noticed a trend where CAL-51 cells with a higher AS displayed increased tumor growth (e.g., C2-56, CN-81, C2-42, Fig. 19c, Fig. 20d). However, not all highly aneuploid cells showed increased growth (e.g., C1-06). Our data are consistent with previous reports that aneuploidy can be either tumor-promoting or tumor suppressive (Vasudevan et al., 2020, 2021). Additionally, cell line CN-19 displayed no detectable aneuploidy but was the most tumorigenic (Fig. 19c, Fig. 20d). To further investigate the observed correlation between tumor growth and aneuploidy, we isolated a diploid and tetraploid sub-clonal cell line from C2-09, a CAL-51 R273H mutant cell line with an intermediate growth phenotype (Fig. 19d). The tetraploid clone 9B6 displayed significantly increased xenograft tumor growth ($P = 0.001$, Fig. 19e) and final tumor weight ($P = 0.019$, Fig. 19f) compared to

the diploid clone 9B11. Analysis of tumor DNA through CMA revealed the 9B6 clone was highly aneuploid compared to clone 9B11 (Fig. 19g). In summary, cell lines with mutant p53 did not preferentially show increased tumorigenicity *in vivo*; rather, the feature of increased aneuploidy in p53 mutant cells was associated with increased tumorigenicity *in vivo*.

Metastatic phenotypes are associated with aneuploidy and not mutant p53 expression

Mutant p53 has been associated with cellular features leading to metastatic progression, such as enhanced migration (Adorno et al., 2009; Lang et al., 2004; Olive et al., 2004; Subramanian et al., 2015; Sun et al., 2020; Yeudall et al., 2012). We performed trans-well migration assays to determine if mutant p53 alters cellular migration in our isogenic cell line models. We did not observe a statistical difference in the average relative migration in either MCF10A or CAL-51 clonally derived cell lines across *TP53* genotypes (Fig. 21a), and knockdown of p53 did not significantly alter migration relative to any genotype in MCF10A or CAL-51 cells (Fig. 21b, Fig. 16a, b). While the level of migration was variable across each clonal cell line, the CAL-51 R273H mutant lines with the highest overall relative migration were among those with the most elevated AS (Fig. 21a, clones C2-60, C2-56 and C2-22). Note that not all aneuploid cell lines showed increased migration (e.g., MCF10A M1-33, CAL-51 CN-81 and C1-06), suggesting specific chromosomal alterations and not the degree of aneuploidy resulted in increased migration.

To determine if cells with *TP53* mutations have increased metastasis *in vivo*, we utilized the MetMap500, MetMap125, and MetMap Basal-like datasets from the metastasis map (MetMap) project, which provided the metastatic potential of barcoded and pooled cancer cell lines following cardiac injection in mice (Fig. 21c) (Jin et al., 2020). We compared the metastatic potential of cell lines that were p53 WT or contained either missense or truncating mutations in *TP53*. Across all three datasets, we found no statistical difference in the metastatic potential of cell lines based on *TP53* genotype (Fig. 21d). While there is no correlation between total aneuploidy and metastatic potential in these datasets (Jin et al., 2020), others have shown that chromosomal alterations are enriched and drive metastatic tumor formation (Bakhoum et al., 2018; Vasudevan et al., 2020). Similarly, our results indicate that differences in metastatic phenotypes such as increased migration are not dependent on the expression of mutant p53 or total levels of aneuploidy but are likely the result of specific chromosomal alterations.

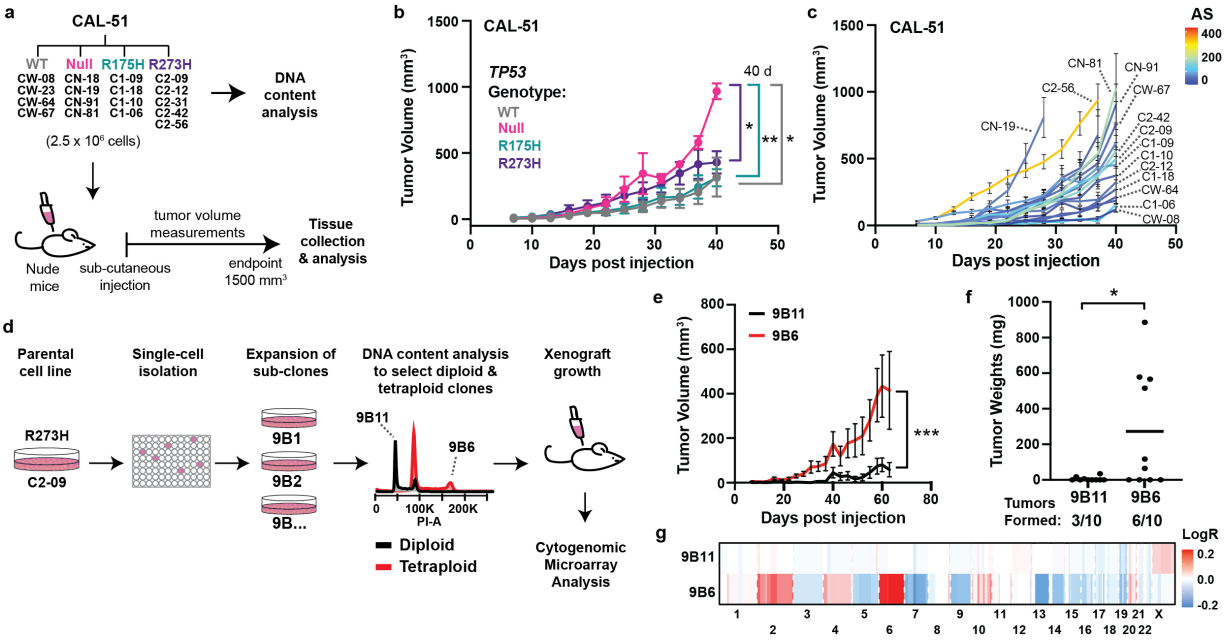

Figure 19: Clonal differences in tumorigenicity are associated with aneuploidy and not mutant p53 expression.

a Diagram demonstrating workflow for CAL-51 xenograft tumor growth experiment. **b, c** Tumor volume (in cubic millimeters) of CAL-51 cell lines. Data shown represent the mean ± standard error of the mean (s.e.m.) tumor volume (n = 10 tumors per cell line) measured across CAL-51 cell lines indicated in (**a**) averaged by (**b**) *TP53* genotype or (**c**) colored by aneuploidy score (AS). **d** Diagram demonstrating workflow for single cell isolation and subcutaneous xenograft experiment of CAL-51 diploid (9B11) and tetraploid (9B6) R273H mutant p53 sub-clones. **e**, **f**, Tumor volume (**e**) and tumor weights (**f**) for 9B11 and 9B6 sub-clone xenografts. Data shown represent the mean ± s.e.m. tumor volume measured every three days (n = 10 tumors per cell line). **g** Copy number alterations from cytogenomic microarray analyses in 9B11 and 9B6 sub-clones (Log_2 ratios, LogR). Chromosomal gain (red) and loss (blue). Significance tested using (**b**) mixed-effects analysis with Dunnett's multiple comparison test, (**e, f**) Two-tailed student's t-tests. **P* < 0.05, ***P* < 0.01, ****P* < 0.001. Xenograft experiments were conducted with the assistance of Brian Lehmann and Clayton Marshall.

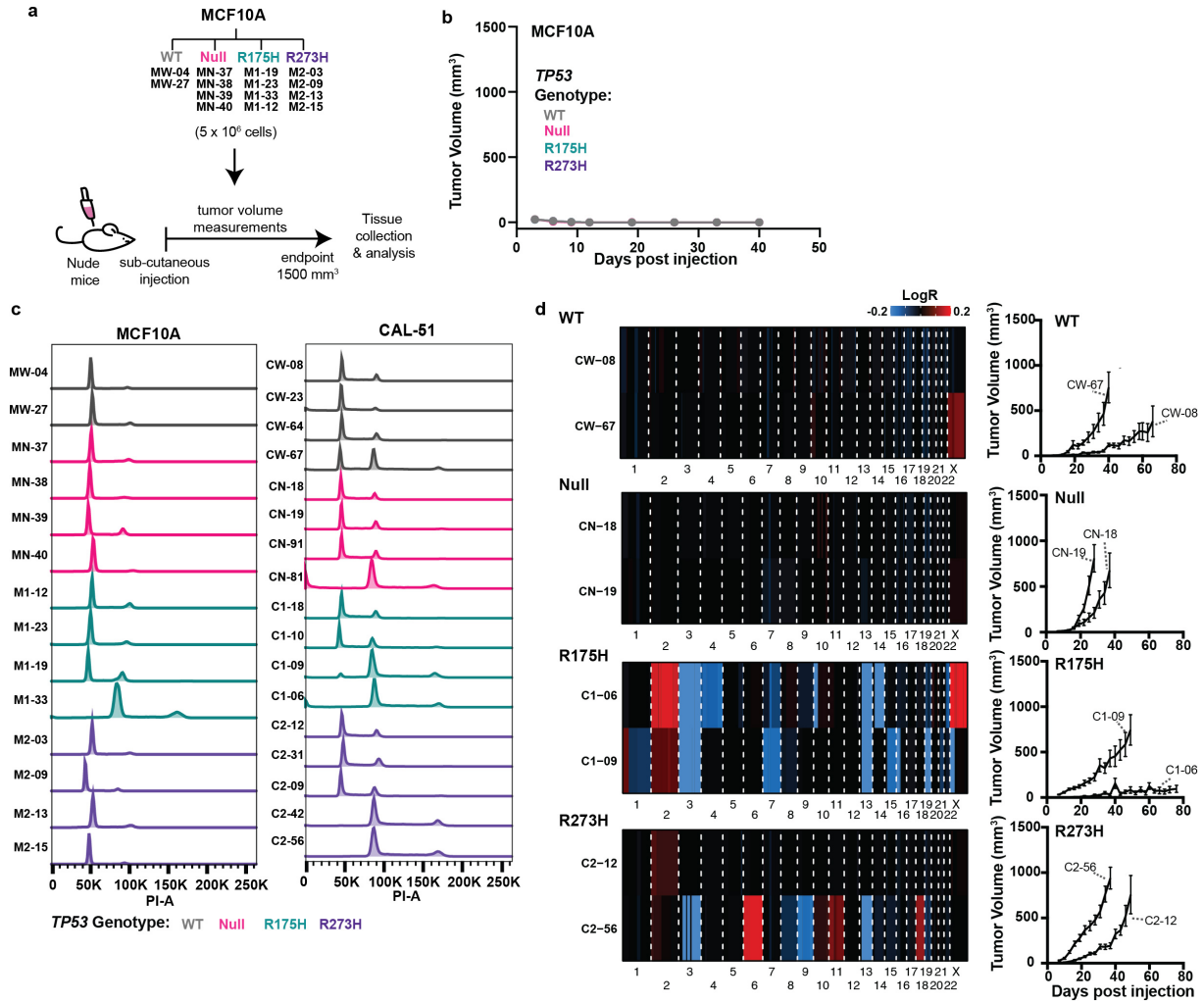

Figure 20. Analysis of tumorigenicity and aneuploidy in MCF10A and CAL-51 cells.
a Diagram demonstrating workflow for MCF10A xenograft tumor growth experiment. **b** Tumor volume (in cubic millimeters) of MCF10A cell lines. Data shown represent the mean ± s.e.m. of tumor volume (*n* = 10 tumors per cell line) measured every three days (for palpable tumors) or weekly for mice with no detectable tumor across MCF10A cells indicated in (**a**) by *TP53* genotype. **c** Histograms showing DNA content of injected MCF10A (left) and CAL-51 (right) xenograft cells by flow cytometry of propidium iodide (PI) stained cells. Colors represent *TP53* genotype. **d** Copy number alterations from cytogenomic microarray analyses of tumor DNA (left) from select corresponding CAL-51 cell line xenografts (right). Xenograft growth was measured as tumor volume (in cubic millimeters) and represents the mean ± s.e.m of *n* = 10 tumors per cell line. Chromosomal gain (red) and loss (blue). Xenograft experiments were conducted with the assistance of Brian Lehmann and Clayton Marshall.

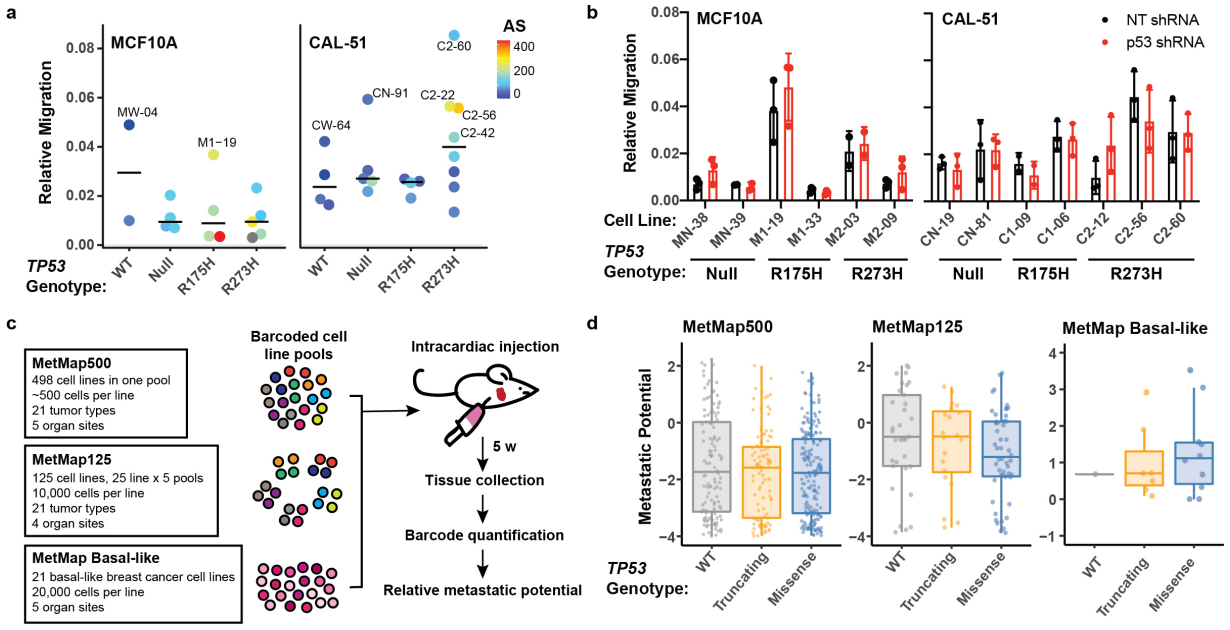

Figure 21: Metastatic phenotypes are associated with aneuploidy and not mutant p53 expression. **a** Quantification of the relative migration (mean cells per field from three technical replicates normalized to the number of cells seeded, arbitrary units) of MCF10A (left) and CAL51 (right) cells that crossed the membrane in transwell assays. Each dot represents the mean relative migration for each cell line (MCF10A *n* = 2 WT, 4 Null, 4 R175H, and 5 R273H cell lines; CAL-51 *n* = 4 WT, 5 Null, 4 R175H and 8 R273H cell lines) from at least two independent experiments. Bars represent the median value per *TP53* genotypes. Dots are colored by aneuploidy score, and those colored in gray were not profiled in cytogenomic microarray experiments. **b** Quantification of relative migration, as described above, in MCF10A (left) and CAL-51 (right) cells containing non-targeting (NT, black) or p53 shRNAs (red). Mean ± s.d. from *n* = 3 independent experiments (except MN-39, M2-03, and C1-09 cell lines, *n* = 2). Western blots showing knockdown of p53 are shown in Fig. 16a, b. **c** Diagram demonstrating workflow for metastatic datasets generated in the MetMap project(Jin et al., 2020). **d** Box and whisker plots of the metastatic potential in cells with wild-type (WT), missense or truncating mutations in *TP53* in the MetMap500 (left; WT n = 129, Trunc. N = 101, Miss. N = 195), MetMap125 (middle; WT n = 33, Trunc. N = 20, Miss. N = 50) and MetMap Basal-like (right; WT n = 1, Trunc. N = 7, Miss. N = 10) datasets. Points represent mean metastatic potential across all sites. Boxplot elements: center line, median; box limits, upper and lower quartiles; whiskers, 1.5x interquartile range. Significance tested using (**a**) one-way analysis of variance (ANOVA) with Dunnett's multiple comparisons test, (**d**) two-way ANOVA with Sidak's multiple comparisons test and (**c**) one-way ANOVA with Tukey's multiple comparison test. Migration images were quantified with the help of Johanna Schafer.

Aneuploidy and loss of p53 function associate with unfavorable prognosis

TP53 mutation strongly correlates with the development of aneuploidy (Ciriello et al., 2013; Taylor et al., 2018), and both *TP53* mutation and aneuploidy have been associated with unfavorable prognostic features in multiple cancer types (Hieronymus et al., 2018; Kandoth et al., 2013; Olivier et al., 2006; Silwal-Pandit et al., 2014; Smith and Sheltzer, 2018; Stopsack et al., 2019). Thus, we determined the relationship between missense *TP53* mutations, aneuploidy status, and survival across human tumor types. We first analyzed the fraction of the genome altered (FGA) by aneuploidy in tumors across 19 cancer types (TCGA, n = 6682; abbreviations defined in Table 3) that contained either missense or truncating mutations in *TP53*. Similar to previous findings (Smith and Sheltzer, 2018), the FGA was significantly increased across a majority of tumor types with either truncating or missense mutations in *TP53* compared to those with WT p53 (Fig. 22a). Uterine carcinosarcoma (UCS), uterine corpus endometrial carcinoma (UCEC), lung squamous cell carcinoma (LUSC), ovarian (OV), and breast cancers (BRCA) with missense *TP53* mutations displayed the highest median FGA across all cancer types (Fig. 22a). Breast and sarcomas were the only cancer types that displayed a significant difference between missense and truncating *TP53* mutations, with tumors containing truncating *TP53* mutations having increased FGA. Not all missense mutations in *TP53* equally disrupt p53 function, so we assessed aneuploidy in the top five most frequent missense and truncating amino acid changes across the above tumor types with the highest median FGA (UCS, UCEC, OV, BRCA, and LUSC). Tumors with WT p53 had a significantly lower FGA compared to truncating or missense mutations ($P < 0.0001$); however, there was no statistical difference between high-

frequency missense and truncating p53 alterations (Fig. 22b). This data suggests that loss of p53 function leads to increased aneuploidy, irrespective of the type of point mutation.

To determine if individuals with tumors containing missense versus truncating mutations experienced differential survival, we compared the progression-free survival in individuals with BRCA, OV, UCEC, UCS, and LUSC. Individuals with tumors containing either missense or truncating mutations in *TP53* displayed significantly worse survival when compared to those with WT p53 ($P < 0.0001$). There was no statistical difference in survival between individuals with tumors containing either missense or truncating mutations in p53 (Fig. 22c). To assess the relationship of tumor aneuploidy with survival, independent from *TP53* mutation, we stratified individuals with tumors containing WT, missense, or truncating mutations in *TP53* into either aneuploid-high (upper quantile FGA) or aneuploid-low (lower quantile FGA) groups. All individuals with aneuploid-high tumors, regardless of p53 genotype, showed significantly worse survival outcomes compared to aneuploid-low tumors (WT $P = 0.008$, truncating $P = 0.004$, missense $P < 0.0001$) (Fig. 22d-f). In summary, these data indicate that progression-free survival is not directly associated with *TP53* mutation type (truncating vs. missense). Instead, an individual's outcome is associated with the loss of p53 function and increased genomic alterations in their tumor(s).

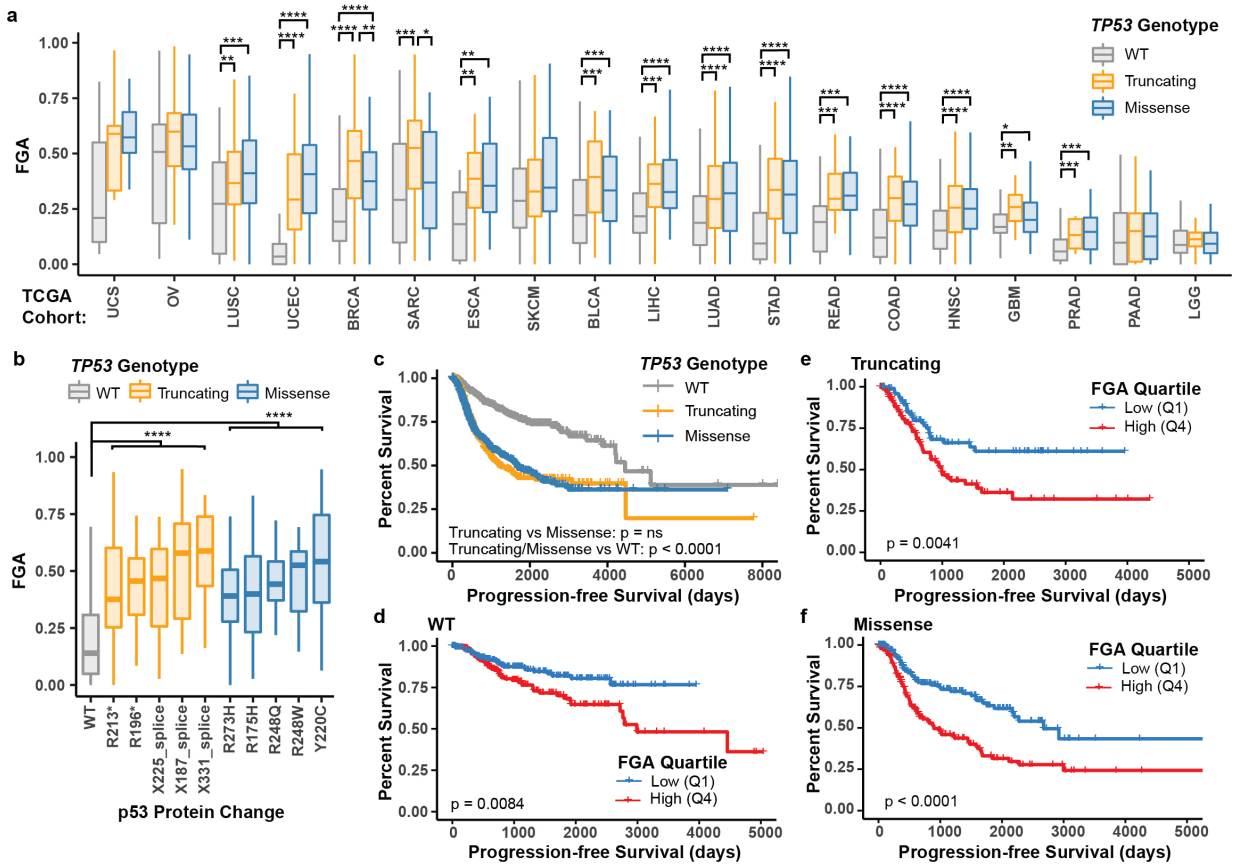

Figure 22: Aneuploidy and loss of p53 function associate with unfavorable prognosis.
a, b Box and whisker plots of the fraction of the genome altered (FGA) in tumors with wild-type (WT), missense or truncating mutations in *TP53* compared (**a**) across cancer types (source: The Cancer Genome Atlas [TCGA]), or (**b**) in BRCA, OV, UCEC, UCS and LUSC cancer types across the five most frequent truncating or missense mutations. Cohort acronyms and values for *n* can be found in Table 3. Pairwise two-sided Wilcoxon test with Benjamini-Hochberg *P* value correction, **P* < 0.05, ***P* <0.01, ****P* < 0.001, *****P* < 0.0001. Boxplot elements: center line, median; box limits, upper and lower quartiles; whiskers, 1.5x interquartile range. **c – f** Kaplan-Meier curves showing progression-free survival of individuals with BRCA, OV, UCEC, UCS, and LUSC separated by *TP53* genotype (**c**) or further divided into aneuploid-low (blue, lower quantile FGA, Q1) or aneuploid-high (red, upper quantile FGA, Q4) groups in individuals with tumors containing WT (**d**), truncating (**e**), or missense (**f**) mutant *TP53*. Log-rank tests.

			Tumors per indicated TP53 Genotype		
Study Abbreviation	**Study Name**	**Tumors (total)**	**WT**	**Truncating**	**Missense**
BLCA	Bladder urothelial carcinoma	344	196	51	97
BRCA	Breast invasive carcinoma	985	658	130	197
COAD	Colon adenocarcinoma	339	163	40	136
ESCA	Esophageal carcinoma	131	17	44	70
GBM	Glioblastoma multiforme	333	244	16	73
HNSC	Head and Neck squamous cell carcinoma	352	128	102	122
LGG	Brain lower grade glioma	425	255	23	147
LIHC	Kidney renal papillary cell carcinoma	342	245	37	60
LUAD	Lung adenocarcinoma	432	220	75	137
LUSC	Lung squamous cell carcinoma	380	55	118	207
OV	Ovarian serous cystadenocarcinoma	352	29	125	198
PAAD	Pancreatic adenocarcinoma	152	55	39	58
PRAD	Prostate adenocarcinoma	461	409	16	36
READ	Rectum adenocarcinoma	128	36	30	62
SARC	Sarcoma	231	153	37	41
SKCM	Skin cutaneous Melanoma	409	345	28	36
STAD	Stomach adenocarcinoma	376	201	69	106
UCEC	Uterine corpus endometrial carcinoma	461	304	40	117
UCS	Uterine carcinosarcoma	49	5	8	36

Table 3. TCGA cohort acronyms and the number of tumors analyzed.
Cancer studies from The Cancer Genome Atlas, study abbreviations and the number of tumors analyzed for each *TP53* genotype.

Discussion

The concept of mutant p53 GOF was introduced over 30 years ago (Dittmer et al., 1993; Halevy et al., 1990). Since then, many publications have reported context-specific and conflicting evidence for oncogenic phenotypes arising from overexpression of the mutant protein. As described in this chapter, we generated and characterized two breast epithelial isogenic models with cells differing only by the presence or absence of mutant p53 protein. We examined several reported mutant p53 GOF phenotypes in our cell line models and found no evidence for GOF activities by mutant p53 protein.

Two prominent hallmarks of human tumors are aneuploidy and mutation *TP53*. Given the strong associations between p53 mutations and the development of aneuploidy in human tumors (Ciriello et al., 2013; Davoli et al., 2017; Taylor et al., 2018), and the diverse cellular consequences that accompany aneuploidy (Beach et al., 2017; Chunduri and Storchová, 2019; Santaguida and Amon, 2015; Sheltzer and Amon, 2011), we speculated that aneuploidy itself could be a mechanism accounting for the diversity of reported GOF phenotypes. Through the use of our clonally derived cell lines which originated from the same near-diploid parental genetic background, we assessed the molecular heterogeneity and genomic alterations that occurred following mutation of *TP53*. Through our comparative analyses of isogenic epithelial cells, which initially differed only by *TP53* genotype, we discovered that increased aneuploidy is consistently observed in our mutant p53-expressing cell lines. Further, we discovered that *in vitro* GOF phenotypes are only present in mutant p53-expressing cell lines that display increased aneuploidy and that these phenotypes are not dependent on mutant p53

protein expression. Mutant p53-containing cell lines did not have increased tumorigenicity or metastasis *in vivo*, and analysis of human tumors revealed that loss of p53 function and increased aneuploidy were associated with unfavorable prognoses. Importantly, our results reveal aneuploidy as a mechanism contributing to the diversity of reported mutant p53 GOF phenotypes. Given our findings and current efforts to target mutant p53 protein for therapeutic purposes, it will be of interest to determine if other GOF activities exist independent from aneuploidy development.

Proponents of the mutant p53 GOF hypothesis have argued that the accumulation of specific high-frequency hotspot p53 mutants suggests that GOF activities confer a fitness advantage. However, many hotspot mutations, including R273 and R175, contain methylated CpG dinucleotides, rendering them more likely to mutate by spontaneous deamination (Rideout et al., 1990). Recent findings confirmed that natural mutational processes combined with LOF and dominant-negative activities select for the spectrum of *TP53* mutations (Giacomelli et al., 2018); additionally, this work found that the growth of an extensive panel of cell lines was not dependent on mutant p53 protein expression. These findings were corroborated by a study of mutant p53 isogenic models of myeloid malignancies showing no evidence of GOF, but instead LOF and dominant-negative activities over WT p53 protein (Boettcher et al., 2019). Two concurrent studies of mouse models harboring the knock-in *TP53* mutations equivalent to R175H and R273H showed persuasive but conflicting evidence for GOF *in vivo*, with an increased incidence of carcinomas in R175H/- (Olive et al., 2004) but not R175H/R175H (Lang et al., 2004) mice. The latter inconsistency was attributed to differing murine genetic backgrounds. Of note, tumors from R175H/- mice displaying

altered tumor spectra also showed enlarged nuclei and polyploid cells in hematoxylin and eosin-stained tumor sections (Olive et al., 2004), consistent with the notion that aneuploidy could underlie differences in tumor development and GOF activities reported using these models.

The increased aneuploidy observed in our mutant p53 cell lines is consistent with previous studies (Duensing and Duensing, 2005; Hanel and Moll, 2012). There is a strong correlation between *TP53* mutation and aneuploidy in human tumors (Ciriello et al., 2013; Taylor et al., 2018), and analyses of medulloblastoma tumors and acute myeloid leukemias from Li-Fraumeni Syndrome (LFS) individuals with somatic *TP53* mutations showed increased chromothripsis (Rausch et al., 2012). Fibroblasts from LFS individuals accumulate aneuploid cells (Bischoff et al., 1990; Boyle et al., 1998), as do normal human and murine fibroblasts with exogenous expression of *TP53* missense mutations (Gualberto et al., 1998; Liu et al., 1996; Talos et al., 2007). Further, a study of LFS individuals revealed that those who developed cancer had a striking enrichment in germline copy number variation (Shlien et al., 2008), suggesting that aneuploidy following p53 LOF leads to tumorigenesis. The latter is supported by the wide range of tumorigenic phenotypes caused by aneuploidy (Ben-David and Amon, 2020; Chunduri and Storchová, 2019; Zhu et al., 2018), many of which have been associated with mutant p53 GOF activities, including, but not limited to: altered proliferation (Williams et al., 2008); altered metabolism (Hwang et al., 2017; Stingele et al., 2012); transcriptional reprogramming and drug resistance (Kim et al., 2018); immune evasion (Davoli et al., 2017); migration (Vasudevan et al., 2020); and invasion and metastasis (Bakhoum et al., 2018). Given the strong propensity for cells containing mutant p53 to become

aneuploid and the overlap of tumorigenic phenotypes related to both alterations, GOF phenotypes identified in mutant p53 models must be carefully validated relative to corresponding chromosomal changes.

The underlying mechanisms behind the increased aneuploidy we observed in our engineered lines require further study, although many potential mechanisms, such as loss of cell cycle checkpoints, have been previously reported (Hanel and Moll, 2012). Our study was limited by the number of independent cell lines assayed and the technology available to evaluate aneuploidy. Finally, our work only examined two specific hotspot p53 missense mutations in two cell line models; thus, we cannot exclude the existence of select GOF activities occurring in cells containing other p53 missense mutants or existing in different tissue-specific cellular contexts. In addition, further studies are needed to determine the effect of oncogenic mutations, not present in the model systems used in the current study, on potential mutant p53 GOF activities.

In summary, our study demonstrates that the acquisition of aneuploidy can generate a variety of the previously ascribed mutant p53 GOF phenotypes. Further, our data showed the heterogeneity of genomic alterations that can occur following mutation of p53, consistent with the diverse and sometimes conflicting phenotypes observed in prior reports. While we cannot rule out the existence of p53 mutant-specific GOF effects in other models, future studies should carefully consider how the genomic changes that occur after the loss of WT p53 can confound and contribute to GOF phenotypes. Acquisition of aneuploidy after the loss of WT p53 function provides a unifying mechanism that accounts for the wide array and context-specific nature of GOF phenotypes previously attributed to p53 mutant proteins.

CHAPTER IV

ANALYSIS OF MUTANT P53 PROTEIN ACCUMULATION

Introduction

Proper regulation of p53 protein stability is critical for its tumor suppressor activities. In addition to mutation or deletion of *TP53*, dysregulation of p53 protein stability also contributes to p53 inactivation through both MDM2-dependent and independent mechanisms. For example, tumor cells that maintain wild-type p53 often overexpress the E3 ubiquitin ligase, MDM2, or other negative regulators of the protein (Bulavin et al., 2002; Momand et al., 1998). Less is known about mutant p53 regulation; however, similar to the WT protein, mutant p53 can be stabilized in response to various cellular stresses (Boettcher et al., 2019; Redman-Rivera et al., 2021; Terzian et al., 2008). Compared to WT p53, which has a half-life of approximately 30 minutes (Reich and Levine, 1984), mutant p53 proteins have significantly increased half-lives of several hours (Giaccia and Kastan, 1998; Oren et al., 1981).

A commonly observed feature of cancer cells that contain *TP53* missense mutations is elevated levels of p53 protein. This accumulation is not an intrinsic property of the mutant protein as high expression is not seen in most normal tissues of mutant p53 murine models and LFS patients (Lang et al., 2004; Olive et al., 2004; Soussi, 2007; Terzian et al., 2008). However, mutant p53 accumulation has been shown in some normal tissues, such as proliferating cells of small intestinal crypts of engineered murine models containing mutant p53, in a manner dependent on gene dosage and cell

type (Goh et al., 2015). Thus, it is hypothesized that elevated mutant p53 protein in some normal tissues, transformed cells and tumors requires secondary events (Terzian et al., 2008).

Mechanisms underlying the accumulation of mutant p53 protein are poorly understood, although it was initially thought that mutant accumulation is primarily due to loss of WT p53-mediated MDM2 transactivation and thus negative regulation. However, mutant p53 murine models with MDM2 knockout display stabilized mutant p53 in some but not all tissues, indicating that other factors besides MDM2 contribute to mutant p53 stability. Other cancer cell-specific factors, such as oncogenic alterations like c-Myc and PTEN overexpression, have been identified to contribute to mutant p53 protein accumulation (Suh et al., 2011; Terzian et al., 2008).

Mutant p53 accumulation has been proposed to be necessary for mutant p53 proteins to exert putative GOF effects (Brosh and Rotter, 2009; Yue et al., 2017). A study of mutant p53 mice with MDM2 knockout and stabilized mutant protein showed the animals had significantly decreased survival and increased frequency of metastatic lesions compared to mice with stabilized mutant p53 protein (Terzian et al., 2008). However, MDM2 loss may have other cellular consequences that contribute to this phenotype. Song and colleagues have suggested that protein accumulation can enhance novel interactions between mutant p53 and other cellular proteins, further contributing to proposed GOF activities (Song et al., 2007).

Because of the reported roles for mutant p53 accumulation contributing to GOF phenotypes in cells, destabilization of mutant p53 protein is currently being studied as a potential cancer therapy (Parrales and Iwakuma, 2015). The hypothesis is that this

frequent tumor alteration represents an actionable therapeutic target for certain cancer types such as basal-like/triple-negative breast cancers, which display a high frequency of *TP53* mutation and relatively homogeneous accumulation of the mutant protein in patient tumors (Fig. 2b) (Bouchalova et al., 2014). However, as mutant and wild-type p53 can be regulated similarly, the use of p53 destabilizing agents could cause significant damage to normal cells containing the WT protein. For this reason, an improved understanding of the overlapping and distinct mechanisms that contribute to WT and mutant p53 stabilization is critical.

This chapter reports results from a study using our isogenic clonal cell lines developed from breast epithelial cells to investigate mechanisms contributing to mutant p53 accumulation. Through comparative analyses of our transformed CAL-51 cell lines, we identified heterogeneous protein stabilization between and within clonal cell lines *in vitro* and *in vivo*. We found that aneuploidy, but not whole-genome doubling or nuclear area, is correlated with increased mutant p53 protein accumulation. Highly aneuploid cells displayed increased mutant p53 ubiquitination and increased cytoplasmic localization. We also identified that mutant proteins are ubiquitinated and degraded through proteasomal and non-proteasomal mechanisms independent of MDM2 expression. Further study of mechanisms contributing to mutant p53 accumulation in our cell lines is needed, however through these preliminary analyses, we show that our isogenic cell lines represent ideal model systems for the study of mutant p53 regulation.

Results

Missense mutant p53 expression is increased in basal-like and highly aneuploid breast cancers

Mutant p53 accumulation has been highly studied for prognostic relevance and contribution to GOF activities in breast cancers (Bouchalova et al., 2014; Olivier et al., 2006). As expected, analysis of *TP53* mRNA and protein expression reverse-phase protein array (RPPA) data from breast tumors revealed that missense mutant p53 protein is elevated compared to other *TP53* mutations (Fig. 23a). To identify clinical and molecular features associated with increased missense mutant protein expression, we stratified breast (BRCA) *TP53* missense tumors into either p53-high (upper quantile RPPA) or p53-low (lower quantile RPPA) groups with significant differences in p53 protein levels (Fig. 23b). Analysis of clinical features associated with differences in p53 protein revealed that patients with the basal-like breast subtype had significantly increased enrichment in the p53-high group (Fig. 23c). Basal-like/triple-negative breast cancers have high levels of chromosomal instability, and similarly, the fraction of the genome altered by aneuploidy was also increased in patient tumors with high levels of p53 protein, which are enriched for the basal-like subtype (Fig. 23d). The CAL-51 and MCF10A isogenic cell line models described in Chapter III are considered “triple-negative” since they lack estrogen and progesterone hormone receptor expression and *HER2* amplification (Lehmann et al., 2011; Neve et al., 2006), and thus represent improved model systems to study further the molecular mechanisms associated with mutant p53 protein accumulation in this cancer subtype.

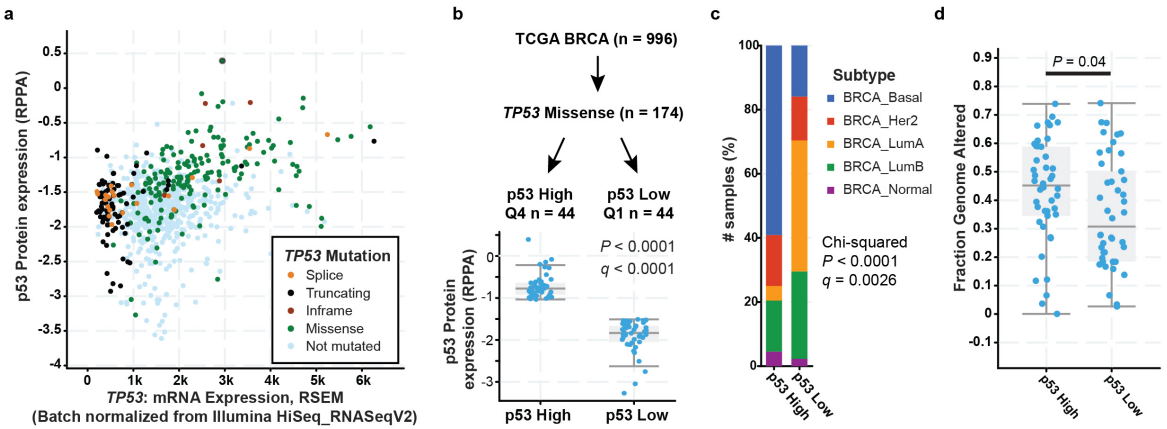

Figure 23. Missense mutant p53 protein is elevated in basal-like and highly aneuploid breast cancers.

a Scatter plot showing TP53 mRNA expression and p53 protein expression in human breast tumors. Dots are colored by *TP53* mutation. **b** Diagram showing the workflow to classify breast (BRCA) tumors containing *TP53* missense mutations into quantiles with high or low p53 protein expression (source: The Cancer Genome Atlas, TCGA). Protein expression is from TCGA reverse-phase protein array (RPPA) datasets. **c** Stacked bar plots showing enrichment of BRCA subtypes in p53-high and -low groups. Enrichment was calculated using a chi-squared test. **d** The fraction of the genome altered in tumors with either high or low p53 protein. Wilcoxon Test.

Mutant p53 expression is heterogeneous in transformed isogenic cell lines

Mutant p53 is associated with oncogenic transformation; however, accumulation is context-specific, occurring in some but not all tumors in murine models and patient tumors expressing mutant p53 (Terzian et al., 2008; Xue et al., 2019). To study mechanisms contributing to heterogeneous mutant p53 accumulation, we first evaluated p53 protein expression within the CAL-51 clonally derived cancer cell lines described in Chapter III of this dissertation (Redman-Rivera et al., 2021). Immunoblotting for p53 in R273H, p53 WT and null (negative control) cell lines revealed that mutant p53 levels were elevated in all mutant cell lines compared to the WT control (Fig. 24a). To analyze mutant p53 expression in individual cells, we conducted tyramide signal-amplified immunofluorescence (TSA-IF) staining for p53. We found that mutant p53 cell lines displayed a range of p53 protein levels, with several mutant-containing cell lines maintaining low levels of p53 similar to WT p53 cell lines (Fig. 24b). Cell lines with low levels of p53 expression also had a smaller percentage of cells that stained positive for p53, indicating that p53 mutant expression is heterogeneous between and within clonal cell lines (Fig. 24b).

To further analyze mutant p53 expression, we conducted p53 immunohistochemistry (IHC) on a formalin-fixed and paraffin-embedded tissue microarray (TMA) consisting of CAL-51 cell line xenograft tumors as described in Chapter III (Fig. 19a-c). p53 IHC specificity was validated by staining CAL-51 p53 null cell lines and the R273H mutant cell line MD-AMB-468, respectively, as negative and positive controls. IHC staining was consistent with immunoblot analysis, with p53

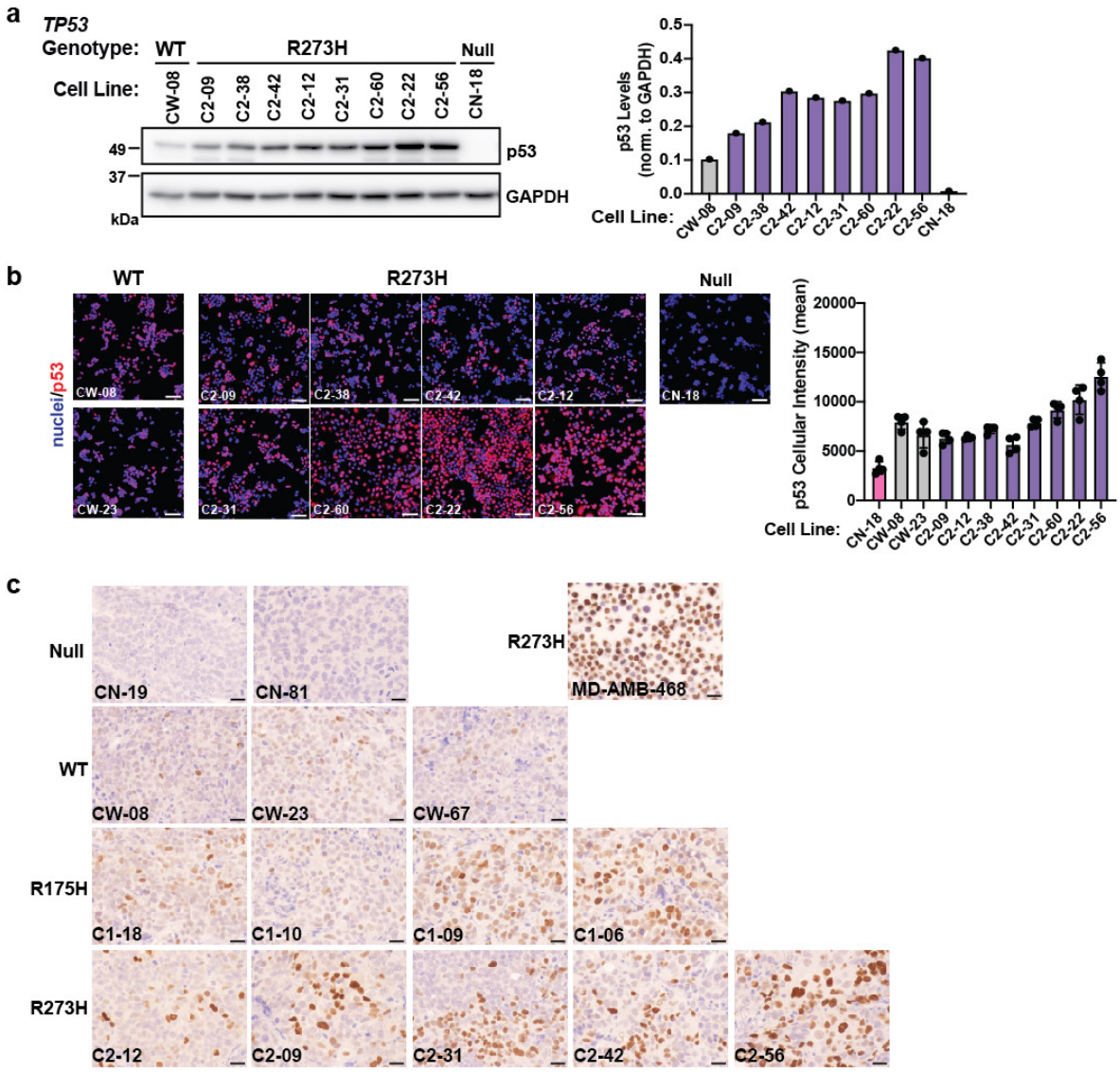

Figure 24. Mutant p53 protein expression is heterogeneous across and within CAL-51 cells.
a Western blot of relative p53 and GAPDH protein levels in the indicated CAL-51 cell lines (left panel) and quantification of p53 protein levels normalized to the loading control GAPDH (right panel). Results are representative of at least two independent experiments. Colors indicate *TP53* genotype (WT, gray; R273H, purple; Null, pink). **b** Representative tyramide signal-amplified (TSA) immunofluorescence images stained for p53 (CY3/red) and nuclei (Hoechst/blue) in the indicated CAL-51 cells (left panel), from at least two independent experiments. Scale bar, 100 μM. Quantification of the mean cellular p53 protein immunofluorescence intensity (right panel). Colors indicate *TP53* genotype (WT, gray; R273H, purple; Null, pink). **c** Representative p53 immunohistochemistry (IHC) images of CAL-51 cell line xenograft tissue or the MD-AMB-468 cell line used as a positive control. Scale, 20 μM.

protein expression higher in R175H and R273H mutant cells compared to WT p53 (Fig. 24c). In addition, p53 staining was heterogeneous between cell lines and within tumors, indicating that sub-clonal heterogeneity or environmental factors contribute to mutant p53 expression (Fig. 24c). Collectively, these results indicate that mutant p53 accumulation is heterogeneous in our transformed CAL-51 cell lines, consistent with previous reports (Lang et al., 2004; Song et al., 2007; Suh et al., 2011; Terzian et al., 2008; Xue et al., 2019).

Mutant p53 accumulation is correlated with aneuploidy

Analysis of TCGA BRCA cancers with missense mutations in *TP53* revealed that the fraction of the genome altered by aneuploidy was increased in patient tumors with high levels of p53 protein (Fig. 23d). Further, analyses conducted in Chapter III revealed that mutant p53 GOF phenotypes were associated with aneuploidy development (Redman-Rivera et al., 2021). To determine if mutant p53 accumulation was also associated with aneuploidy in our isogenic cell line models, we performed immunoblot analyses in isogenic p53 WT and R273H CAL-51 and MCF10A cell lines. Aneuploidy score was significantly correlated with p53 protein levels in CAL-51 cells and a similar trend observed in MCF10A cells, although not reaching statistical significance (CAL-51, $P = 0.0084$; MCF10A, $P = 0.0536$; Fig. 25a).

The aneuploidy observed in mutant p53 CAL-51 cell lines occurs over time in passage (Fig. 26). To analyze p53 protein levels following aneuploidy development within the same cell line, temporal DNA-content and p53 immunoblot analyses were conducted in parallel with CAL-51 p53 WT and R273H cell lines. The p53 WT (CW-64)

and R273H (C2-38) cell lines remained diploid over time in passage and had consistently low levels of p53 protein. In contrast, the R273H mutant cell line C2-56 displayed aneuploidy at all passages and had high levels of p53 protein (Fig. 25b-c). Interestingly, the R273H cell line C2-09 developed aneuploidy over time in passage, with a corresponding increase in p53 protein levels (Fig. 25b-c). However, this mutant p53 protein accumulation was not associated with amplification of the *TP53* locus analyzed at passage 30 (Fig. 25d) or with increased *TP53* transcript measured in the corresponding cells by RNA-seq at passages 5 and 30 (Fig. 25e).

To further evaluate how DNA content and aneuploidy affect p53 accumulation, we isolated sub-clonal cell lines from the CAL-51 C2-09 R273H mutant cell line, which displayed a mixed population of diploid and tetraploid cells at an intermediate passage (Fig. 25c and Fig. 27a). DNA-content analysis revealed that the C2-09 sub-clones had varied content, with several clones undergoing whole-genome doubling (WGD) (Fig. 27b). TSA-IF staining on the same cells showed that p53 staining intensity and the percent of p53 positive cells did not correlate with DNA content or increased nuclear area (Fig. 27c-d). These results indicate that mutant p53 accumulation is associated with aneuploidy but not WGD or nuclear area in CAL-51 cells and suggest that specific chromosomal alterations may contribute to dysregulation of mutant p53 protein and mutant p53 stabilization.

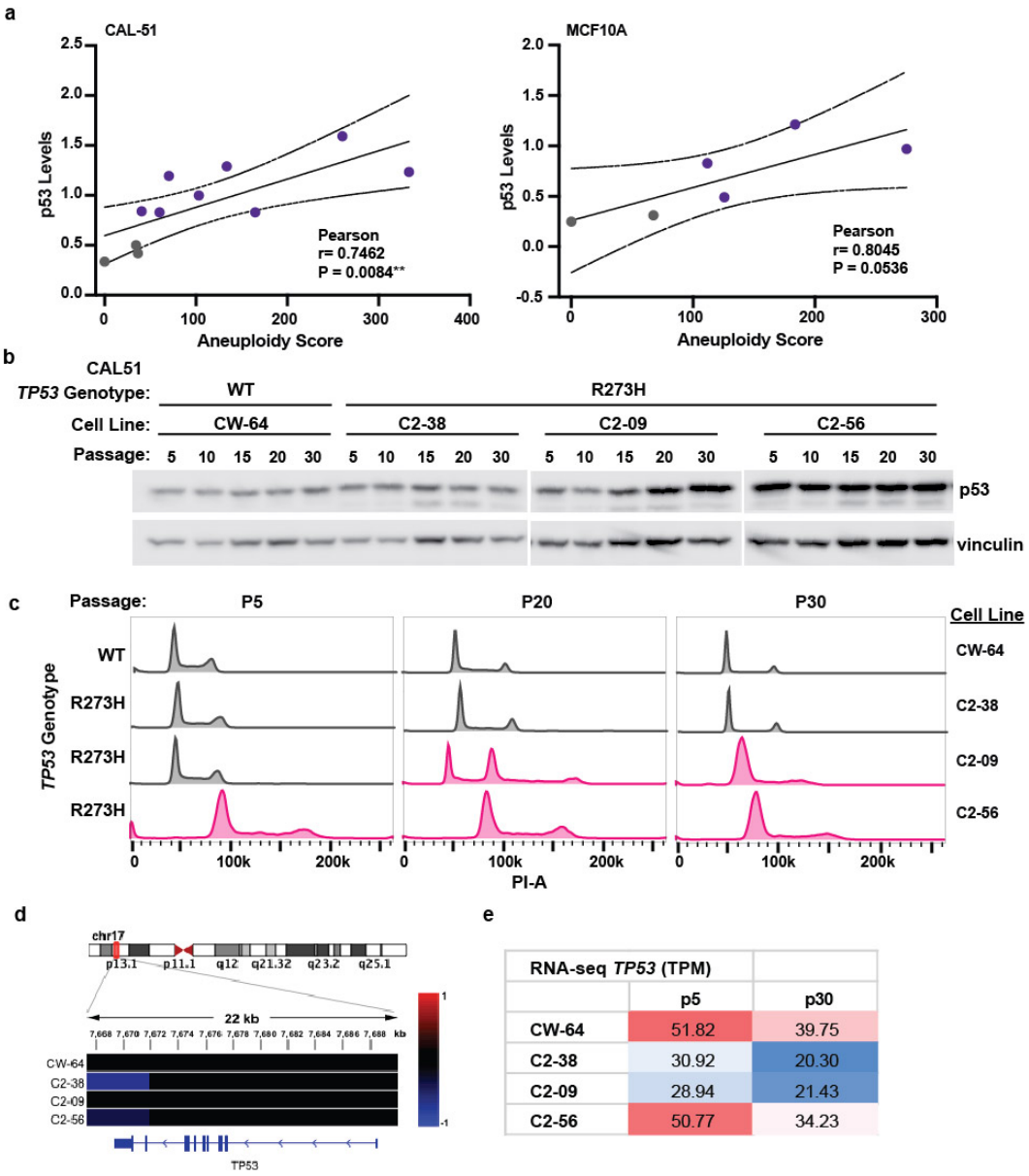

Figure 25. Mutant p53 accumulation is correlated with aneuploidy but not *TP53* DNA or RNA levels.

a Scatter plot showing immunoblot quantification of p53 levels versus aneuploidy score in CAL-51 (left panel) and MCF10A (right panel) isogenic cell lines. The black line represents a linear model of the best fit, with the dotted lines indicating the 95% confidence intervals. Significance was determined using Pearson correlation. **b** Western blot of relative p53 and vinculin protein levels in the indicated CAL-51 cell lines over time at various passages in culture. **c** Histograms showing DNA content of CAL-51 cell lines by flow cytometry of propidium iodide (PI) stained CAL-51 cells at indicated passages (P5, P20, and P30). Cells were collected in parallel to western blot samples displayed in panel (**b**). **d** DNA copy number alterations (Log2 ratios) of the corresponding CAL-51 cell lines indicated in panels **b** and **c** at passage 30. **e** RNA-seq transcript per million (TPM) values for *TP53* in CAL-51 cells of the indicated passage.

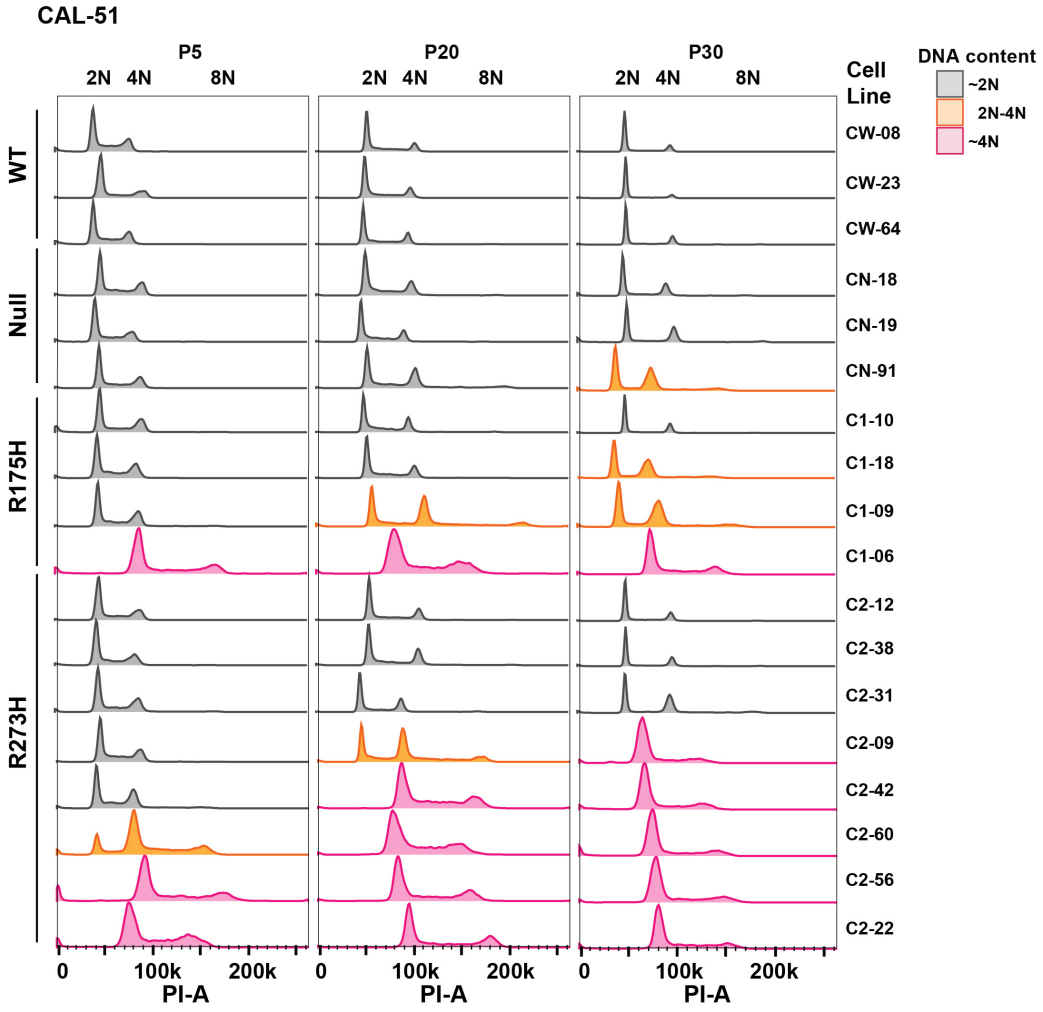

Figure 26. CAL-51 cell lines become aneuploid over time in passage.
Histograms showing DNA content of CAL-51 isogenic cell line populations by flow cytometry of propidium iodide (PI) stained cells at passage 5 (P5), 20 (P20) and 30 (P30) after clonal expansion. Colors represent DNA content (gray = ~2N, orange = 2N-4N, pink = ~4N). These experiments are representative of n = 2 independent experiments. Flow cytometry was conducted with the help of Hailing Jin.

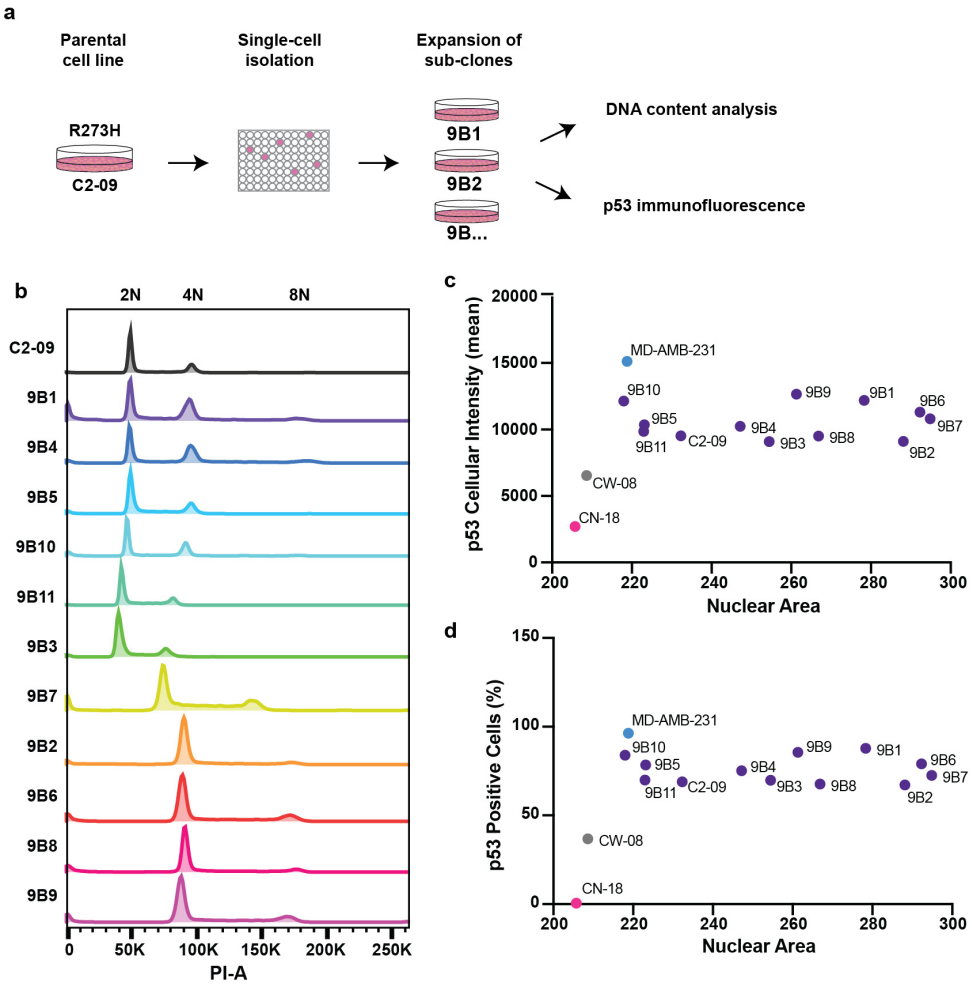

Figure 27. Mutant p53 accumulation is not correlated with whole-genome doubling or nuclear area.

a Diagram demonstrating workflow for single-cell isolation of CAL-51 C2-09 sub-clones, and parallel DNA content analysis and p53 TSA-IF analyses. **b** Histograms showing DNA content of CAL-51 C2-09 sub-clones by flow cytometry of propidium iodide (PI) stained cells. **c-d** The mean cellular p53 fluorescence intensity (**c**) and mean percentage of cells with positive p53 TSA-IF staining (**d**) from immunofluorescence staining of CAL-51 WT CW-08, Null CN-18 and the R273H parental C2-09 cell line, as well as C2-09 sub-clones and the MD-AMB-231 cell line used as a positive control from n = 2 independent experiments. Colors indicate *TP53* genotype (pink, Null; gray, WT; purple, R273H; blue, R280L). Analyses were conducted with the help of Hailing Jin.

Mutant p53 is ubiquitinated and degraded in CAL-51 cells, independent of MDM2

WT p53 protein is typically maintained at low levels through MDM2-mediated ubiquitination and proteasomal degradation (Haupt et al., 1997; Rodriguez et al., 2000). However, ubiquitination of mutant p53 protein is controversial: studies have reported both increased and decreased mutant p53 ubiquitination occurring in cells (Li et al., 2011a; Lukashchuk and Vousden, 2007). To determine if altered mutant p53 ubiquitination underlies protein accumulation in clonal CAL-51 cell lines, we treated WT and R273H mutant p53 cells with the cell-permeable proteasome inhibitor MG132 to prevent protein degradation. Immunoblotting showed higher molecular weight forms of p53 in all cells treated with MG132, indicating that p53 ubiquitination may occur regardless of the *TP53* genotype (Fig. 28a).

To determine if the higher molecular weight bands were ubiquitinated forms of p53, we conducted ubiquitination assays by transfecting cells with HA-tagged ubiquitin (HA-Ub) and immunoprecipitating p53 protein. Immunoblot analysis of immunoprecipitates showed that ubiquitinated p53 protein was detectable in all WT and R273H clonal cell lines analyzed and not in the p53 null negative control (Fig. 28b). Mutant p53 ubiquitination levels increased in several mutant clones compared to a p53 WT cell line, although ubiquitination varied by cell line and depended on total HA-Ub expression (Fig. 28b). In a separate analysis across mutant cell lines with similar HA-Ub transfection efficiencies, the highly aneuploid (Fig. 7) mutant C2-56 and C2-22 cell lines that express higher levels of mutant p53 protein (Fig. 24a-b) also displayed increased p53 ubiquitination levels compared to other R273H mutant cell lines (Fig. 28c). Mutant p53 ubiquitination was independent of MDM2 expression, as p53 mutant CAL-51 clonal

cell lines with genotoxic stress induced through doxorubicin or ultraviolet irradiation did not upregulate MDM2 expression (Fig. 29). Together, these data indicate that mutant p53 proteins are ubiquitinated through an MDM2-independent mechanism and that increased mutant p53 ubiquitination is associated with aneuploidy in these transformed cell lines.

Increased MDM2-independent ubiquitination of mutant p53 protein has been reported previously, although increased ubiquitination in these cells did not lead to a corresponding increase in protein degradation (Lukashchuk and Vousden, 2007). To characterize mutant p53 degradation in our CAL-51 cell lines, we examined p53 protein levels by immunoblotting at various timepoints following inhibition of protein translation with cycloheximide (Fig. 30a). In contrast to WT p53, which was efficiently degraded and had a short half-life, all cell lines with mutant p53 displayed a variable but increased half-life of p53 protein (Fig. 30b-c). Even though mutant p53 half-lives were increased, the protein was still degraded in clonal R273H CAL-51 cell lines but not the MDA-MB-468 cell line (Fig. 30b).

To determine if mutant p53 degradation was dependent on the proteasome, we analyzed p53 protein at various timepoints following cycloheximide treatment in the presence of the proteasome inhibitor MG132 (Fig. 31a). Whereas proteasome inhibition completely blocked WT p53 degradation, it reduced but did not completely abrogate mutant p53 degradation (Fig. 31b-c). These data suggest that mutant p53 protein is ubiquitinated independently of MDM2, and degraded through proteasomal and non-proteasomal mechanisms.

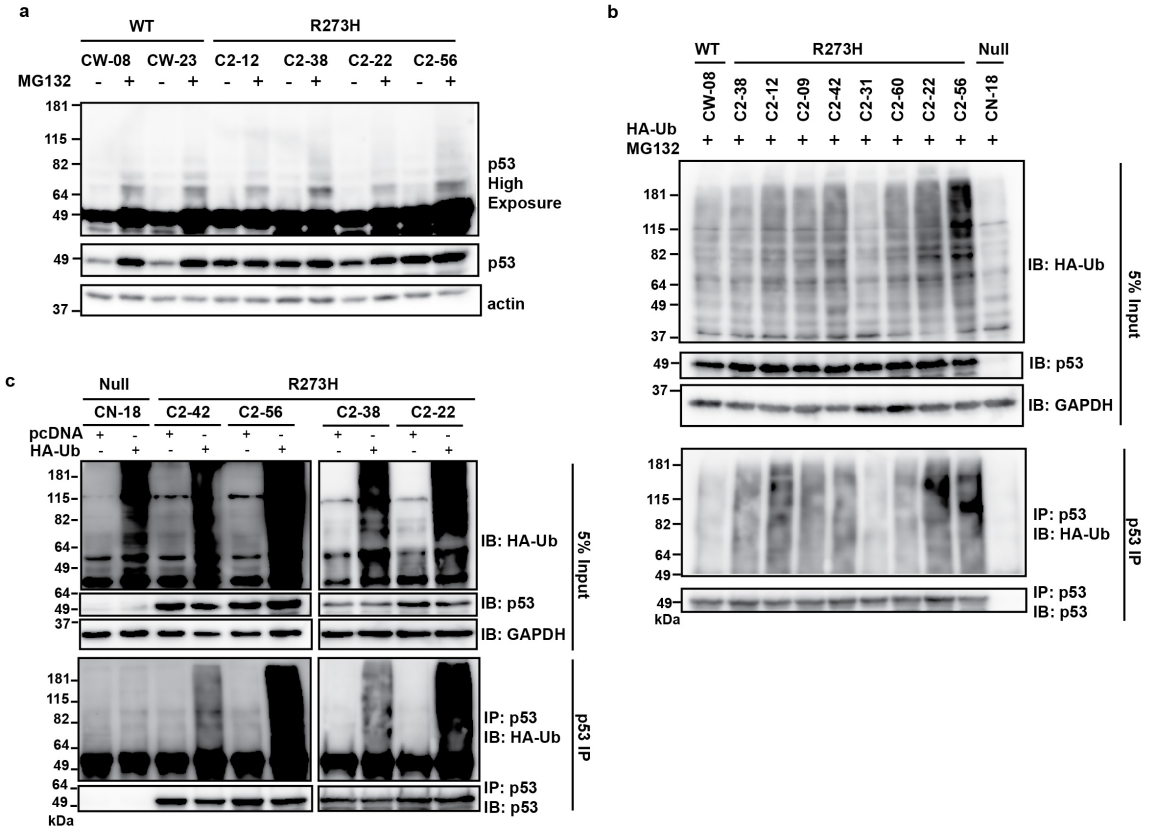

Figure 28. Mutant p53 is ubiquitinated in CAL-51 cells.
a Western blot using a p53-specific antibody showing higher molecular weight protein bands after 5 h treatment with 10 μM MG132. p53 levels are shown at high and low exposures along with the loading control actin in the indicated CAL-51 WT and R273H mutant cell lines. Western blot is representative of n = 2 independent experiments across multiple clonal cell lines. **b-c** Western blots showing p53 ubiquitination in CAL-51 cells of the indicated *TP53* genotype following 48 h transfection with HA-tagged ubiquitin (HA-Ub) and 5 h treatment with 10μM MG132. Upper panel shows 5% of the input used for immunoprecipitation of p53 shown in the lower panel. Western blots are representative of at least n = 2 independent experiments. All experiments were conducted by Hailing Jin.

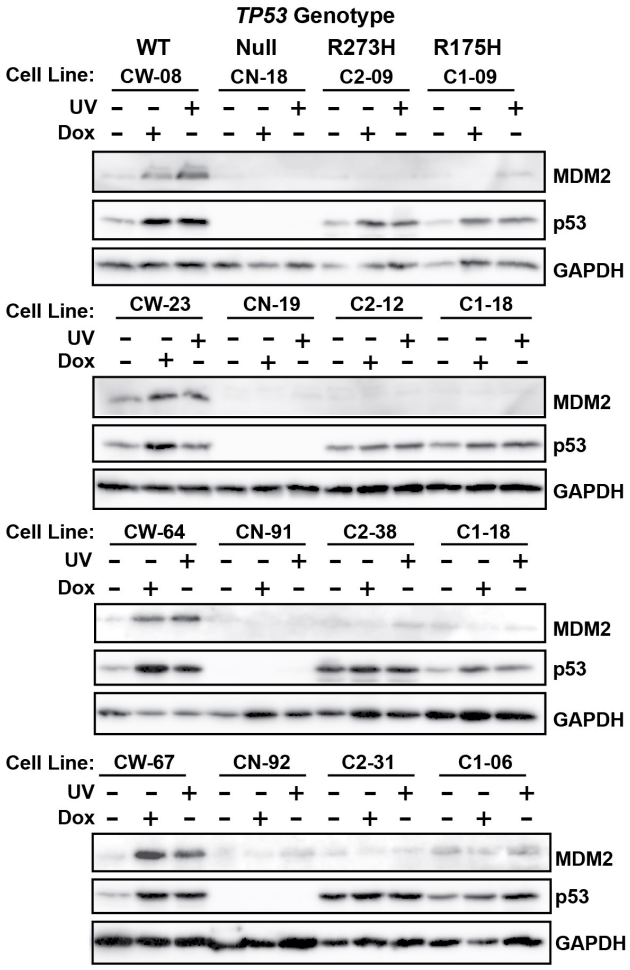

Figure 29. Increases in MDM2 protein levels are not detectable in p53 null and mutant cell lines after treatment with agents that induce genotoxic stress.
Western blots showing relative p53, MDM2, and GAPDH protein levels in the indicated CAL-51 clonal cell lines containing WT, null, R175H or R273H *TP53* genotypes after treatment with doxorubicin (Dox, 0.2 μM, 6h) or ultraviolet radiation (UV, 20J, 6h).

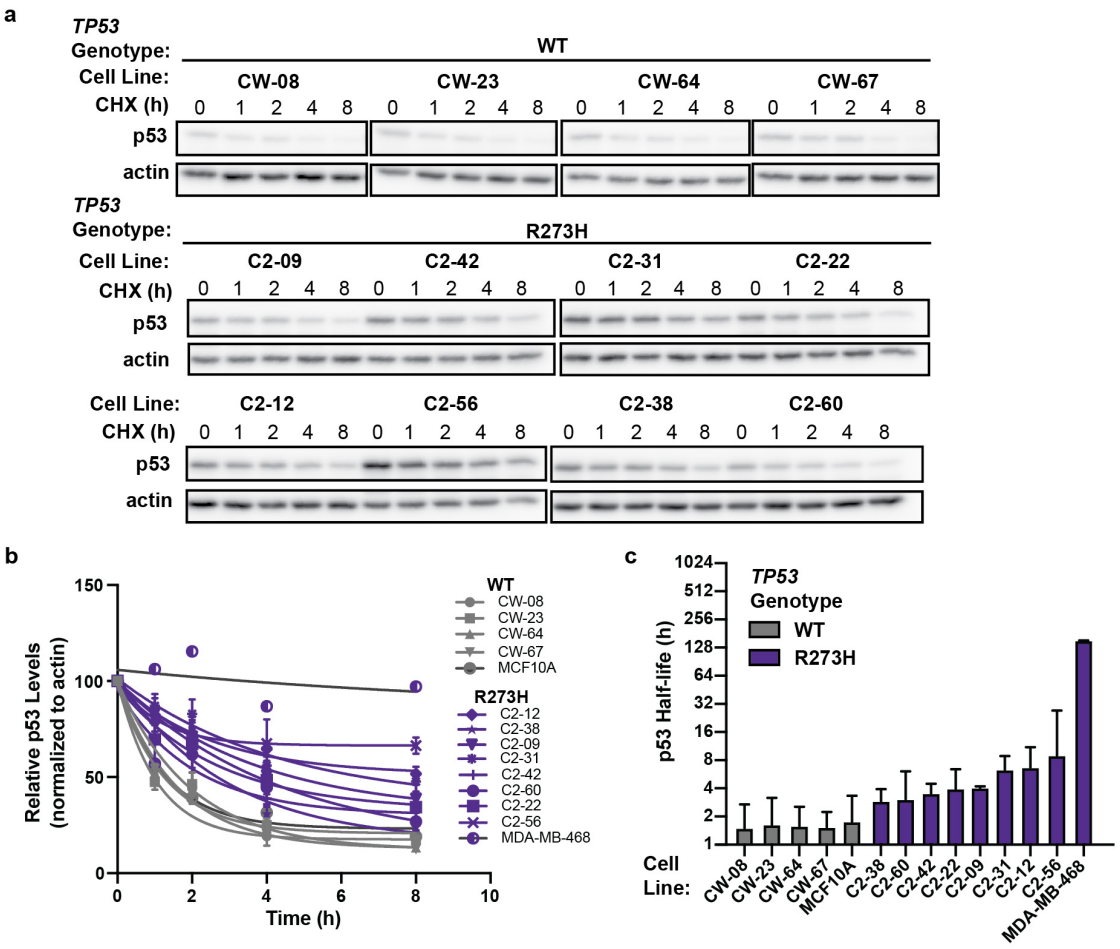

Figure 30. Mutant p53 has increased half-life but is degraded in CAL-51 cells.
a Representative western blots showing p53 and actin protein levels at various timepoints following cycloheximide (CHX) treatment (100 µg/µL) in CAL-51 p53 WT and R273H mutant cell lines. **b** Quantification of western blots shown in (**a**) showing p53 degradation following cycloheximide treatment, along with MCF10A and MD-AMB-468 cell lines (blots not shown). The mean p53 levels from n = 3 independent experiments are shown normalized to the actin loading control and relative to the untreated sample. Colors indicate *TP53* genotype (WT, gray; R273H, purple). **c** Bar plot of p53 half-lives calculated from nonlinear regression of data shown in (**b**). Data indicate the mean ± 95% confidence intervals. Colors indicate *TP53* genotype (WT, gray; R273H, purple). Western blot analyses were conducted with the help of Hailing Jin.

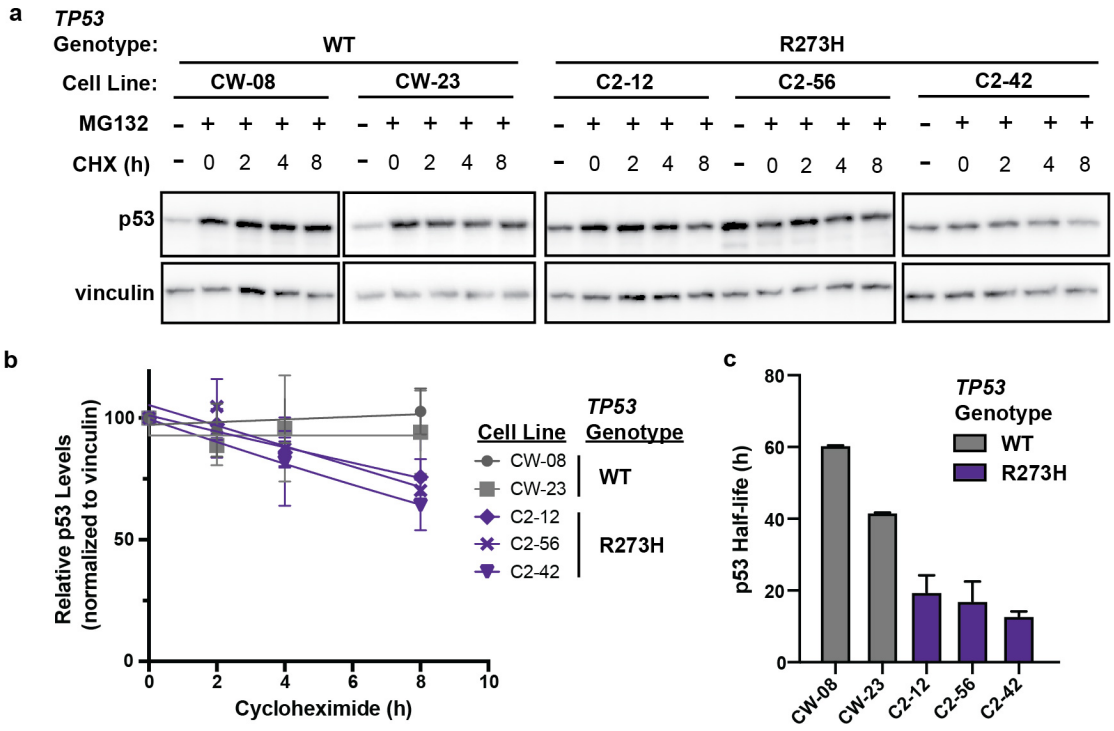

Figure 31. Mutant p53 degradation occurred after proteasome inhibition in CAL-51 cells.
a Representative western blots showing p53 and vinculin protein levels following MG132 treatment (10 μM, 5 h) at various timepoints following cycloheximide (CHX) treatment (100 μg/μL). **b** Quantification of western blots in n = 2 WT and n = 3 R273H mutant cell lines following MG132 and cycloheximide treatment as shown in (**a**). p53 levels are shown normalized to the vinculin loading control and relative to the untreated sample. Data shown represent the mean ± standard deviation from 3 independent experiments. Colors indicate *TP53* genotype (WT, gray; R273H, purple). **c** Bar plots of p53 half-lives calculated from nonlinear regression of data shown in (**b**). Data shown represent the mean ± 95% confidence intervals. Colors indicate *TP53* genotype (WT, gray; R273H, purple). Western blot analyses were conducted with the help of Hailing Jin.

Mutant p53 cytoplasmic localization is increased in aneuploid cells

Although mutant p53 accumulation is typically nuclear (Rotter et al., 1983; Shaulsky et al., 1990), cytoplasmic localization has been reported to be associated with MDM2-independent mutant p53 ubiquitination (Lukashchuk and Vousden, 2007). To determine the localization of mutant p53 in CAL-51 isogenic cells, we conducted subcellular fractionation and immunoblotting in addition to several p53 WT and R273H cell lines. Fractionation was confirmed by immunoblotting for GAPDH and PARP as cytoplasmic and nuclear controls, respectively. In WT cell lines, p53 protein levels were increased in nuclear cell extracts, whereas in mutant cell lines, p53 protein was increased in the cytoplasmic cellular extracts (Fig. 32a-b). This increase in cytoplasmic mutant p53 was especially pronounced in the highly aneuploid cell line C2-56. To validate p53 localization in a larger panel of cell lines, we conducted p53 TSA-IF staining with α-tubulin immunofluorescent staining as a cytoplasmic marker. WT and R273H mutant p53 clonal cell lines had similar levels of cytoplasmic p53 staining, except for three cell lines determined to be aneuploid by flow cytometry analysis, which had increased levels of cytoplasmic mutant p53 staining (Fig. 32c-d). Of note, the mutant cell line C2-12 did not show increased cytoplasmic p53 staining, contrary to the cellular fractionation experiments (Fig. 32a-b); however, this inconsistency could be due to differences in experimental sensitivity. In total, this data indicates that aneuploidy is associated with cytoplasmic localization of mutant p53 protein.

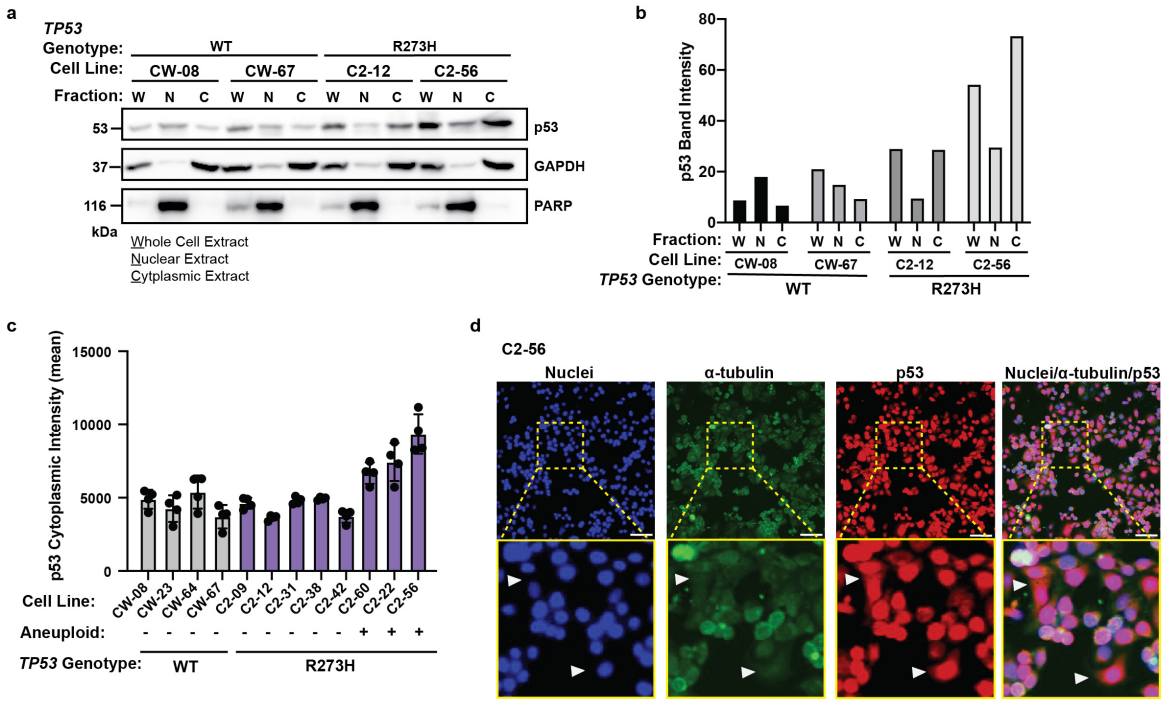

Figure 32. Mutant p53 cytoplasmic localization is increased in aneuploid cells.
a Western blot showing relative p53, GAPDH, and PARP protein levels in the indicated whole-cell, nuclear or cytoplasmic extracts in the indicated CAL-51 cell lines. Data are representative of three independent experiments. **b** Quantification of p53 levels in the indicated cellular fractions (W, whole-cell extract; N, nuclear extract; C, cytoplasmic extract) in CAL-51 cell lines with varying *TP53* genotypes. **c** Quantification of p53 cytoplasmic localization from tyramide signal-amplified immunofluorescence (TSA-IF) in the indicated CAL-51 cell lines. Aneuploidy status for each cell line was determined by flow cytometry and shown as having diploid (-) or tetraploid (+) DNA content. Colors indicate *TP53* genotype (gray, WT; purple, R273H) **d** Representative TSA-IF images stained for p53 (CY3/red), a-tubulin (FITC/green), and nuclei (Hoechst/blue) in the CAL-51 C2-56 cell line. Arrows indicate examples of mutant p53 cytoplasmic staining. Scale bar, 100 μM. Analyses were conducted with the help of Hailing Jin.

Mutant p53 is destabilized by the HDAC inhibitor SAHA but not with HSP90 inhibitors or statins

Therapeutic targeting and destabilization of mutant p53 protein is an active area of research, and several compounds have been identified to destabilize mutant p53 in cells. For example, HSP90 or HDAC inhibitors have been shown to alter mutant p53 protein levels and are being considered as an exploitable therapeutic option for tumors containing mutant p53 (Alexandrova et al., 2015; Li et al., 2011b). In addition, the use of statins has been reported to specifically induce degradation of mutant p53 protein in breast cancer cell lines (Parrales et al., 2016; Turrell et al., 2017). Therefore, we determined if compounds previously reported to destabilize mutant p53 protein could decrease mutant p53 levels in our isogenic CAL-51 cell line models. CAL-51 clonal cell lines containing WT or R273H mutant p53 were treated with the HSP90 inhibitors 17-AAG and ganetespib, or with the HDAC inhibitor SAHA and protein levels evaluated by immunoblot. Only the HDAC inhibitor SAHA specifically decreased mutant p53 protein levels (Fig. 33a). Neither HSP90 inhibitor nor two different statins (lovastatin and atorvastatin) resulted in decreased mutant p53 protein in CAL-51 cells, contrary to previous reports (Fig. 33b) (Freed-Pastor et al., 2012; Parrales et al., 2016).

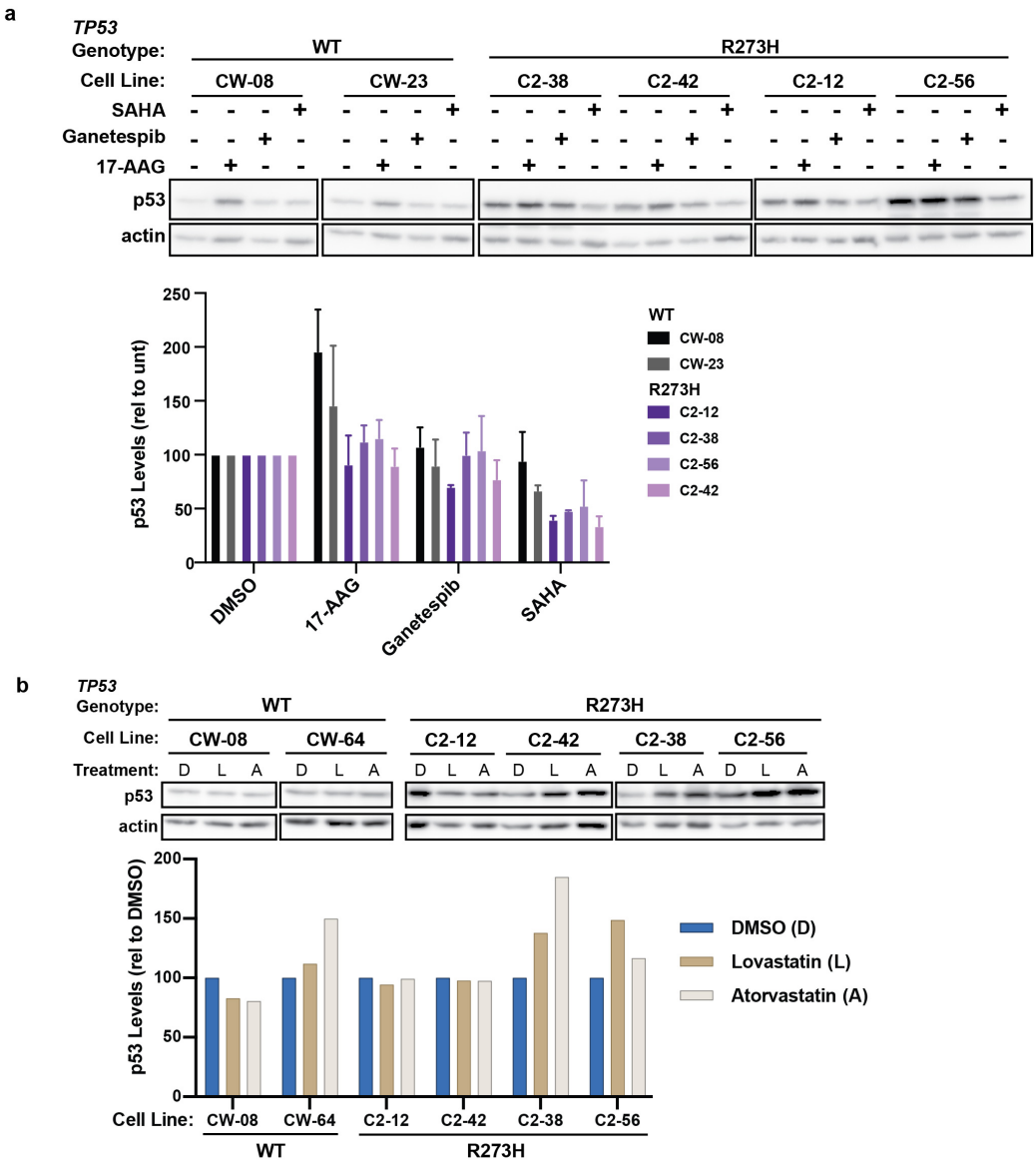

Figure 33. Mutant p53 is destabilized by the HDAC inhibitor SAHA but not HSP90 inhibitors or statins.

a Western blots showing relative p53 and actin levels in the indicated CAL-51 WT and R273H cell lines following treatment with the HDAC inhibitor SAHA (5 μM, 24h), or the HSP90 inhibitors ganetespib (30 nM, 24 h) and 17-AAG (5 μM, 24 h) or a DMSO control (upper panel). Quantification of p53 levels normalized to actin and shown relative to the DMSO treated control (lower panel) from n = 2 independent experiments. **b** Western blots showing relative p53 and actin levels in the indicated CAL-51 WT and R273H cell lines following treatment with the statins lovastatin (8 μM, 24h) and atorvastatin (8 μM, 24h), or a DMSO control (upper panel). Quantification of p53 levels normalized to actin and shown relative to the DMSO treated control (lower panel), representative of n = 2 independent experiments. Western blot analyses were conducted with the help of Hailing Jin.

Discussion

Accumulation of mutant p53 protein is a hallmark feature of transformed cells and human tumors, and this phenotype is especially prominent in basal-like/triple-negative breast cancers (Bártek et al., 1991; Bouchalova et al., 2014). Increased protein accumulation has been reported to enhance supposed mutant p53 GOF phenotypes such as increased metastasis (Terzian et al., 2008). Given the high frequency of p53 mutations, there is significant interest in developing mutant p53 destabilizing compounds for therapeutic purposes. However, very little is known about the mechanisms underlying mutant p53 stabilization and if they are unique to mutant p53 or shared with the WT protein. The latter is highly relevant given that it is unlikely that compounds that destabilize mutant p53 will reach therapeutic utility if they also destabilize WT p53 protein. As described in this chapter, we utilized our isogenic triple-negative breast cell line models to study mechanisms contributing to mutant p53 accumulation.

Similar to previous reports (Terzian et al., 2008; Xue et al., 2019), we observed heterogeneous mutant p53 accumulation in our cell line models. Utilizing our clonally derived cell lines, which originated from a near-diploid parental genetic background, we showed that increased p53 protein levels in R273H mutant cell lines correlated with the acquisition of aneuploidy in those cells. Comparative analyses conducted with our cell lines revealed that aneuploidy is also associated with the ubiquitination and cytoplasmic localization of mutant p53 protein. Because aneuploidy, but not whole-genome doubling, correlated with increased mutant p53 protein stability, it is likely that specific chromosomal gains or losses, and potentially the gain or loss of novel mutant p53

regulators, contributes to protein stabilization. We identified that mutant p53 is ubiquitinated and degraded by an MDM2-independent mechanism through proteasomal and non-proteasomal pathways. These data suggest that ubiquitin ligases other than MDM2 are responsible for mutant p53 ubiquitination. Further studies are needed, however, identification of novel mutant p53 regulators and ubiquitin ligases will be of value to the p53 field and perhaps attractive therapeutic targets if mutant GOF activity is identified and confirmed in future studies. Finally, determining whether the alteration of other cellular degradation pathways such as autophagy contribute to mutant p53 stabilization requires further investigation.

Aneuploidy has been shown to activate wild-type p53 protein (Li et al., 2010; Santaguida and Amon, 2015; Soto et al., 2017; Thompson and Compton, 2010), although there is some debate over the specific types of aneuploidy and contexts that cause p53 activation. For example, stable aneuploid murine embryonic fibroblasts do not show elevated p53 levels (Tang et al., 2011), and whole chromosome aneuploidies are tolerated and propagated in a p53-proficient background (Soto et al., 2017). Aneuploidy has not previously been attributed to mutant p53 protein stabilization; however, mutant and wild-type p53 are stabilized similarly in response to cellular stress (Boettcher et al., 2019; Redman-Rivera et al., 2021; Terzian et al., 2008). Thus, it is reasonable to hypothesize that cellular stresses associated with aneuploidy may be contributing to mutant p53 stabilization in cells.

Mutant p53 accumulation has been reported to underlie mutant p53 GOF phenotypes (Brosh and Rotter, 2009; Terzian et al., 2008). While we have observed overlapping associations between the acquisition of aneuploidy, mutant p53

accumulation, the presence of mutant p53 associated GOF phenotypes, and mutant p53 knockdown, the experiments described in Chapter III revealed GOF phenotypes were not dependent on mutant p53 protein levels. Similar to the findings of Chapter III, in this chapter, we show that acquisition of aneuploidy contributes to phenotypes associated with mutant p53 protein. More work is needed to validate these findings and determine how aneuploidy contributes to mutant p53 stabilization.

Finally, although aneuploidy was associated with mutant p53 accumulation in CAL-51 cell lines, other mechanisms contributing to mutant p53 stabilization likely exist. Notably, the varying levels of mutant p53 protein in our cell line models, which originated from the same genetic background, provide improved models for the study of p53 protein regulation. A better understanding of the mechanistic basis for mutant p53 protein accumulation is needed, especially as studies are attempting to modulate the stability of both mutant and WT p53 proteins for therapeutic purposes. Even if this protein accumulation is not contributing to mutant p53 GOF activity, it may be useful as a prognostic marker indicative of other cellular alterations that could be targeted therapeutically, especially in some aggressive cancer types that have high frequency of p53 mutation and accumulation like triple-negative breast cancers.

CHAPTER V

CONCLUSIONS AND FUTURE DIRECTIONS

Summary

The work presented in this dissertation was performed to advance the field's understanding of mutant p53 protein function in human cancers. Although the role of mutant p53 in tumorigenesis has been studied for over 40 years, the model systems used for experimentation have yielded contradictory results and generated confusion over whether mutant p53 has oncogenic gain-of-function (GOF) activities. The advent of CRISPR/Cas9 genome editing technology has allowed the generation of improved biological models, like those utilized in this dissertation, which control for confounding effects caused by ectopic expression of protein and other cellular modification techniques. Further, genomic sequencing advances have improved the ability to detect complex genomic and chromosomal alterations in cells.

We deployed experimental and technological improvements to generate two isogenic cell line models, consisting of 36 clonal cell lines derived from relatively diploid non-transformed and transformed epithelial cells. These isogenic cell lines initially differed only by *TP53* genotype and allowed for the systematic study of mutant p53 LOF and GOF. In Chapter III, I presented evidence that various cellular phenotypes, which had previously been attributed to the oncogenic activities of mutant p53 proteins, were not dependent on the mutant p53 protein but the acquisition of aneuploidy. Further, I could not identify inhibitory protein-protein interactions between mutant p53 and p73 or

changes in gene expression, previously reported as mechanisms for mutant p53 GOF activities. In Chapter IV, I extended my investigation to another phenotype common to mutant p53 expressing cells: accumulation of the mutant p53 protein. Similar to the theme of Chapter III, my results in Chapter IV showed that aneuploidy contributes to the accumulation of the mutant protein. Highly aneuploid cells displayed increased mutant p53 ubiquitination and increased cytoplasmic localization, and mutant p53 protein degradation occurred through proteasomal and non-proteasomal mechanisms, independent of MDM2. Finally, in Chapter III, I reported that human cancer cell lines containing *TP53* missense mutations do not display increased metastasis in murine models. Further, patients with highly aneuploid tumors have unfavorable clinical outcomes, regardless of *TP53* status (mutant or null).

Analyses of the collective data generated from my dissertation research suggest that the mutant p53 proteins analyzed herein (R175H and R273H) have LOF but not GOF activity. This notion is supported by other studies utilizing isogenic cell lines and next-generation sequencing techniques (Boettcher et al., 2019; Giacomelli et al., 2018). Further, this dissertation work provides valuable insight to whether mutant p53 has an oncogenic function. I discovered that aneuploidy, which frequently occurs in cells following p53 LOF, can generate many GOF phenotypes previously attributed to the mutant p53 protein. Aneuploidy has diverse cellular consequences that contribute to tumorigenesis (Ben-David and Amon, 2020; Chunduri and Storchová, 2019; Vasudevan et al., 2021), and cells with p53 mutations frequently display aneuploidy (Ciriello et al., 2013; Davoli et al., 2017; Taylor et al., 2018; Zack et al., 2013). Yet, most publications claiming mutant p53 GOF effects often disregard the confounding effects caused by the

genomic instability following p53 LOF. The contribution of aneuploidy in mutant p53 GOF had not previously been assessed, and our findings reveal aneuploidy as an explanation for the diverse array of reported mutant p53 GOF phenotypes. These findings are significant given the extent of pre-clinical and clinical investigation currently underway to target the GOF activities of mutant p53 for cancer therapy.

Future Studies and Ongoing Analyses

In the remainder of this chapter, I will discuss the ongoing analyses and future studies that can address questions developed from our findings. Several important questions remain: (i) Does mutant p53 GOF activity exist in other contexts, for example, with other p53 mutations, other oncogenic mutations in the same cell like activating Ras mutations, or phenotypes not yet analyzed in our models?; (ii) Is the increased metastasis reported in mutant p53 murine models also driven by aneuploidy?; (iii) Does mutant p53 contribute to the development of aneuploidy?; and (iv) What cellular factors and processes contribute to mutant p53 stabilization and can they be utilized as prognostic markers indicative of other cellular alterations that could be targeted for therapeutic purposes?

Determining Mutant p53 GOF in Other Contexts

Our isogenic cell lines represent improved models for the study of both WT and mutant p53 functions. Much work remains to determine if mutant p53 GOF activities exist in other contexts. Early studies of mutant p53 (then thought to be the wild-type

protein) found that the protein could facilitate cellular transformation in cooperation with other oncogenes such as activated Ras (Eliyahu et al., 1984; Jenkins et al., 1984; Parada et al., 1984). However, in the studies above, it was not determined if the cellular transformation was due to dominant-negative or GOF effects. Dominant-negative functions of mutant p53 often complicate the understanding of GOF activities as many prior studies claiming GOF have been conducted in cells that retain a WT allele. For example, the pancreatic ductal adenocarcinoma *Kras*$^{G12D/+}$;*Trp53*$^{R172H/+}$;*Pdx1-Cre* mice (KPC) mice contain Kras and heterozygous p53 mutations (with a p53 WT allele intact) and have been commonly used to define mutant p53 GOF (Ghosh et al., 2021; Morton et al., 2010). It would be interesting to determine if mutant p53 can exert GOF activities in cooperation with other alterations such as Ras, PIK3CA, or PTEN mutations in cells that do not retain the WT protein. Our p53 null and mutant isogenic MCF10A or CAL-51 cell lines could be efficiently CRISPR/Cas9 engineered to add oncogene mutations of interest (e.g., Kras G12D). The resulting modified lines could be used in xenograft mouse models to determine if both mutant p53- and Kras G12D-expressing cells display GOF phenotypes such as increased tumorigenicity compared to p53 null cells with a Kras G12D mutation.

We were not able to analyze all mutant p53 GOF phenotypes previously described. Using murine models of p53 mutations, investigators have reported increased metastasis (Lang et al., 2004; Morton et al., 2010; Terzian et al., 2008), however, we were unsuccessful in our attempt to study metastasis through tail-vein injection experiments using our CAL-51 cell line models (data not shown). Although we found no evidence supporting metastatic mutant p53 GOF activities by analyzing

publicly available data on the metastatic potential of cancer cell lines in mice (Fig. 21c-d), further work to optimize experimental conditions and study metastasis using our isogenic cell line models could be conducted.

Recent work shows that mutant p53-containing cells with loss-of-heterozygosity (LOH), which are aneuploid, have increased metastasis in mice (Nakayama et al., 2020). Other studies have shown that chromosomal instability contributes to metastasis (Bakhoum et al., 2018). Further, a study of KPC cells revealed that cells expressing heterozygous p53 R172H (human R175H) and activating Kras (G12D) mutations undergo p53 LOH, display widespread chromosomal instability and develop highly metastatic disease compared to cells containing either the p53 mutation or Kras mutation alone (Hingorani et al., 2005). However, there is limited understanding of how mutant p53 contributes to cancer metastasis. Further studies are needed to determine if mutant p53 GOF activity (and not dominant-negative activity) or chromosomal alterations drive the increased metastasis seen in several engineered mouse models with heterozygous mutations in p53. Given the unfavorable outcomes for patients diagnosed with metastatic disease, any mechanistic insights in this area would be significant.

Other reported mutant p53 GOF phenotypes of interest for further study include cellular plasticity and immune modulation (Ghosh et al., 2021; Loizou et al., 2019). Uncovering whether mutant p53 or aneuploidy contribute to these phenotypes would also provide insight to mutant p53 function. Finally, not all p53 mutations are equivalent in terms of their effect on protein structure. As we only analyzed two p53 mutations (R175H and R273H), it will also be interesting to determine if other hotspot p53 mutants

have GOF activities. For example, the R248Q mutation has been reported to have GOF activity, and its ablation in murine models has been shown to cause tumor regression (Alexandrova et al., 2015; Schulz-Heddergott et al., 2018). Isogenic models of this mutation and others can easily be created and analyzed using the methods and analyses described in Chapter II of this dissertation.

Determining Mechanisms of Aneuploidy Development

Analyses described in Chapter III show that mutant p53 containing cell lines displayed an increased frequency of aneuploidy consistent with previous studies (Ciriello et al., 2013; Duensing and Duensing, 2005; Gualberto et al., 1998; Hanel and Moll, 2012; Hingorani et al., 2005; Liu et al., 1996; Rausch et al., 2012; Talos et al., 2007; Taylor et al., 2018). However, the underlying mechanisms behind this increased aneuploidy require further study. We have assessed several mechanisms by which mutant p53 has been reported to generate aneuploidy. We evaluated cell cycle arrest after DNA damage and double-strand break formation in our cell lines but found no significant differences between p53 mutant and null cells (Fig. 34a-b). Another potential mechanism could be through direct interactions between mutant p53 and the p53 family member p73. Previously, p73 has been reported to maintain chromosomal stability and ploidy in the absence of p53 (Talos et al., 2007). As described in Chapter III, no interactions were observed between mutant p53 and p73 proteins in MCF10A or CAL-51 isogenic cell lines (Fig. 10a-c). Additionally, overexpression of exogenous mutant p53 protein in non-aneuploid CAL-51 null cell lines and subsequent DNA content analysis by metaphase spreads or flow cytometry showed changes in DNA content (Fig.

34c-e). These data suggest the expression of the mutant protein is not sufficient to induce aneuploidy. Mutant p53 GOF activities associated with genomic and chromosomal instability have been reported previously (Gualberto et al., 1998; Murphy et al., 2000; Song et al., 2007). Even though it is well established that aneuploidy is a consequence of p53 LOF, it remains possible that mutant p53 proteins have GOF activities that contribute to the development of aneuploidy. Additional studies such as immunofluorescence analyses of centrosome duplication and live-cell imaging experiments to monitor and dissect mechanisms of aneuploidy development are one area of focus for future studies.

Elucidating Mechanisms of Mutant p53 Stabilization

In Chapter IV, we utilized our cell line models with varying levels of mutant p53 protein to study mechanisms contributing to mutant p53 accumulation. We identified that aneuploidy, but not whole-genome duplication, contributes to mutant p53 stabilization. However, further experiments are needed to uncover additional mechanisms contributing to mutant p53 stability and the exact mechanisms for how aneuploidy is promoting mutant p53 accumulation. One potential hypothesis is that aneuploidy results in the gain or loss of proteins regulating mutant p53. Alternatively, the cellular stresses associated with aneuploidy, such as proteotoxicity or metabolic imbalances, could cause accumulation of the mutant protein. Further experiments to induce aneuploidy through chemical (spindle checkpoint inhibitors) or genetic (CRISPR/Cas9) methods to create specific chromosomal amplifications or deletions can be utilized to analyze the effects of these perturbations on mutant p53 accumulation.

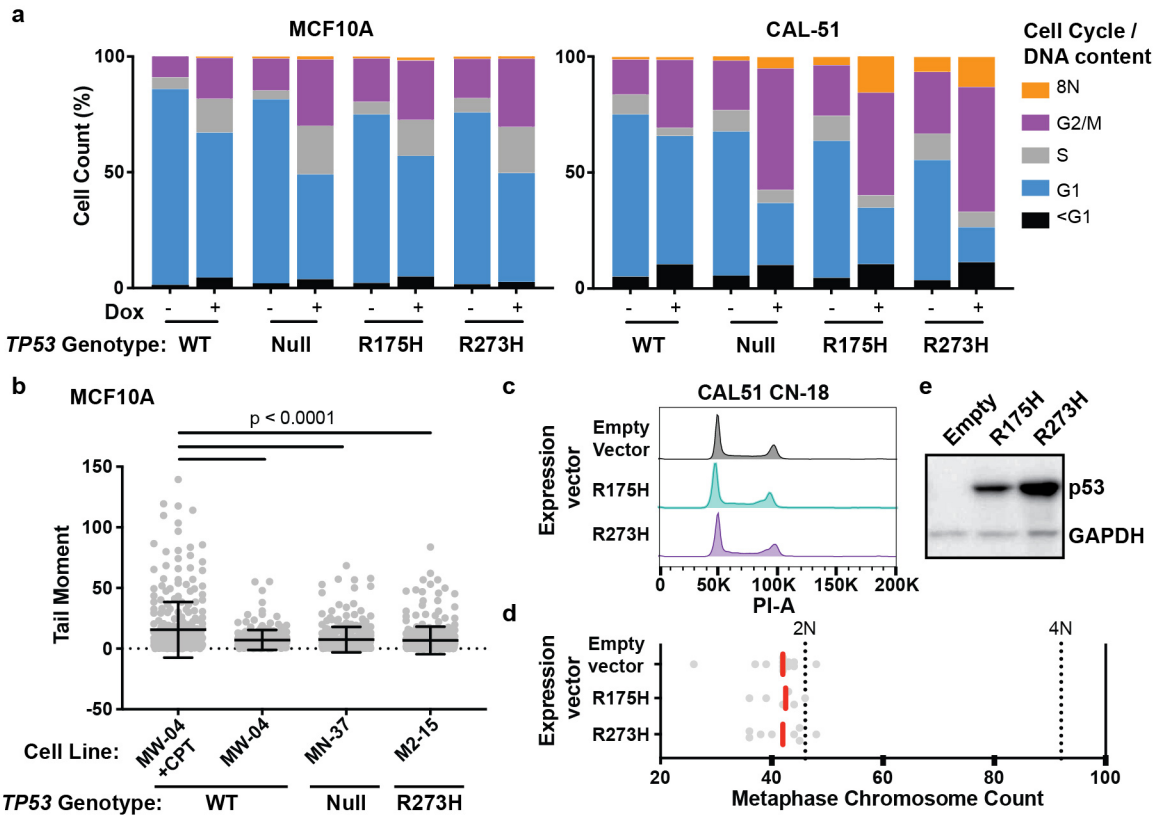

Figure 34. Analysis of mechanisms for aneuploidy development in mutant p53 containing isogenic cell lines.

a Cell cycle checkpoint analysis of MCF10A and CAL-51 cell lines after treatment with doxorubicin (Dox, 2 μM, 24 h). Data from two independent experiments represent the average percentage of cells in each cell cycle phase from multiple cell lines of the indicated *TP53* genotype. Colors represent the cell cycle phase/DNA content (black, <G1; blue, G1; gray, S; purple, G2/M; and yellow, 8N). **b** Comet assay (conducted in collaboration with Archana Krishnamoorthy, David Cortez Laboratory, Vanderbilt University) showing the average tail moment of the indicated MCF10A cell lines. The p53 WT cell line MW-04 was treated with camptothecin (+CPT, 10 μM, 2 h) and used as a positive control. At least 200 cells were scored for tail moment using Opencomet software in Fiji. Samples were compared using one-way ANOVA with Tukey's multiple comparisons test. **c** DNA content analysis of CAL-51 CN-18 cells transduced to overexpress R175H or R273H mutant p53. Cell cycle distributions represent DNA content measured by flow cytometry of propidium iodide (PI) stained cells and **d** quantification of chromosomes using metaphase spreads (10 cells per cell line) at approximately 10 passages after viral transduction. **e** Immunoblot showing expression of the indicated p53 protein or GAPDH loading control following viral transduction.

Our results show that mutant p53 proteins are still ubiquitinated and degraded in CAL-51 cell lines through an MDM2-independent mechanism (Fig. 28-30). These data indicate that other E3 ubiquitin ligases exist that can contribute to mutant p53 ubiquitination. E3 ligases CHIP and Pirh2 have been shown to ubiquitinate and regulate mutant p53 protein (Lukashchuk and Vousden, 2007; Parrales et al., 2016); thus, genetic modulation through knock-in and knockdown experiments followed by immunoblotting analyses can be utilized to determine if these proteins are contributing to the mutant p53 ubiquitination seen in our cell lines. Current and ongoing analyses also focus on identifying novel proteins that potentially regulate mutant p53 stability. We are currently optimizing conditions to immunoprecipitate p53 from CAL-51 WT, Null and mutant p53 cell lines followed by mass spectrometry to identify novel mutant p53 interacting proteins. In Chapter IV, we determined that a non-proteasomal mechanism contributes to mutant p53 degradation (Fig. 31). Analysis of other cellular degradation pathways, such as cellular autophagy, could be further investigated for their potential role in mutant p53 degradation.

Finally, further analysis of genomic datasets comparing cell lines with high and low levels of p53 protein could provide useful information as to the cellular pathways contributing to mutant p53 stabilization and degradation. Bioinformatics analyses of publicly available human cell line and tumor datasets are currently being conducted to identify genes with genetic dependencies or expression levels that correlate with mutant p53 expression. Given the interest in destabilizing mutant p53 for therapeutic purposes, any discoveries made regarding mutant p53 stabilization utilizing our cell line models will be of value.

Concluding Remarks

In conclusion, the research presented herein has provided new insight to mutant p53 function and uncovered that aneuploidy contributes to several phenotypes previously associated with mutant p53 GOF activity and accumulation of the mutant protein. Additionally, this dissertation research and the work of others utilizing advanced technologies have shown no evidence for mutant p53 GOF (Boettcher et al., 2019; Giacomelli et al., 2018; Redman-Rivera et al., 2021). These findings build on nearly three decades of research, much of which has claimed oncogenic functions of mutant p53. Thus, the research described herein will benefit the p53 field and catalyze discoveries that may be translated into clinical advancements for patients with cancer.

REFERENCES

Aas, T., Børresen, A.L., Geisler, S., Smith-Sørensen, B., Johnsen, H., Varhaug, J.E., Akslen, L.A., and Lønning, P.E. (1996). Specific P53 mutations are associated with de novo resistance to doxorubicin in breast cancer patients. Nat. Med. *2*, 811–814.

Adorno, M., Cordenonsi, M., Montagner, M., Dupont, S., Wong, C., Hann, B., Solari, A., Bobisse, S., Rondina, M.B., Guzzardo, V., et al. (2009). A Mutant-p53/Smad Complex Opposes p63 to Empower TGFβ-Induced Metastasis. Cell *137*, 87–98.

Agapova, L.S., Ilyinskaya, G. V, Turovets, N.A., Ivanov, A. V, Churnakov, P.M., and Kopnin, B.P. (1996). Chromosome changes caused by alterations of p53 expression. Mutat. Res. *354*, 129–138.

Di Agostino, S., Strano, S., Emiliozzi, V., Zerbini, V., Mottolese, M., Sacchi, A., Blandino, G., and Piaggio, G. (2006). Gain of function of mutant p53: The mutant p53/NF-Y protein complex reveals an aberrant transcriptional mechanism of cell cycle regulation. Cancer Cell *10*, 191–202.

Alexandrova, E.M., Yallowitz, A.R., Li, D., Xu, S., Schulz, R., Proia, D.A., Lozano, G., Dobbelstein, M., and Moll, U.M. (2015). Improving survival by exploiting tumour dependence on stabilized mutant p53 for treatment. Nature *523*, 352–356.

Allen, M.A., Andrysik, Z., Dengler, V.L., Mellert, H.S., Guarnieri, A., Freeman, J.A., Sullivan, K.D., Galbraith, M.D., Luo, X., Lee Kraus, W., et al. (2014). Global analysis of p53-regulated transcription identifies its direct targets and unexpected regulatory mechanisms. Elife *2014*, 1–29.

Allton, K., Jain, A.K., Herz, H.-M., Tsai, W.-W., Jung, S.Y., Qin, J., Bergmann, A., Johnson, R.L., and Barton, M.C. (2009). Trim24 targets endogenous p53 for degradation. Proc. Natl. Acad. Sci. U. S. A. *106*, 11612–11616.

Alsner, J., Jensen, V., Kyndi, M., Vrou Offersen, B., Vu, P., Børresen-Dale, A.-L., and Overgaard, J. (2008). A comparison between p53 accumulation determined by immunohistochemistry and TP53 mutations as prognostic variables in tumours from breast cancer patients. Acta Oncol. (Madr). *47*, 600–607.

Andreeff, M., Kelly, K.R., Yee, K., Assouline, S., Strair, R., Popplewell, L., Bowen, D., Martinelli, G., Drummond, M.W., Vyas, P., et al. (2016). Results of the phase i trial of RG7112, a small-molecule MDM2 antagonist in leukemia. Clin. Cancer Res. *22*, 868–876.

Andrews, S. (2010). FastQC: A Quality Control Tool for High Throughput Sequence Data.

Baker, S.J., Fearon, E.R., Nigro, J.M., Hamilton, S.R., Preisinger, A.C., Jessup, J.M., VanTuinen, P., Ledbetter, D.H., Barker, D.F., Nakamura, Y., et al. (1989). Chromosome 17 deletions and p53 gene mutations in colorectal carcinomas. Science *244*, 217–221.

Bakhoum, S.F., Ngo, B., Laughney, A.M., Cavallo, J.A., Murphy, C.J., Ly, P., Shah, P., Sriram, R.K., Watkins, T.B.K., Taunk, N.K., et al. (2018). Chromosomal instability drives metastasis through a cytosolic DNA response. Nature *553*, 467–472.

Bargonetti, J., Friedman, P.N., Kern, S.E., Vogelstein, B., and Prives, C. (1991). Wild-Type but Not Mutant p53 Immunopurified Proteins Bind to Sequences Adjacent to the SV40 Origin of Replication.

Barretina, J., Caponigro, G., Stransky, N., Venkatesan, K., Margolin, A.A., Kim, S., Wilson, C.J., Lehár, J., Kryukov, G. V., Sonkin, D., et al. (2012). The Cancer Cell Line Encyclopedia enables predictive modelling of anticancer drug sensitivity. Nature *483*, 603–607.

Bártek, J., Bártková, J., Vojtěsek, B., Stasková, Z., Lukás, J., Rejthar, A., Kovarík, J., Midgley, C.A., Gannon, J. V, and Lane, D.P. (1991). Aberrant expression of the p53 oncoprotein is a common feature of a wide spectrum of human malignancies. Oncogene *6*, 1699–1703.

Beach, R.R., Ricci-Tam, C., Brennan, C.M., Moomau, C.A., Hsu, P. hsin, Hua, B., Silberman, R.E., Springer, M., and Amon, A. (2017). Aneuploidy Causes Non-genetic Individuality. Cell *169*, 229-242.e21.

Belyi, V.A., Ak, P., Markert, E., Wang, H., Hu, W., Puzio-Kuter, A., and Levine, A.J. (2010). The origins and evolution of the p53 family of genes. Cold Spring Harb. Perspect. Biol. *2*, a001198.

Ben-David, U., and Amon, A. (2020). Context is everything: aneuploidy in cancer. Nat. Rev. Genet. *21*, 44–62.

Beroukhim, R., Mermel, C.H., Porter, D., Wei, G., Raychaudhuri, S., Donovan, J., Barretina, J., Boehm, J.S., Dobson, J., Urashima, M., et al. (2010). The landscape of somatic copy-number alteration across human cancers. Nature *463*, 899–905.

Bischoff, F.Z., Yim, S.O., Pathak, S., Grant, G., Siciliano, M.J., Giovanella, B.C., Strong, L.C., and Tainsky, M.A. (1990). Spontaneous Abnormalities in Normal Fibroblasts from Patients with Li-Fraumeni Cancer Syndrome: Aneuploidy and Immortalization. Cancer Res. *50*, 7979–7984.

Blandino, G., Levine, A.J., and Oren, M. (1999). Mutant p53 gain of function: Differential effects of different p53 mutants on resistance of cultured cells to chemotherapy. Oncogene *18*, 477–485.

Boettcher, S., Miller, P.G., Sharma, R., McConkey, M., Leventhal, M., Krivtsov, A. V., Giacomelli, A.O., Wong, W., Kim, J., Chao, S., et al. (2019). A dominant-negative effect drives selection of TP53 missense mutations in myeloid malignancies. Science *365*, 599–604.

Bouchalova, P., Nenutil, R., Muller, P., Hrstka, R., Appleyard, M.V., Murray, K., Jordan, L.B., Purdie, C.A., Quinlan, P., Thompson, A.M., et al. (2014). Mutant p53 accumulation in human breast cancer is not an intrinsic property or dependent on structural or functional disruption but is regulated by exogenous stress and receptor status. J. Pathol. *233*, 238–246.

Bougeard, G., Renaux-Petel, M., Flaman, J.-M., Charbonnier, C., Fermey, P., Belotti, M., Gauthier-Villars, M., Stoppa-Lyonnet, D., Consolino, E., Brugières, L., et al. (2015). Revisiting Li-Fraumeni Syndrome From TP53 Mutation Carriers. J. Clin. Oncol. *33*, 2345–2352.

Boveri, T. (2008). Concerning the Origin of Malignant Tumours by Theodor Boveri. Translated and annotated by Henry Harris. J. Cell Sci. *121*, 1–84.

Boyle, J.M., Mitchell, E.L., Greaves, M.J., Roberts, S.A., Tricker, K., Burt, E., Varley, J.M., Birch, J.M., and Scott, D. (1998). Chromosome instability is a predominant trait of fibroblasts from Li-Fraumeni families. Br. J. Cancer *77*, 2181–2192.

Braicu, C., Pileczki, V., Irimie, A., and Berindan-Neagoe, I. (2013). p53siRNA therapy reduces cell proliferation, migration and induces apoptosis in triple negative breast cancer cells. Mol. Cell. Biochem. *381*, 61–68.

Brosh, R., and Rotter, V. (2009). When mutants gain new powers: news from the mutant p53 field. Nat. Rev. Cancer *9*, 701–713.

Bulavin, D. V., Demidov, O.N., Saito, S., Kauraniemi, P., Phillips, C., Amundson, S.A., Ambrosino, C., Sauter, G., Nebreda, A.R., Anderson, C.W., et al. (2002). Amplification of PPM1D in human tumors abrogates p53 tumor-suppressor activity. Nat. Genet. *31*, 210–215.

Bykov, V.J.N., Issaeva, N., Shilov, A., Hultcrantz, M., Pugacheva, E., Chumakov, P., Bergman, J., Wiman, K.G., and Selivanova, G. (2002). Restoration of the tumor suppressor function to mutant p53 by a low-molecular-weight compound. Nat. Med. *8*, 282–288.

Bykov, V.J.N., Eriksson, S.E., Bianchi, J., and Wiman, K.G. (2017). Targeting mutant p53 for efficient cancer therapy. Nat. Rev. Cancer *18*, 89–102.

Campbell, P.J., Getz, G., Korbel, J.O., Stuart, J.M., Jennings, J.L., Stein, L.D., Perry, M.D., Nahal-Bose, H.K., Ouellette, B.F.F., Li, C.H., et al. (2020). Pan-cancer analysis of whole genomes. Nature *578*, 82–93.

Carpenter, A.E., Jones, T.R., Lamprecht, M.R., Clarke, C., Kang, I.H., Friman, O., Guertin, D.A., Chang, J.H., Lindquist, R.A., Moffat, J., et al. (2006). CellProfiler: Image analysis software for identifying and quantifying cell phenotypes. Genome Biol. *7*, R100.

Cerami, E., Gao, J., Dogrusoz, U., Gross, B.E., Sumer, S.O., Aksoy, B.A., Jacobsen, A., Byrne, C.J., Heuer, M.L., Larsson, E., et al. (2012). The cBio Cancer Genomics Portal: An open platform for exploring multidimensional cancer genomics data. Cancer Discov. *2*, 401–404.

Chandar, N., Billig, B., McMaster, J., and Novak, J. (1992). Inactivation of p53 gene in human and murine osteosarcoma cells. Br. J. Cancer *65*, 208–214.

Chang, C.-J., Chao, C.-H., Xia, W., Yang, J.-Y., Xiong, Y., Li, C.-W., Yu, W.-H., Rehman, S.K., Hsu, J.L., Lee, H.-H., et al. (2011). p53 regulates epithelial–mesenchymal transition and stem cell properties through modulating miRNAs. Nat. Cell Biol. *13*, 317–323.

Cho, Y., Gorina, S., Jeffrey, P.D., and Pavletich, N.P. (1994). Crystal structure of a p53 tumor suppressor-DNA complex: understanding tumorigenic mutations. Science *265*, 346–355.

Chunduri, N.K., and Storchová, Z. (2019). The diverse consequences of aneuploidy. Nat. Cell Biol. *21*, 54–62.

Ciriello, G., Miller, M.L., Aksoy, B.A., Senbabaoglu, Y., Schultz, N., and Sander, C. (2013). Emerging landscape of oncogenic signatures across human cancers. Nat. Genet. *45*, 1127–1133.

Clarke, A.., Purdie, C.A., Harrison, D.J., Morris, R.G., Bird, C.C., Hooper, M.L., and Wyllie, A.H. (1993). Thymocyte apoptosis induced by p53-dependent and independent pathways. Nature *362*, 849–852.

Clinical Lung Cancer Genome Project (CLCGP), and Network Genomic Medicine (NGM) (2013). A genomics-based classification of human lung tumors. Sci. Transl. Med. *5*, 209ra153-209ra153.

Coffill, C.R., Muller, P.A.J., Oh, H.K., Neo, S.P., Hogue, K.A., Cheok, C.F., Vousden, K.H., Lane, D.P., Blackstock, W.P., and Gunaratne, J. (2012). Mutant p53 interactome identifies nardilysin as a p53R273H-specific binding partner that promotes invasion. EMBO Rep. *13*, 638–644.

Di Como, C.J., Gaiddon, C., and Prives, C. (1999). P73 Function Is Inhibited By Tumor-Derived P53 Mutants in Mammalian Cells. Mol. Cell. Biol. *19*, 1438–1449.

Cordani, M., Butera, G., Dando, I., Torrens-Mas, M., Butturini, E., Pacchiana, R., Oppici, E., Cavallini, C., Gasperini, S., Tamassia, N., et al. (2018). Mutant p53 blocks SESN1/AMPK/PGC-1α/UCP2 axis increasing mitochondrial $O2^{-}\cdot$ production in cancer cells. Br. J. Cancer *119*, 994–1008.

Crawford, L.V., Pim, D.C., and Bulbrook, R.D. (1982). Detection of antibodies against the cellular protein p53 in sera from patients with breast cancer. Int. J. Cancer *30*, 403–408.

Daemen, A., Griffith, O.L., Heiser, L.M., Wang, N.J., Enache, O.M., Sanborn, Z., Pepin, F., Durinck, S., Korkola, J.E., Griffith, M., et al. (2013). Modeling precision treatment of breast cancer. Genome Biol. *14*, R110.

Davoli, T., Uno, H., Wooten, E.C., and Elledge, S.J. (2017). Tumor aneuploidy correlates with markers of immune evasion and with reduced response to immunotherapy. Science *355*.

Deleo, A.B., Jayt, G., Appellat, E., Duboist, G.C., Lawt, L.W., and Old, L.J. (1979). Detection of a transformation-related antigen in chemically induced sarcomas and other transformed cells of the mouse. Immunology *76*, 2420–2424.

Dittmer, D., Pati, S., Zambetti, G., Chu, S., Teresky, A.K., Moore, M., Finlay, C., and Levine, A.J. (1993). Gain of function mutations in p53. Nat. Genet. *4*, 42–46.

Dodt, M., Roehr, J.T., Ahmed, R., and Dieterich, C. (2012). FLEXBAR-flexible barcode and adapter processing for next-generation sequencing platforms. Biology (Basel). *1*, 895–905.

Donehower, L.A., Harvey, M., Slagle, B.L., McArthur, M.J., Montgomery, C.A., Butel, J.S., and Bradley, A. (1992). Mice deficient for p53 are developmentally normal but susceptible to spontaneous tumours. Nature *356*, 215–221.

Donehower, L.A., Soussi, T., Korkut, A., Liu, Y., Schultz, A., Cardenas, M., Li, X., Babur, O., Hsu, T.-K., Lichtarge, O., et al. (2019). Integrated Analysis of TP53 Gene and Pathway Alterations in The Cancer Genome Atlas. Cell Rep. *28*, 1370–1384.

Dornan, D., Wertz, I., Shimizu, H., Arnott, D., Frantz, G.D., Dowd, P., O' Rourke, K., Koeppen, H., and Dixit, V.M. (2004). The ubiquitin ligase COP1 is a critical negative regulator of p53. Nature *429*, 86–92.

Dowell, S.P., Wilson, P.O., Derias, N.W., Lane, D.P., and Hall, P.A. (1994). Clinical utility of the immunocytochemical detection of p53 protein in cytological specimens. Cancer Res. *54*, 2914–2918.

Duensing, A., and Duensing, S. (2005). Guilt by association? p53 and the development of aneuploidy in cancer. Biochem. Biophys. Res. Commun. *331*, 694–700.

Dumaz, N., and Meek, D.W. (1999). Serine15 phosphorylation stimulates p53 transactivation but does not directly influence interaction with HDM2. EMBO J. *18*, 7002–7010.

Eby, K.G., Rosenbluth, J.M., Mays, D.J., Marshall, C.B., Barton, C.E., Sinha, S., Johnson, K.N., Tang, L., and Pietenpol, J.A. (2010). ISG20L1 is a p53 family target gene that modulates genotoxic stress-induced autophagy. Mol. Cancer *9*, 95.

El-Deiry, W.S., Kern, S.E., Pietenpol, J.A., Kinzler, K.W., and Vogelstein, B. (1992). Definition of a consensus binding site for p53. Nat. Genet. *1*, 45–49.

El-Deiry, W.S., Tokino, T., Velculescu, V.E., Levy, D.B., Parsons, R., Trent, J.M., Lin, D., Edward Mercer, W., Kinzler, K.W., and Vogelstein, B. (1993). WAF1, a Potential Mediator of p53 Tumor Suppression. Cell *75*, 817–825.

Eliyahu, D., Raz, A., Gruss, P., Givol, D., and Oren, M. (1984). Participation of p53 cellular tumour antigen in transformation of normal embryonic cells. Nature *312*, 646–649.

Eliyahu, D., Goldfinger, N., Pinhasi-Kimhi, O., Shaulsky, G., Skurnik, Y., Arai, N., Rotter, V., and Oren, M. (1988). Meth A fibrosarcoma cells express two transforming mutant p53 species. Oncogene *3*, 313–321.

Eliyahu, D., Michalovitz, D., Eliyahu, S., Pinhasi-Kimhi, O., and Oren, M. (1989). Wild-type p53 can inhibit oncogene-mediated focus formation. Proc. Natl. Acad. Sci. U. S. A. *86*, 8763–8767.

Ellrott, K., Bailey, M.H., Saksena, G., Covington, K.R., Kandoth, C., Stewart, C., Hess, J., Ma, S., Chiotti, K.E., McLellan, M., et al. (2018). Scalable Open Science Approach for Mutation Calling of Tumor Exomes Using Multiple Genomic Pipelines. Cell Syst. *6*, 271–281.

Eriksson, M., Ambroise, G., Ouchida, A.T., Lima Queiroz, A., Smith, D., Gimenez-Cassina, A., Iwanicki, M.P., Muller, P.A., Norberg, E., and Vakifahmetoglu-Norberg, H. (2017). Effect of Mutant p53 Proteins on Glycolysis and Mitochondrial Metabolism. Mol. Cell. Biol. *37*.

Escobar-Hoyos, L.F., Penson, A., Kannan, R., Cho, H., Pan, C.-H., Singh, R.K., Apken, L.H., Hobbs, G.A., Luo, R., Lecomte, N., et al. (2020). Altered RNA Splicing by Mutant p53 Activates Oncogenic RAS Signaling in Pancreatic Cancer. Cancer Cell *38*, 198-211.e8.

Ewels, P., Magnusson, M., Lundin, S., and Käller, M. (2016). MultiQC: summarize analysis results for multiple tools and samples in a single report. Bioinformatics *32*, 3047–3048.

Farmer, G., Bargonetti, J., Zhu, H., Friedman, P., Prywes, R., and Prives, C. (1992). Wild-type p53 activates transcription in vitro. Nature *358*, 83–86.

Fearon, E.R., and Vogelstein, B. (1990). A genetic model for colorectal tumorigenesis. Cell *61*, 759–767.

Finlay, C.A., Hinds, P.W., Tan, T.H., Eliyahu, D., Oren, M., and Levine, A.J. (1988). Activating mutations for transformation by p53 produce a gene product that forms an hsc70-p53 complex with an altered half-life. Mol. Cell. Biol. *8*, 531–539.

Finlay, C.A., W. Hinds, P., and Levine, A.J. (1989). The p53 Proto-Oncogene Can Act as a Suppressor of Transformation.

Fischer, M. (2017). Census and evaluation of p53 target genes. Oncogene *36*, 3943–3956.

Flores, E.R., Tsai, K.Y., Crowley, D., Sengupta, S., Yang, A., McKeon, F., and Jacks, T. (2002). p63 and p73 are required for p53-dependent apoptosis in response to DNA damage. Nature *416*, 560–564.

Franch-Expósito, S., Bassaganyas, L., Vila-Casadesús, M., Hernández-Illán, E., Esteban-Fabró, R., Díaz-Gay, M., Lozano, J.J., Castells, A., Llovet, J.M., Castellví-Bel, S., et al. (2020). CNApp, a tool for the quantification of copy number alterations and integrative analysis revealing clinical implications. Elife *9*.

Freed-Pastor, W.A., Mizuno, H., Zhao, X., Langerød, A., Moon, S.H., Rodriguez-Barrueco, R., Barsotti, A., Chicas, A., Li, W., Polotskaia, A., et al. (2012). Mutant p53 disrupts mammary tissue architecture via the mevalonate pathway. Cell *148*, 244–258.

Fuchs, S.Y., Adler, V., Buschmann, T., Yin, Z., Wu, X., Jones, S.N., and Ronai, Z. (1998). JNK targets p53 ubiquitination and degradation in nonstressed cells. Genes Dev. *12*, 2658–2663.

Fujiwara, T., Bandi, M., Nitta, M., Ivanova, E. V, Bronson, R.T., and Pellman, D. (2005). Cytokinesis failure generating tetraploids promotes tumorigenesis in p53-null cells.

Gaiddon, C., Lokshin, M., Ahn, J., Zhang, T., and Prives, C. (2001). A Subset of Tumor-Derived Mutant Forms of p53 Down-Regulate p63 and p73 through a Direct Interaction with the p53 Core Domain. Mol. Cell. Biol. *21*, 1874–1887.

Gao, J., Aksoy, B.A., Dogrusoz, U., Dresdner, G., Gross, B., Sumer, S.O., Sun, Y., Jacobsen, A., Sinha, R., Larsson, E., et al. (2013). Integrative analysis of complex cancer genomics and clinical profiles using the cBioPortal. Sci. Signal. *6*, pl1–pl1.

Gerstung, M., Jolly, C., Leshchiner, I., Dentro, S.C., Gonzalez, S., Rosebrock, D., Mitchell, T.J., Rubanova, Y., Anur, P., Yu, K., et al. (2020). The evolutionary history of 2,658 cancers. Nature *578*, 122–128.

Ghosh, M., Saha, S., Bettke, J., Nagar, R., Parrales, A., Iwakuma, T., van der Velden, A.W.M., and Martinez, L.A. (2021). Mutant p53 suppresses innate immune signaling to promote tumorigenesis. Cancer Cell *39*, 494-508.e5.

Giaccia, A.J., and Kastan, M.B. (1998). The complexity of p53 modulation: emerging patterns from divergent signals. Genes Dev. *12*, 2973–2983.

Giacomelli, A.O., Yang, X., Lintner, R.E., McFarland, J.M., Duby, M., Kim, J., Howard, T.P., Takeda, D.Y., Ly, S.H., Kim, E., et al. (2018). Mutational processes shape the landscape of TP53 mutations in human cancer. Nat. Genet. *50*, 1381–1387.

Gioanni, J., Le François, D., Mazeau, C., Ettore, F., Lambert, J.C., and Dutrillaux, B. (1990). Establishment and characterisation of a new tumorigenic cell line with a normal karyotype derived from a human breast adenocarcinoma. Br. J. Cancer *62*, 8–13.

Goh, A.M., Xue, Y., Leushacke, M., Li, L., Wong, J.S., Chiam, P.C., Rahmat, S.A.B., Mann, M.B., Mann, K.M., Barker, N., et al. (2015). Mutant p53 accumulates in cycling and proliferating cells in the normal tissues of p53 R172H mutant mice. Oncotarget *6*, 17968–17980.

Gourley, C., Green, J., Gabra, H., Vergote, I., Basu, B., Brenton, J.D., Björklund, U., Smith, A.M., and Von Euler, M. (2016). PISARRO: A EUTROC phase Ib study of APR-246 in combination with carboplatin (C) and pegylated liposomal doxorubicin (PLD) in platinum sensitive relapsed high grade serous ovarian cancer (HGSOC). J. Clin. Oncol. *34*, 5571–5571.

Gu, W., and Roeder, R.G. (1997). Activation of p53 sequence-specific DNA binding by acetylation of the p53 C-terminal domain. Cell *90*, 595–606.

Gualberto, A., Aldape, K., Kozakiewicz, K., and Tlsty, T.D. (1998). An oncogenic form of p53 confers a dominant, gain-of-function phenotype that disrupts spindle checkpoint control. Genetics *95*, 5166–5171.

Gudas, J.M., Nguyen, H., Klein, R.C., Katayose, D., Seth, P., and Cowan, K.H. (1995). Differential Expression of Multiple MDM2 Messenger RNAs and Proteins in Normal and Tumorigenic Breast Epithelial Cells.

Hainaut, P., and Pfeifer, G.P. (2016). Somatic TP53 Mutations in the Era of Genome Sequencing. Cold Spring Harb. Perspect. Med. *6*.

Halevy, O., Michalovitz, D., and Oren, M. (1990). Different tumor-derived p53 mutants exhibit distinct biological activities. Science *250*, 113–116.

Hall, P.A., and Lane, D.P. (1994). p53 In tumour pathology: Can we trust immunohistochemistry?—revisited! J. Pathol. *172*, 1–4.

Hallek, M. (2019). Chronic lymphocytic leukemia: 2020 update on diagnosis, risk stratification and treatment. Am. J. Hematol. *94*, 1266–1287.

Hanel, W., and Moll, U.M. (2012). Links between mutant p53 and genomic instability. J. Cell. Biochem. *113*, 433–439.

Hansemann, V.D. (1890). Ueber asymmetrische Zelltheilung in Epithelkrebsen und deren biologische Bedeutung. Arch. Für Pathol. Anat. Und Physiol. Und Für Klin. Med. *119*, 299–326.

Harper, J.W., Adami, G.R., Wei, N., Keyomarsi, K., and Elledge', S.J. (1993). The p21 Cdk-Interacting Protein Cip1 Is a Potent Inhibitor of G1 Cyclin-Dependent Kinases. Cell *75*, 805–816.

Harvey, M., Vogel, H., Morris, D., Bradley, A., Bernstein, A., and Donehower, L.A. (1995). A mutant p53 transgene accelerates tumour development in heterozygous but not nullizygous p53–deficient mice. Nat. Genet. *9*, 305–311.

Haupt, Y., Maya, R., Kazaz, A., and Oren, M. (1997). Mdm2 promotes the rapid degradation of p53. Nature *387*, 296–299.

Hieronymus, H., Murali, R., Tin, A., Yadav, K., Abida, W., Moller, H., Berney, D., Scher, H., Carver, B., Scardino, P., et al. (2018). Tumor copy number alteration burden is a pan-cancer prognostic factor associated with recurrence and death. Elife *7*, 1–18.

Hingorani, S.R., Wang, L., Multani, A.S., Combs, C., Deramaudt, T.B., Hruban, R.H., Rustgi, A.K., Chang, S., and Tuveson, D.A. (2005). Trp53R172H and KrasG12D cooperate to promote chromosomal instability and widely metastatic pancreatic ductal adenocarcinoma in mice. Cancer Cell *7*, 469–483.

Hsiue, E.H.-C., Wright, K.M., Douglass, J., Hwang, M.S., Mog, B.J., Pearlman, A.H., Paul, S., DiNapoli, S.R., Konig, M.F., Wang, Q., et al. (2021). Targeting a neoantigen derived from a common TP53 mutation. Science *371*.

Humpton, T.J., Hock, A.K., Maddocks, O.D.K., and Vousden, K.H. (2018). p53-mediated adaptation to serine starvation is retained by a common tumour-derived mutant. Cancer Metab. *6*, 18.

Hwang, S., Gustafsson, H.T., O'Sullivan, C., Bisceglia, G., Huang, X., Klose, C., Schevchenko, A., Dickson, R.C., Cavaliere, P., Dephoure, N., et al. (2017). Serine-Dependent Sphingolipid Synthesis Is a Metabolic Liability of Aneuploid Cells. Cell Rep. *21*, 3807–3818.

Ignatiadis, N., Klaus, B., Zaugg, J.B., and Huber, W. (2016). Data-driven hypothesis weighting increases detection power in genome-scale multiple testing. Nat. Methods *13*, 577–580.

Ingallina, E., Sorrentino, G., Bertolio, R., Lisek, K., Zannini, A., Azzolin, L., Severino, L.U., Scaini, D., Mano, M., Mantovani, F., et al. (2018). Mechanical cues control mutant p53 stability through a mevalonate–RhoA axis. Nat. Cell Biol. *20*, 28–35.

Invitae Corporation (2018). Invitae Multi-Cancer Panel.

Ito, A., Kawaguchi, Y., Lai, C.-H., Kovacs, J.J., Higashimoto, Y., Appella, E., and Yao, T.-P. (2002). MDM2–HDAC1-mediated deacetylation of p53 is required for its degradation. EMBO J. *21*, 6236–6245.

Jenkins, J.R., Rudge, K., and Currie, G.A. (1984a). Cellular immortalization by a cDNA clone encoding the transformation-associated phosphoprotein p53. Nature *312*, 651–654.

Jenkins, J.R., Rudge, K., Redmond, S., and Wade-Evans, A. (1984b). Cloning and expression analysis of full length mouse cDNA sequences encoding the transformation associated protein p53. Nucleic Acids Res. *12*, 5609–5626.

Jiang, D., Brady, C.A., Johnson, T.M., Lee, E.Y., Park, E.J., Scott, M.P., and Attardi, L.D. (2011). Full p53 transcriptional activation potential is dispensable for tumor suppression in diverse lineages. Proc. Natl. Acad. Sci. U. S. A. *108*, 17123–17128.

Jin, X., Demere, Z., Nair, K., Ali, A., Ferraro, G.B., Natoli, T., Deik, A., Petronio, L., Tang, A.A., Zhu, C., et al. (2020). A metastasis map of human cancer cell lines. Nature *588*, 331–336.

Jones, S.N., Roe, A.E., Donehower, L.A., and Bradley, A. (1995). Rescue of embryonic lethality in Mdm2-deficient mice by absence of p53. Nature *378*, 206–208.

Jost, C.A., Marin, M.C., and Jr, W.G.K. (1997). p73 is a human p53-related protein that can induce apoptosis. Nature *389*, 191–194.

Juven, T., Barak, Y., Zauberman, A., George, D.L., and Oren, M. (1993). Wild type p53 can mediate sequence-specific transactivation of an internal promoter within the mdm2 gene. Oncogene *8*, 3411–3416.

Kaghad, M., Bonnet, H., Yang, A., Creancier, L., Biscan, J.C., Valent, A., Minty, A., Chalon, P., Lelias, J.M., Dumont, X., et al. (1997). Monoallelically expressed gene related to p53 at 1p36, a region frequently deleted in neuroblastoma and other human cancers. Cell *90*, 809–819.

Kalo, E., Kogan-Sakin, I., Solomon, H., Bar-Nathan, E., Shay, M., Shetzer, Y., Dekel, E., Goldfinger, N., Buganim, Y., Stambolsky, P., et al. (2012). Mutant p53R273H attenuates the expression of phase 2 detoxifying enzymes and promotes the survival of cells with high levels of reactive oxygen species. J. Cell Sci. *125*, 5578–5586.

Kandoth, C., McLellan, M.D., Vandin, F., Ye, K., Niu, B., Lu, C., Xie, M., Zhang, Q., McMichael, J.F., Wyczalkowski, M.A., et al. (2013). Mutational landscape and significance across 12 major cancer types. Nature *502*, 333–339.

Kastan, M.B., Onyekwere, O., Sidransky, D., Vogelstein, B., and Craig, R.W. (1991). Participation of p53 Protein in the Cellular Response to DNA Damage. Cancer Res. *51*, 6304–6311.

Kastenhuber, E.R., and Lowe, S.W. (2017). Putting p53 in Context. Cell *170*, 1062–1078.

Kato, S., Han, S.-Y., Liu, W., Otsuka, K., Shibata, H., Kanamaru, R., and Ishioka, C. (2003). Understanding the function-structure and function-mutation relationships of p53 tumor suppressor protein by high-resolution missense mutation analysis. Proc. Natl. Acad. Sci. U. S. A. *100*, 8424–8429.

Kern, S.E., Pietenpol, J.A., Thiagalingam, S., Seymour, A., Kinzler, K.W., and Vogelstein, B. (1992). Oncogenic forms of p53 inhibit p53-regulated gene expression. Science *256*, 827–830.

Kim, A.L., Raffo, A.J., Brandt-Rauf, P.W., Pincus, M.R., Monaco, R., Abarzua, P., and Fine, R.L. (1999). Conformational and Molecular Basis for Induction of Apoptosis by a p53 C-terminal Peptide in Human Cancer Cells. J. Biol. Chem. *274*, 34924–34931.

Kim, C., Gao, R., Sei, E., Crosetto, N., Foukakis, T., and Navin Correspondence, N.E. (2018). Chemoresistance Evolution in Triple-Negative Breast Cancer Delineated by Single-Cell Sequencing. Cell *173*, 879–893.

Kitayner, M., Rozenberg, H., Kessler, N., Rabinovich, D., Shaulov, L., Haran, T.E., and Shakked, Z. (2006). Structural basis of DNA recognition by p53 tetramers. Mol. Cell *22*, 741–753.

Kratz, C.P., Achatz, M.I., Brugi Eres, L., Frebourg, T., Garber, J.E., Greer, M.-L.C., Hansford, J.R., Janeway, K.A., Kohlmann, W.K., Mcgee, R., et al. (2017). Cancer Screening Recommendations for Individuals with Li-Fraumeni Syndrome. Clin Cancer Res *23*.

Kress, M., May, E., Cassingena, R., and May, P. (1979). Simian virus 40-transformed cells express new species of proteins precipitable by anti-simian virus 40 tumor serum. J. Virol. *31*, 472–483.

Kruiswijk, F., Labuschagne, C.F., and Vousden, K.H. (2015). p53 in survival, death and metabolic health: a lifeguard with a licence to kill. Nat. Rev. Mol. Cell Biol. *16*, 393–405.

Kuhn, E., Kurman, R.J., Vang, R., Sehdev, A.S., Han, G., Soslow, R., Wang, T.-L., and Shih, I.-M. (2012). TP53 mutations in serous tubal intraepithelial carcinoma and concurrent pelvic high-grade serous carcinoma-evidence supporting the clonal relationship of the two lesions. J. Pathol. *226*, 421–426.

Lambert, J.M.R., Gorzov, P., Veprintsev, D.B., Söderqvist, M., Segerbäck, D., Bergman, J., Fersht, A.R., Hainaut, P., Wiman, K.G., and Bykov, V.J.N. (2009). PRIMA-1 reactivates mutant p53 by covalent binding to the core domain. Cancer Cell *15*, 376–388.

Lambert, P.F., Kashanchi, F., Radonovich, M.F., Shiekhattar, R., and Brady, J.N. (1998). Phosphorylation of p53 Serine 15 Increases Interaction with CBP. J. Biol. Chem. *273*, 33048–33053.

Lane, D.P. (1992). p53, guardian of the genome. Nature *358*, 15–16.

Lane, D., and Levine, A. (2010). p53 Research: the past thirty years and the next thirty years. Cold Spring Harb. Perspect. Biol. *2*, a000893.

Lane, D.P., and Crawford, L. V. (1979). T antigen is bound to a host protein in SV40-transformed cells. Nature *278*, 261–263.

Lang, G.A., Iwakuma, T., Suh, Y.-A., Liu, G., Rao, V.A., Parant, J.M., Valentin-Vega, Y.A., Terzian, T., Caldwell, L.C., Strong, L.C., et al. (2004). Gain of Function of a p53 Hot Spot Mutation in a Mouse Model of Li-Fraumeni Syndrome. Cell *119*, 861–872.

Langerød, A., Zhao, H., Borgan, Ø., Nesland, J.M., Bukholm, I.R., Ikdahl, T., Kåresen, R., Børresen-Dale, A.-L., and Jeffrey, S.S. (2007). TP53mutation status and gene expression profiles are powerful prognostic markers of breast cancer. Breast Cancer Res. *9*, R30.

Lehmann, B.D., and Pietenpol, J.A. (2012). Targeting mutant p53 in human tumors. J. Clin. Oncol. *30*, 3648–3650.

Lehmann, B.D., Bauer, J.A., Chen, X., Sanders, M.E., Chakravarthy, A.B., Shyr, Y., and Pietenpol, J.A. (2011). Identification of human triple-negative breast cancer subtypes and preclinical models for selection of targeted therapies. J. Clin. Invest. *121*, 2750–2767.

Lehmann, S., Bykov, V.J.N., Ali, D., Andrén, O., Cherif, H., Tidefelt, U., Uggla, B., Yachnin, J., Juliusson, G., Moshfegh, A., et al. (2012). Targeting p53 in vivo: a first-in-human study with p53-targeting compound APR-246 in refractory hematologic malignancies and prostate cancer. J. Clin. Oncol. *30*, 3633–3639.

Levine, A.J., and Oren, M. (2009). The first 30 years of p53: growing ever more complex. Nat. Rev. Cancer *9*, 749–758.

Li, H., and Durbin, R. (2010). Fast and accurate long-read alignment with Burrows–Wheeler transform. Bioinformatics *26*, 589–595.

Li, D., Marchenko, N.D., Schulz, R., Fischer, V., Velasco-Hernandez, T., Talos, F., and Moll, U.M. (2011a). Functional Inactivation of Endogenous MDM2 and CHIP by HSP90 Causes Aberrant Stabilization of Mutant p53 in Human Cancer Cells. Mol. Cancer Res. *9*, 577–588.

Li, D., Marchenko, N.D., and Moll, U.M. (2011b). SAHA shows preferential cytotoxicity in mutant p53 cancer cells by destabilizing mutant p53 through inhibition of the HDAC6-Hsp90 chaperone axis. Cell Death Differ. *18*, 1904–1913.

Li, M., Chen, D., Shiloh, A., Luo, J., Nikolaev, A.Y., Qin, J., and Gu, W. (2002). Deubiquitination of p53 by HAUSP is an important pathway for p53 stabilization. Nature *416*, 648–653.

Li, M., Fang, X., Baker, D.J., Guo, L., Gao, X., Wei, Z., Han, S., van Deursen, J.M., and Zhang, P. (2010). The ATM-p53 pathway suppresses aneuploidy-induced tumorigenesis. Proc. Natl. Acad. Sci. U. S. A. *107*, 14188–14193.

Li, R., Sutphin, P.D., Schwartz, D., Matas, D., Almog, N., Wolkowicz, R., Goldfinger, N., Pei, H., Prokocimer, M., and Rotter, V. (1998). Mutant p53 protein expression interferes with p53-independent apoptotic pathways. Oncogene *16*, 3269–3277.

Li, Y., Guessous, F., Kwon, S., Kumar, M., Ibidapo, O., Fuller, L., Johnson, E., Lal, B., Hussaini, I., Bao, Y., et al. (2008). PTEN Has Tumor-Promoting Properties in the Setting of Gain-of-Function p53 Mutations. Cancer Res. *68*, 1723–1731.

Lim, L.Y., Vidnovic, N., Ellisen, L.W., and Leong, C.-O. (2009). Mutant p53 mediates survival of breast cancer cells. Br. J. Cancer *101*, 1606–1612.

Linzer, D.I.H., and Levine, A.J. (1979). Characterization of a 54K Dalton cellular SV40 tumor antigen present in SV40-transformed cells and uninfected embryonal carcinoma cells. Cell *17*, 43–52.

Linzer, D.I.H., Maltzman, W., and Levine, A.J. (1979). The SV40 A gene product is required for the production of a 54,000 MW cellular tumor antigen. Virology *98*, 308–318.

Liu, D.P., Song, H., and Xu, Y. (2010). A common gain of function of p53 cancer mutants in inducing genetic instability. Oncogene *29*, 949–956.

Liu, D.S., Duong, C.P., Haupt, S., Montgomery, K.G., House, C.M., Azar, W.J., Pearson, H.B., Fisher, O.M., Read, M., Guerra, G.R., et al. (2017). Inhibiting the system xC−/glutathione axis selectively targets cancers with mutant-p53 accumulation. Nat. Commun. *8*, 14844.

Liu, G., Parant, J.M., Lang, G., Chau, P., Chavez-Reyes, A., El-Naggar, A.K., Multani, A., Chang, S., and Lozano, G. (2004). Chromosome stability, in the absence of apoptosis, is critical for suppression of tumorigenesis in Trp53 mutant mice. Nat. Genet. *36*, 63–68.

Liu, J., Zhang, C., Hu, W., and Feng, Z. (2015). Tumor suppressor p53 and its mutants in cancer metabolism. Cancer Lett. *356*, 197–203.

Liu, J., Lichtenberg, T., Hoadley, K.A., Poisson, L.M., Lazar, A.J., Cherniack, A.D., Kovatich, A.J., Benz, C.C., Levine, D.A., Lee, A. V., et al. (2018). An Integrated TCGA Pan-Cancer Clinical Data Resource to Drive High-Quality Survival Outcome Analytics. Cell *173*, 400–416.

Liu, K., Ling, S., and Lin, W.-C. (2011). TopBP1 Mediates Mutant p53 Gain of Function through NF-Y and p63/p73. Mol. Cell. Biol. *31*, 4464–4481.

Liu, P.K., Kraus, E., Wu, T.A., Strong, L.C., and Tainsky, M.A. (1996). Analysis of genomic instability in Li-Fraumeni fibroblasts with germline p53 mutations. Oncogene *12*, 2267–2278.

Liu, Y., Chen, C., Xu, Z., Scuoppo, C., Rillahan, C.D., Gao, J., Spitzer, B., Bosbach, B., Kastenhuber, E.R., Baslan, T., et al. (2016). Deletions linked to TP53 loss drive cancer through p53-independent mechanisms. Nature *531*, 471–475.

Loizou, E., Banito, A., Livshits, G., Ho, Y.-J., Koche, R.P., Sánchez-Rivera, F.J., Mayle, A., Chen, C.-C., Kinalis, S., Bagger, F.O., et al. (2019). A Gain-of-Function p53-Mutant Oncogene Promotes Cell Fate Plasticity and Myeloid Leukemia through the Pluripotency Factor FOXH1. Cancer Discov. *9*, 962–979.

Love, M.I., Huber, W., and Anders, S. (2014). Moderated estimation of fold change and dispersion for RNA-seq data with DESeq2. Genome Biol. *15*, 550.

Lowe, S.W., Schmitt, E.M., Smitht, S.W., Osbornet, B.A., and Jacks, T. (1993). p53 is required for radiation-induced apoptosis in mouse thymocytes. Nature *362*, 847–849.

Lu, X. (2010). Tied up in loops: positive and negative autoregulation of p53. Cold Spring Harb. Perspect. Biol. *2*, a000984.

Lukashchuk, N., and Vousden, K.H. (2007). Ubiquitination and degradation of mutant p53. Mol. Cell. Biol. *27*, 8284–8295.

Malkin, D., Li, F.P., Strong, L.C., Fraumeni, J.F., Nelson, C.E., Kim, D.H., Kassel, J., Gryka, M.A., Bischoff, F.Z., Tainsky, M.A., et al. (1990). Germ line p53 mutations in a familial syndrome of breast cancer, sarcomas, and other neoplasms. Science *250*, 1233–1238.

Marshall, C.B., Mays, D.J., Beeler, J.S., Rosenbluth, J.M., Boyd, K.L., Santos Guasch, G.L., Shaver, T.M., Tang, L.J., Liu, Q., Shyr, Y., et al. (2016). p73 Is Required for Multiciliogenesis and Regulates the Foxj1-Associated Gene Network. Cell Rep. *14*, 2289–2300.

Martin, M. (2011). Cutadapt removes adapter sequences from high-throughput sequencing reads. EMBnet.Journal *17*, 10.

Masuda, H., Miller, C., Koeffler, H.P., Battifora, H., and Cline, M.J. (1987). Rearrangement of the p53 gene in human osteogenic sarcomas. Proc. Natl. Acad. Sci. U. S. A. *84*, 7716–7719.

Mayakonda, A., Lin, D.C., Assenov, Y., Plass, C., and Koeffler, H.P. (2018). Maftools: Efficient and comprehensive analysis of somatic variants in cancer. Genome Res. *28*, 1747–1756.

Mayrhofer, M., Viklund, B., and Isaksson, A. (2016). Rawcopy: Improved copy number analysis with Affymetrix arrays. Sci. Rep. *6*, 1–11.

McKenna, A., Hanna, M., Banks, E., Sivachenko, A., Cibulskis, K., Kernytsky, A., Garimella, K., Altshuler, D., Gabriel, S., Daly, M., et al. (2010). The genome analysis toolkit: A MapReduce framework for analyzing next-generation DNA sequencing data. Genome Res. *20*, 1297–1303.

Meek, D.W., and Anderson, C.W. (2009). Posttranslational modification of p53: cooperative integrators of function. Cold Spring Harb. Perspect. Biol. *1*, a000950.

Melero, J., Stitt, D.T., Mangel, W.F., and Carroll, R.B. (1979). Identification of new polypeptide species (48–55K) immunoprecipitable by antiserum to purified large T antigen and present in SV40-infected and -transformed cells. Virology *93*, 466–480.

Midgley, C.A., and Lane, D.P. (1997). p53 protein stability in tumour cells is not determined by mutation but is dependent on Mdm2 binding. Oncogene *15*, 1179–1189.

Mills, A.A., Zheng, B., Wang, X.-J., Vogel, H., Roop, D.R., and Bradley, A. (1999). p63 is a p53 homologue required for limb and epidermal morphogenesis. Nature *398*, 708–713.

Milner, J., and Medcalf, E.A. (1991). Cotranslation of activated mutant p53 with wild type drives the wild-type p53 protein into the mutant conformation. Cell *65*, 765–774.

Milner, J., Medcalf, E.A., and Cook, A.C. (1991). Tumor suppressor p53: analysis of wild-type and mutant p53 complexes. Mol. Cell. Biol. *11*, 12–19.

Miyashita, T., Krajewski, S., Krajewska, M., Wang, H., Lin, H., Liebermann, D., Hoffman, B., and Reed, J. (1994). Tumor suppressor p53 is a regulator of bcl-2 and bax gene expression in vitro and in vivo. Oncogene *9*, 1799–1805.

Momand, J., Zambetti, G.P., Olson, D.C., George, D., and Levine, A.J. (1992). The mdm-2 oncogene product forms a complex with the p53 protein and inhibits p53-mediated transactivation. Cell *69*, 1237–1245.

Momand, J., Jung, D., Wilczynski, S., and Niland, J. (1998). The MDM2 gene amplification database. Nucleic Acids Res. *26*, 3453–3459.

Morris, J.P., Yashinskie, J.J., Koche, R., Chandwani, R., Tian, S., Chen, C.-C., Baslan, T., Marinkovic, Z.S., Sánchez-Rivera, F.J., Leach, S.D., et al. (2019). α-Ketoglutarate links p53 to cell fate during tumour suppression. Nature *573*, 595–599.

Morselli, E., Tasdemir, E., Chiara Maiuri, M., Galluzzi, L., Kepp, O., Criollo, A., Vicencio, J.M., Soussi, T., and Kroemer, G. (2008). Mutant p53 protein localized in the cytoplasm inhibits autophagy. Cell Cycle *7*, 3056–3061.

Morton, J.P., Timpson, P., Karim, S.A., Ridgway, R.A., Athineos, D., Doyle, B., Jamieson, N.B., Oien, K.A., Lowy, A.M., Brunton, V.G., et al. (2010). Mutant p53 drives metastasis and overcomes growth arrest/senescence in pancreatic cancer. Proc. Natl. Acad. Sci. U. S. A. *107*, 246–251.

Mowat, M., Cheng, A., Kimura, N., Bernstein, A., and Benchimol, S. (1985). Rearrangements of the cellular p53 gene in erythroleukaemic cells transformed by Friend virus. Nature *314*, 633–636.

Muller, P.A.J., and Vousden, K.H. (2013). p53 mutations in cancer. Nat. Cell Biol. *15*, 2–8.

Muller, P.A.J., and Vousden, K.H. (2014). Mutant p53 in Cancer: New Functions and Therapeutic Opportunities. Cancer Cell *25*, 304–317.

Muller, P.A.J., Caswell, P.T., Doyle, B., Iwanicki, M.P., Tan, E.H., Karim, S., Lukashchuk, N., Gillespie, D.A., Ludwig, R.L., Gosselin, P., et al. (2009). Mutant p53 Drives Invasion by Promoting Integrin Recycling. Cell *139*, 1327–1341.

Murphy, K.L., Dennis, A.P., and Rosen, J.M. (2000). A gain of function p53 mutant promotes both genomic instability and cell survival in a novel p53-null mammary epithelial cell model.

Nakayama, M., Hong, C.P., Oshima, H., Sakai, E., Kim, S.-J., and Oshima, M. (2020). Loss of wild-type p53 promotes mutant p53-driven metastasis through acquisition of survival and tumor-initiating properties. Nat. Commun. *11*, 2333.

Nemajerova, A., Kramer, D., Siller, S.S., Herr, C., Shomroni, O., Pena, T., Gallinas Suazo, C., Glaser, K., Wildung, M., Steffen, H., et al. (2016). TAp73 is a central transcriptional regulator of airway multiciliogenesis. Genes Dev. *30*, 1300–1312.

Neve, R.M., Chin, K., Fridlyand, J., Yeh, J., Baehner, F.L., Fevr, T., Clark, L., Bayani, N., Coppe, J.P., Tong, F., et al. (2006). A collection of breast cancer cell lines for the study of functionally distinct cancer subtypes. Cancer Cell *10*, 515–527.

Nilsen, G., Liestøl, K., Loo, P. Van, Moen Vollan, H.K., Eide, M.B., Rueda, O.M., Chin, S.F., Russell, R., Baumbusch, L.O., Caldas, C., et al. (2012). Copynumber: Efficient algorithms for single- and multi-track copy number segmentation. BMC Genomics *13*, 591.

Noll, J.E., Jeffery, J., Al-Ejeh, F., Kumar, R., Khanna, K.K., Callen, D.F., and Neilsen, P.M. (2012). Mutant p53 drives multinucleation and invasion through a process that is suppressed by ANKRD11. Oncogene *31*, 2836–2848.

O'Farrell, T.J., Ghosh, P., Dobashi, N., Sasaki, C.Y., and Longo, D.L. (2004). Comparison of the Effect of Mutant and Wild-Type p53 on Global Gene Expression. Cancer Res. *64*, 8199–8207.

de Oca Luna, R.M., Wagner, D.S., and Lozano, G. (1995). Rescue of early embryonic lethality in mdm2-deficient mice by deletion of p53. Nature *378*, 203–206.

Olive, K.P., Tuveson, D.A., Ruhe, Z.C., Yin, B., Willis, N.A., Bronson, R.T., Crowley, D., and Jacks, T. (2004). Mutant p53 Gain of Function in Two Mouse Models of Li-Fraumeni Syndrome. Cell *119*, 847–860.

Olivier, M., Langerød, A., Carrieri, P., Bergh, J., Klaar, S., Eyfjord, J., Theillet, C., Rodriguez, C., Lidereau, R., Bièche, I., et al. (2006). The clinical value of somatic TP53 gene mutations in 1,794 patients with breast cancer. Clin. Cancer Res. *12*, 1157–1167.

Olivier, M., Hollstein, M., and Hainaut, P. (2010). TP53 mutations in human cancers: origins, consequences, and clinical use. Cold Spring Harb. Perspect. Biol. *2*, a001008.

Oren, M., Maltzman, W., and Levine, A.J. (1981). Post-translational regulation of the 54K cellular tumor antigen in normal and transformed cells. Mol. Cell. Biol. *1*, 101–110.

Orr, B., Godek, K.M., and Compton, D. (2015). Aneuploidy. Curr. Biol. *25*, R538–R542.

Ozcelik, H., Pinnaduwage, D., Bull, S.B., and Andrulis, I.L. (2007). Type of TP53 mutation and ERBB2 amplification affects survival in node-negative breast cancer. Breast Cancer Res. Treat. *105*, 255–265.

Parada, L.F., Land, H., Weinberg, R.A., Wolf, D., and Rotter, V. (1984). Cooperation between gene encoding p53 tumour antigen and ras in cellular transformation. Nature *312*, 649–651.

Parrales, A., and Iwakuma, T. (2015). Targeting oncogenic mutant p53 for cancer therapy. Front. Oncol. *5*.

Parrales, A., Ranjan, A., Iyer, S.V., Padhye, S., Weir, S.J., Roy, A., and Iwakuma, T. (2016). DNAJA1 controls the fate of misfolded mutant p53 through the mevalonate pathway. Nat. Cell Biol. *18*, 1233–1243.

Patro, R., Duggal, G., Love, M.I., Irizarry, R.A., and Kingsford, C. (2017). Salmon provides fast and bias-aware quantification of transcript expression. Nat. Methods *14*, 417–419.

Petitjean, A., Achatz, M.I.W., Borresen-Dale, A.L., Hainaut, P., and Olivier, M. (2007). TP53 mutations in human cancers: functional selection and impact on cancer prognosis and outcomes. Oncogene *26*, 2157–2165.

Pietenpol, J.A., Tokino, T., Thiagalingam, S., el-Deiry, W.S., Kinzler, K.W., and Vogelstein, B. (1994). Sequence-specific transcriptional activation is essential for growth suppression by p53. Proc. Natl. Acad. Sci. U. S. A. *91*, 1998–2002.

Polotskaia, A., Xiao, G., Reynoso, K., Martin, C., Qiu, W.-G., Hendrickson, R.C., and Bargonetti, J. (2015). Proteome-wide analysis of mutant p53 targets in breast cancer identifies new levels of gain-of-function that influence PARP, PCNA, and MCM4. Proc. Natl. Acad. Sci. U. S. A. *112*, E1220-9.

Quinlan, D.C., Davidson, A.G., Summers, C.L., Warden, H.E., and Doshi, H.M. (1992). Accumulation of p53 Protein Correlates with a Poor Prognosis in Human Lung Cancer.

Ran, F.A., Hsu, P.D., Wright, J., Agarwala, V., Scott, D.A., and Zhang, F. (2013). Genome engineering using the CRISPR-Cas9 system. Nat. Protoc. *8*, 2281–2308.

Rausch, T., Jones, D.T.W., Zapatka, M., Stütz, A.M., Zichner, T., Weischenfeldt, J., Jäger, N., Remke, M., Shih, D., Northcott, P.A., et al. (2012). Genome sequencing of pediatric medulloblastoma links catastrophic DNA rearrangements with TP53 mutations. Cell *148*, 59–71.

Redman-Rivera, L.N., Shaver, T.M., Jin, H., Marshall, C.B., Schafer, J.M., Sheng, Q., Hongo, R.A., Beckermann, K.E., Wheeler, F.C., Lehmann, B.D., et al. (2021). Acquisition of aneuploidy drives mutant p53-associated gain-of-function phenotypes. Nat. Commun. *12*, 5184.

Reich, N.C., and Levine, A.J. (1984). Growth regulation of a cellular tumour antigen, p53, in nontransformed cells. Nature *308*, 199–201.

Rideout, W.M., Coetzee, G.A., Olumi, A.F., and Jones, P.A. (1990). 5-Methylcytosine as an endogenous mutagen in the human LDL receptor and p53 genes. Science *249*, 1288–1290.

Robinson, J.T., Thorvaldsdóttir, H., Winckler, W., Guttman, M., Lander, E.S., Getz, G., and Mesirov, J.P. (2011). Integrative genomics viewer. Nat. Biotechnol. *29*, 24–26.

Robles, A.I., and Harris, C.C. (2010). Clinical outcomes and correlates of TP53 mutations and cancer. Cold Spring Harb. Perspect. Biol. *2*, a001016.

Rodriguez, M.S., Desterro, J.M.P., Lain, S., Lane, D.P., and Hay, R.T. (2000). Multiple C-Terminal Lysine Residues Target p53 for Ubiquitin-Proteasome-Mediated Degradation. Mol. Cell. Biol. *20*, 8458–8467.

Rosenbluth, J.M., and Pietenpol, J.A. (2008). The jury is in: p73 is a tumor suppressor after all. Genes Dev. *22*, 2591–2595.

Rosenbluth, J.M., Mays, D.J., Jiang, A., Shyr, Y., and Pietenpol, J.A. (2011). Differential regulation of the p73 cistrome by mammalian target of rapamycin reveals transcriptional programs of mesenchymal differentiation and tumorigenesis. Proc. Natl. Acad. Sci. U. S. A. *108*, 2076–2081.

Roth, J.A. (1999). p53 prognostication: paradigm or paradox? Clin. Cancer Res. *5*, 3345.

Rotter, V. (1983). p53 a transformation-related cellular-encoded protein, can be used as a biochemical marker for the detection of primary mouse tumor cells. Proc. Natl. Acad. Sci. U. S. A. *80*, 2613–2617.

Rotter, V., Witte, O.., Coffman, R., and Baltimore, D. (1980). Abelson murine leukemia virus-induced tumors elicit antibodies against a host cell protein, P50. J. Virol. *36*, 547–555.

Rotter, V., Abutbul, H., and Ben-Ze'ev, A. (1983). P53 transformation-related protein accumulates in the nucleus of transformed fibroblasts in association with the chromatin and is found in the cytoplasm of non-transformed fibroblasts. EMBO J. *2*, 1041–1047.

Rowan, S., Ludwig, R.L., Haupt, Y., Bates, S., Lu, X., Oren, M., and Vousden, K.H. (1996). Specific loss of apoptotic but not cell-cycle arrest function in a human tumor derived p53 mutant. EMBO J. *15*, 827–838.

Saito, S., Goodarzi, A.A., Higashimoto, Y., Noda, Y., Lees-Miller, S.P., Appella, E., and Anderson, C.W. (2002). ATM mediates phosphorylation at multiple p53 sites, including Ser(46), in response to ionizing radiation. J. Biol. Chem. *277*, 12491–12494.

Saito, S., Yamaguchi, H., Higashimoto, Y., Chao, C., Xu, Y., Fornace, A.J., Appella, E., and Anderson, C.W. (2003). Phosphorylation site interdependence of human p53 post-translational modifications in response to stress. J. Biol. Chem. *278*, 37536–37544.

Sakaguchi, K., Herrera, J.E., Saito, S. 'i., Miki, T., Bustin, M., Vassilev, A., Anderson, C.W., and Appella, E. (1998). DNA damage activates p53 through a phosphorylation-acetylation cascade. Genes Dev. *12*, 2831–2841.

Sakaguchi, K., Saito, S., Higashimoto, Y., Roy, S., Anderson, C.W., and Appella, E. (2000). Damage-mediated phosphorylation of human p53 threonine 18 through a cascade mediated by a casein 1-like kinase. Effect on Mdm2 binding. J. Biol. Chem. *275*, 9278–9283.

Salehi, S., Kabeer, F., Ceglia, N., Andronescu, M., Williams, M.J., Campbell, K.R., Masud, T., Wang, B., Biele, J., Brimhall, J., et al. (2021). Clonal fitness inferred from time-series modelling of single-cell cancer genomes. Nature *595*, 585–590.

Sallman, D.A., DeZern, A.E., Garcia-Manero, G., Steensma, D.P., Roboz, G.J., Sekeres, M.A., Cluzeau, T., Sweet, K.L., McLemore, A., McGraw, K.L., et al. (2021). Eprenetapopt (APR-246) and Azacitidine in TP53-Mutant Myelodysplastic Syndromes. J. Clin. Oncol. *39*, 1584–1594.

Santaguida, S., and Amon, A. (2015). Short- and long-term effects of chromosome mis-segregation and aneuploidy. Nat. Rev. Mol. Cell Biol. *16*, 473–485.

Schindelin, J., Arganda-Carreras, I., Frise, E., Kaynig, V., Longair, M., Pietzsch, T., Preibisch, S., Rueden, C., Saalfeld, S., Schmid, B., et al. (2012). Fiji: an open-source platform for biological-image analysis. Nat. Methods *9*, 676–682.

Schulz-Heddergott, R., Stark, N., Edmunds, S.J., Li, J., Conradi, L.-C., Bohnenberger, H., Ceteci, F., Greten, F.R., Dobbelstein, M., and Moll, U.M. (2018). Therapeutic Ablation of Gain-of-Function Mutant p53 in Colorectal Cancer Inhibits Stat3-Mediated Tumor Growth and Invasion. Cancer Cell *34*, 298-314.e7.

Scian, M.J., Stagliano, K.E.R., Ellis, M.A., Hassan, S., Bowman, M., Miles, M.F., Deb, S.P., and Deb, S. (2004a). Modulation of gene expression by tumor-derived p53 mutants. Cancer Res. *64*, 7447–7454.

Scian, M.J., Stagliano, K.E.R., Deb, D., Ellis, M.A., Carchman, E.H., Das, A., Valerie, K., Deb, S.P., and Deb, S. (2004b). Tumor-derived p53 mutants induce oncogenesis by transactivating growth-promoting genes. Oncogene *23*, 4430–4443.

Shah, S.P., Roth, A., Goya, R., Oloumi, A., Ha, G., Zhao, Y., Turashvili, G., Ding, J., Tse, K., Haffari, G., et al. (2012). The clonal and mutational evolution spectrum of primary triple-negative breast cancers. Nature *486*, 395–399.

Shahbandi, A., Nguyen, H.D., and Jackson, J.G. (2020). TP53 Mutations and Outcomes in Breast Cancer: Reading beyond the Headlines. Trends in Cancer *6*, 98–110.

Shaulsky, G., Goldfinger, N., Ben-Ze'ev, A., and Rotter, V. (1990). Nuclear accumulation of p53 protein is mediated by several nuclear localization signals and plays a role in tumorigenesis. Mol. Cell. Biol. *10*, 6565–6577.

Shaulsky, G., Goldfinger, N., and Rotter, V. (1991). Alterations in Tumor Development in Vivo Mediated by Expression of Wild Type or Mutant p53 Proteins.

Shay, J.W., Pereira-Smith, O.M., and Wright, W.E. (1991). A role for both RB and p53 in the regulation of human cellular senescence. Exp. Cell Res. *196*, 33–39.

Sheltzer, J.M. (2013). A Transcriptional and Metabolic Signature of Primary Aneuploidy Is Present in Chromosomally Unstable Cancer Cells and Informs Clinical Prognosis. Cancer Res. *73*, 6401–6412.

Sheltzer, J.M., and Amon, A. (2011). The aneuploidy paradox: Costs and benefits of an incorrect karyotype. Trends Genet. *27*, 446–453.

Sheng, Q., Zhao, S., Guo, M., and Shyr, Y. (2015). NGSPERL: a semi-automated framework for large scale next generation sequencing data analysis. Int. J. Comput. Biol. Drug Des. *8*, 203.

Shieh, S.Y., Ikeda, M., Taya, Y., and Prives, C. (1997). DNA damage-induced phosphorylation of p53 alleviates inhibition by MDM2. Cell *91*, 325–334.

Shirole, N.H., Pal, D., Kastenhuber, E.R., Senturk, S., Boroda, J., Pisterzi, P., Miller, M., Munoz, G., Anderluh, M., Ladanyi, M., et al. (2016). TP53 exon-6 truncating mutations produce separation of function isoforms with pro-tumorigenic functions. Elife *5*, 1–25.

Shlien, A., Tabori, U., Marshall, C.R., Pienkowska, M., Feuk, L., Novokmet, A., Nanda, S., Druker, H., Scherer, S.W., and Malkin, D. (2008). Excessive genomic DNA copy number variation in the Li-Fraumeni cancer predisposition syndrome. Proc. Natl. Acad. Sci. U. S. A. *105*, 11264–11269.

Silvestrini, R., Daidone, M.G., Benini, E., Faranda, A., Tomasic, G., Boracchi, P., Salvadori, B., and Veronesi, U. (1996). Validation of p53 accumulation as a predictor of distant metastasis at 10 years of follow-up in 1400 Node-negative breast cancers. Clin. Cancer Res. *2*, 2007–2013.

Silwal-Pandit, L., Vollan, H.K.M., Chin, S.F., Rueda, O.M., McKinney, S., Osako, T., Quigley, D.A., Kristensen, V.N., Aparicio, S., Børresen-Dale, A.L., et al. (2014). TP53 mutation spectrum in breast cancer is subtype specific and has distinct prognostic relevance. Clin. Cancer Res. *20*, 3569–3580.

Singh, S., Vaughan, C.A., Frum, R.A., Grossman, S.R., Deb, S., and Deb, S.P. (2017). Mutant p53 establishes targetable tumor dependency by promoting unscheduled replication. J. Clin. Invest. *127*, 1839–1855.

Smith, J.C., and Sheltzer, J.M. (2018). Systematic identification of mutations and copy number alterations associated with cancer patient prognosis. Elife *7*, 1–26.

Smith, A.E., Smith, R., and Paucha, E. (1979). Characterization of different tumor antigens present in cells transformed by simian virus 40. Cell *18*, 335–346.

Soneson, C., Love, M.I., and Robinson, M.D. (2016). Differential analyses for RNA-seq: transcript-level estimates improve gene-level inferences. F1000Research *4*, 1521.

Song, H., Hollstein, M., and Xu, Y. (2007). p53 gain-of-function cancer mutants induce genetic instability by inactivating ATM. Nat. Cell Biol. *9*, 573–580.

Soto, M., Raaijmakers, J.A., Bakker, B., Spierings, D.C.J., Lansdorp, P.M., Foijer, F., and Medema, R.H. (2017). p53 Prohibits Propagation of Chromosome Segregation Errors that Produce Structural Aneuploidies. Cell Rep. *19*, 2423–2431.

Soule, H.D., Maloney, T.M., Wolman, S.R., Peterson, W.D., Brenz, R., McGrath, C.M., Russo, J., Pauley, R.J., Jones, R.F., and Brooks, S.C. (1990). Isolation and Characterization of a Spontaneously Immortalized Human Breast Epithelial Cell Line, MCF-10. Cancer Res. *50*, 6075–6086.

Soussi, T. (2000). p53 Antibodies in the sera of patients with various types of cancer: A review. Cancer Res. *60*, 1777–1788.

Soussi, T. (2007). p53 alterations in human cancer: more questions than answers. Oncogene *26*, 2145–2156.

Soussi, T., and Lozano, G. (2005). p53 mutation heterogeneity in cancer. Biochem. Biophys. Res. Commun. *331*, 834–842.

Srivastava, S., Zou, Z., Pirollo, K., Blattner, W., and Chang, E.H. (1990). Germ-line transmission of a mutated p53 gene in a cancer-prone family with Li–Fraumeni syndrome. Nature *348*, 747–749.

Stephens, M. (2016). False discovery rates: a new deal. Biostatistics *18*, 275–294.

Stilgenbauer, S., Schnaiter, A., Paschka, P., Zenz, T., Rossi, M., Döhner, K., Bühler, A., Böttcher, S., Ritgen, M., Kneba, M., et al. (2014). Gene mutations and treatment outcome in chronic lymphocytic leukemia: results from the CLL8 trial. Blood *123*, 3247–3254.

Stingele, S., Stoehr, G., Peplowska, K., Cox, J., Mann, M., and Storchova, Z. (2012). Global analysis of genome, transcriptome and proteome reveals the response to aneuploidy in human cells. Mol. Syst. Biol. *8*, 608.

Stopsack, K.H., Whittaker, C.A., Gerke, T.A., Loda, M., Kantoff, P.W., Mucci, L.A., and Amon, A. (2019). Aneuploidy drives lethal progression in prostate cancer. Proc. Natl. Acad. Sci. U. S. A. *166*, 11390–11395.

Strano, S., Munarriz, E., Rossi, M., Cristofanelli, B., Shaul, Y., Castagnoli, L., Levine, A.J., Sacchi, A., Cesareni, G., Oren, M., et al. (2000). Physical and functional interaction between p53 mutants and different isoforms of p73. J. Biol. Chem. *275*, 29503–29512.

Strano, S., Dell 'orso, S., Agostino, S. Di, Fontemaggi, G., Sacchi, A., and Blandino, G. (2007). Mutant p53: an oncogenic transcription factor. Oncogene *26*, 2212–2219.

Subramanian, A., Tamayo, P., Mootha, V.K., Mukherjee, S., Ebert, B.L., Gillette, M.A., Paulovich, A., Pomeroy, S.L., Golub, T.R., Lander, E.S., et al. (2005). Gene set enrichment analysis: a knowledge-based approach for interpreting genome-wide expression profiles. Proc. Natl. Acad. Sci. U. S. A. *102*, 15545–15550.

Subramanian, M., Francis, P., Bilke, S., Li, X.L., Hara, T., Lu, X., Jones, M.F., Walker, R.L., Zhu, Y., Pineda, M., et al. (2015). A mutant p53/let-7i-axis-regulated gene network drives cell migration, invasion and metastasis. Oncogene *34*, 1094–1104.

Suh, Y.-A., Post, S.M., Elizondo-Fraire, A.C., Maccio, D.R., Jackson, J.G., El-Naggar, A.K., Van Pelt, C., Terzian, T., and Lozano, G. (2011). Multiple Stress Signals Activate Mutant p53 In Vivo. Cancer Res. *71*, 7168–7175.

Sun, S., Chen, H., Sun, L., Wang, M., Wu, X., and Xiao, Z.X.J. (2020). Hotspot mutant p53-R273H inhibits KLF6 expression to promote cell migration and tumor metastasis. Cell Death Dis. *11*, 1–9.

Talos, F., Nemajerova, A., Flores, E.R., Petrenko, O., and Moll, U.M. (2007). p73 Suppresses Polyploidy and Aneuploidy in the Absence of Functional p53. Mol. Cell *27*, 647–659.

Tang, Y.C., Williams, B.R., Siegel, J.J., and Amon, A. (2011). Identification of aneuploidy-selective antiproliferation compounds. Cell *144*, 499–512.

Tasdemir, E., Maiuri, M.C., Galluzzi, L., Vitale, I., Djavaheri-Mergny, M., D'Amelio, M., Criollo, A., Morselli, E., Zhu, C., Harper, F., et al. (2008). Regulation of autophagy by cytoplasmic p53. Nat. Cell Biol. *10*, 676–687.

Taylor, A.M., Shih, J., Ha, G., Gao, G.F., Zhang, X., Berger, A.C., Schumacher, S.E., Wang, C., Hu, H., Liu, J., et al. (2018). Genomic and Functional Approaches to Understanding Cancer Aneuploidy. Cancer Cell *33*, 676–689.

Terzian, T., Suh, Y.A., Iwakuma, T., Post, S.M., Neumann, M., Lang, G.A., Van Pelt, C.S., and Lozano, G. (2008). The inherent instability of mutant p53 is alleviated by Mdm2 or p16 INK4a loss. Genes Dev. *22*, 1337–1344.

The Cancer Genome Atlas Network (2012). Comprehensive molecular portraits of human breast tumours. Nature *490*, 61–70.

Therneau, T.M. (2020). A Package for Survival Analysis in R.

Thompson, S.L., and Compton, D.A. (2010). Proliferation of aneuploid human cells is limited by a p53-dependent mechanism. J. Cell Biol. *188*, 369–381.

Tomasini, R., Mak, T.W., and Melino, G. (2008). The impact of p53 and p73 on aneuploidy and cancer. Trends Cell Biol. *18*, 244–252.

Tsuchihara, K., Tsuda, C., Lau, S.K., Ruffini, A., Tsao, M., Iovanna, J.L., Jurisicova, A., Melino, G., Mak, T.W., Tomasini, R., et al. (2018). TAp73 regulates the spindle assembly checkpoint by modulating BubR1 activity. Proc. Natl. Acad. Sci. *115*, E8812–E8812.

Turrell, F.K., Kerr, E.M., Gao, M., Thorpe, H., Doherty, G.J., Cridge, J., Shorthouse, D., Speed, A., Samarajiwa, S., Hall, B.A., et al. (2017). Lung tumors with distinct p53 mutations respond similarly to p53 targeted therapy but exhibit genotype-specific statin sensitivity. Genes Dev. *31*, 1339–1353.

Ungerleider, N.A., Rao, S.G., Shahbandi, A., Yee, D., Niu, T., Frey, W.D., and Jackson, J.G. (2018). Breast cancer survival predicted by TP53 mutation status differs markedly depending on treatment. Breast Cancer Res. *20*, 115.

Vassilev, L.T., Vu, B.T., Graves, B., Carvajal, D., Podlaski, F., Filipovic, Z., Kong, N., Kammlott, U., Lukacs, C., Klein, C., et al. (2004). In Vivo Activation of the p53 Pathway by Small-Molecule Antagonists of MDM2. Science *303*, 844–848.

Vasudevan, A., Baruah, P.S., Smith, J.C., Wang, Z., Sayles, N.M., Andrews, P., Kendall, J., Leu, J., Chunduri, N.K., Levy, D., et al. (2020). Single-Chromosomal Gains Can Function as Metastasis Suppressors and Promoters in Colon Cancer. Dev. Cell *52*, 413–428.

Vasudevan, A., Schukken, K.M., Sausville, E.L., Girish, V., Adebambo, O.A., and Sheltzer, J.M. (2021). Aneuploidy as a promoter and suppressor of malignant growth. Nat. Rev. Cancer *21*, 89–103.

Vermeij, R., Leffers, N., van der Burg, S.H., Melief, C.J., Daemen, T., and Nijman, H.W. (2011). Immunological and Clinical Effects of Vaccines Targeting p53-Overexpressing Malignancies. J. Biomed. Biotechnol. *2011*, 1–11.

Vijayakumaran, R., Tan, K.H., Miranda, P.J., Haupt, S., and Haupt, Y. (2015). Regulation of Mutant p53 Protein Expression. Front. Oncol. *5*, 284.

Vogiatzi, F., Brandt, D.T., Schneikert, J., Fuchs, J., Grikscheit, K., Wanzel, M., Pavlakis, E., Charles, J.P., Timofeev, O., Nist, A., et al. (2016). Mutant p53 promotes tumor progression and metastasis by the endoplasmic reticulum UDPase ENTPD5. Proc. Natl. Acad. Sci. U. S. A. *113*, E8433–E8442.

Walerych, D., Lisek, K., Sommaggio, R., Piazza, S., Ciani, Y., Dalla, E., Rajkowska, K., Gaweda-Walerych, K., Ingallina, E., Tonelli, C., et al. (2016). Proteasome machinery is instrumental in a common gain-of-function program of the p53 missense mutants in cancer. Nat. Cell Biol. *18*, 897–909.

Wang, K., Li, M., and Hakonarson, H. (2010). ANNOVAR: functional annotation of genetic variants from high-throughput sequencing data. Nucleic Acids Res. *38*, e164–e164.

Wang, S., Zhao, Y., Aguilar, A., Bernard, D., and Yang, C.-Y. (2017). Targeting the MDM2-p53 Protein-Protein Interaction for New Cancer Therapy: Progress and Challenges. Cold Spring Harb. Perspect. Med. *7*, a026245.

Weaver, B.A., and Cleveland, D.W. (2006). Does aneuploidy cause cancer? Curr. Opin. Cell Biol. *18*, 658–667.

Weisz, L., Oren, M., and Rotter, V. (2007). Transcription regulation by mutant p53. Oncogene *26*, 2202–2211.

Williams, A.B., and Schumacher, B. (2016). p53 in the DNA-Damage-Repair Process. Cold Spring Harb. Perspect. Med. *6*, a026070.

Williams, B.R., Prabhu, V.R., Hunter, K.E., Glazier, C.M., Whittaker, C.A., Housman, D.E., and Amon, A. (2008). Aneuploidy affects proliferation and spontaneous immortalization in mammalian cells. Science *322*, 703–709.

Wolf, D., and Rotter, V. (1984). Inactivation of p53 gene expression by an insertion of Moloney murine leukemia virus-like DNA sequences. Mol. Cell. Biol. *4*, 1402–1410.

Wolf, D., and Rotter, V. (1985). Major deletions in the gene encoding the p53 tumor antigen cause lack of p53 expression in HL-60 cells. Proc. Natl. Acad. Sci. U. S. A. *82*, 790–794.

Xu, J., Qian, J., Hu, Y., Wang, J., Zhou, X., Chen, H., and Fang, J.-Y. (2015). Heterogeneity of Li-Fraumeni Syndrome links to unequal gain-of-function effects of p53 mutations. Sci. Rep. *4*, 4223.

Xue, Y., San Luis, B., and Lane, D.P. (2019). Intratumour heterogeneity of p53 expression; causes and consequences. J. Pathol. *249*, 274–285.

Yamamoto, M., Hosoda, M., Nakano, K., Jia, S., Hatanaka, K.C., Takakuwa, E., Hatanaka, Y., Matsuno, Y., and Yamashita, H. (2014). p53 accumulation is a strong predictor of recurrence in estrogen receptor-positive breast cancer patients treated with aromatase inhibitors. Cancer Sci. *105*, 81–88.

Yang, A., and McKeon, F. (2000). p63 and p73: p53 mimics, menaces and more. Nat. Rev. Mol. Cell Biol. *1*, 199–207.

Yang, A., Kaghad, M., Wang, Y., Gillett, E., Fleming, M.D., Dötsch, V., Andrews, N.C., Caput, D., and McKeon, F. (1998). p63, a p53 homolog at 3q27-29, encodes multiple products with transactivating, death-inducing, and dominant-negative activities. Mol. Cell *2*, 305–316.

Yang, A., Schweitzer, R., Sun, D., Kaghad, M., Walker, N., Bronson, R.T., Tabin, C., Sharpe, A., Caput, D., Crum, C., et al. (1999). p63 is essential for regenerative proliferation in limb, craniofacial and epithelial development. Nature *398*, 714–718.

Yang, A., Walker, N., Bronson, R., Kaghad, M., Oosterwegel, M., Bonnin, J., Vagner, C., Bonnet, H., Dikkes, P., Sharpe, A., et al. (2000). p73-deficient mice have neurological, pheromonal and inflammatory defects but lack spontaneous tumours. Nature *404*, 99–103.

Yemelyanova, A., Vang, R., Kshirsagar, M., Lu, D., Marks, M.A., Shih, I.M., and Kurman, R.J. (2011). Immunohistochemical staining patterns of p53 can serve as a surrogate marker for TP53 mutations in ovarian carcinoma: an immunohistochemical and nucleotide sequencing analysis. Mod. Pathol. *24*, 1248–1253.

Yeudall, W.A., Vaughan, C.A., Miyazaki, H., Ramamoorthy, M., Choi, M.-Y., Chapman, C.G., Wang, H., Black, E., Bulysheva, A.A., Deb, S.P., et al. (2012). Gain-of-function mutant p53 upregulates CXC chemokines and enhances cell migration. Carcinogenesis *33*, 442–451.

Yue, X., Zhao, Y., Xu, Y., Zheng, M., Feng, Z., and Hu, W. (2017). Mutant p53 in Cancer: Accumulation, Gain-of-Function, and Therapy. J. Mol. Biol. *429*, 1595–1606.

Zack, T.I., Schumacher, S.E., Carter, S.L., Cherniack, A.D., Saksena, G., Tabak, B., Lawrence, M.S., Zhang, C.Z., Wala, J., Mermel, C.H., et al. (2013). Pan-cancer patterns of somatic copy number alteration. Nat. Genet. *45*, 1134–1140.

Zalcenstein, A., Stambolsky, P., Weisz, L., Müller, M., Wallach, D., Goncharov, T.M., Krammer, P.H., Rotter, V., and Oren, M. (2003). Mutant p53 gain of function: repression of CD95(Fas/APO-1) gene expression by tumor-associated p53 mutants. Oncogene *22*, 5667–5676.

Zhang, C., Liu, J., Liang, Y., Wu, R., Zhao, Y., Hong, X., Lin, M., Yu, H., Liu, L., Levine, A.J., et al. (2013). Tumour-associated mutant p53 drives the Warburg effect. Nat. Commun. *4*, 2935.

Zhang, Q., Bykov, V.J.N., Wiman, K.G., and Zawacka-Pankau, J. (2018). APR-246 reactivates mutant p53 by targeting cysteines 124 and 277. Cell Death Dis. *9*, 439.

Zhang, Y., Xiong, Y., and Yarbrough, W.G. (1998). ARF promotes MDM2 degradation and stabilizes p53: ARF-INK4a locus deletion impairs both the Rb and p53 tumor suppression pathways. Cell *92*, 725–734.

Zhu, J., Sammons, M.A., Donahue, G., Dou, Z., Vedadi, M., Getlik, M., Barsyte-Lovejoy, D., Al-awar, R., Katona, B.W., Shilatifard, A., et al. (2015). Gain-of-function p53 mutants co-opt chromatin pathways to drive cancer growth. Nature *525*, 206–211.

Zhu, J., Tsai, H.J., Gordon, M.R., and Li, R. (2018). Cellular Stress Associated with Aneuploidy. Dev. Cell *44*, 420–431.